NUMERICAL INVESTIGATION OF FEMORAL AUGMENTATION

María Ester Santana Artiles

Thesis submitted in partial fulfilment of the requirements of Kingston University for the degree of Doctor of Philosophy

December 2019

Declaration

I declare that this thesis and the work presented in it are my own and have been generated as the result of my original research, with all references to other sources clearly identified. I declare that no material contained here has been used in any other academic award submission. I confirm that while registered for a research degree at Kingston University, I have not been a registered candidate or enrolled student at any other academic or professional institution.

List of Publications and Conference Papers

Publications

- Santana Artiles, M.E. and Venetsanos, D.T. (2017). A new evolutionary optimization method for osteoporotic bone augmentation, *Computer Methods in Biomechanics and Biomedical Engineering*, 20(7), pp. 691-700.
- Santana Artiles, M. E. and Venetsanos, D. T. (2018) Numerical investigation of the effect of bone cement porosity on osteoporotic femoral augmentation, *International Journal for Numerical Methods in Biomedical Engineering*, pp. e2989.

Conferences

- Santana Artiles, M.E. and Venetsanos, D.T. (2017). Simulation of PMMA bone cement injection and polymerization for bone augmentation. Kingston University Science, Engineering and Computing (SEC) Conference 2017. London, 5 April 2017.
- Santana Artiles, M.E. and Venetsanos, D.T. (2017). Optimal osteoporotic femoral augmentation under multiple load cases. 23rd Congress of the European Society of Biomechanics (ESB). Seville, 2-5 July 2017
- Santana Artiles, M. E. and Venetsanos, D. T. (2018) Injection of bone cement into osteoporotic femora along curved canals. 5th SIMBIO-M conference. Stratford upon Avon, 18-19 June 2018.
- Santana Artiles, M. E. and Venetsanos, D. T. (2018) Computational study of femoral augmentation using curved injection channels. PhD Symposium 2018: Improving and understanding health. Liverpool Medical Institution, 4 July 2018.

- Santana Artiles, M. E. and Venetsanos, D. T. (2018) Prophylactic augmentation of the proximal femur by injecting bone cement through curved drilled channels. 8th World Congress of Biomechanics (WCB). Dublin, 8-12 July 2018.

Abstract

Femoral augmentation is a minimally invasive procedure involving injection of bone cement into osteoporotic femora in order to enhance their load capacity. However, this treatment poses significant risks such as bone thermal necrosis or embolism when large amounts of bone cement are injected in the femur. This thesis presents methods developed to find the ideal bone cement volume and distribution needed to restore the load capacity of osteoporotic femora depending on their level of osteoporosis. Material properties of augmented tissue were modelled using a proposed scheme that combines Voigt-Reuss-Hill average and bone cement porosity. These ideal bone cement distributions were used as a reference to propose several feasible and generalised augmentation strategies, which comprised placing bone cement in up to three spheres or in up to two pre-drilled channels. Bone cement location was found to be more significant in the augmentation result than bone cement volume or augmentation strategy. Fracture analysis of augmented femora was also conducted, demonstrating that approximately 7ml of bone cement can result in an increase of 74% in yield load, 62% in fracture load, and 117% in energy to fracture. After finding the optimum bone cement volume and distribution, the bone cement injection and polymerisation process was studied in a 2D femur model, and results suggest that risk of thermal necrosis was limited to the regions in the bone-PMMA interface while stress levels required to develop debonding between the materials were not reached. However, results were obtained from a 2D model and the bone-PMMA interface was not modelled in detail. Some other limitations involved in the present study are the use of a single femur, with

virtually introduced osteoporosis that only represents senile osteoporosis and a single set of boundary conditions. Additionally, despite results were compared against experiments in the literature, an experimental validation may be necessary to ensure the validity of the model. Despite the limitations of the present study and lack of direct experimental validation, the methods presented in this thesis can be applied to any femur to evaluate the requirements of femoral augmentation and the risks that it may entail. When applied to the studied femur, we conclude that femoral augmentation can increase significantly the femur yield and fracture load and only present risk of thermal necrosis in the bone-PMMA interface.

Acknowledgments

Firstly, I would like to express my gratitude to Dr Demetrios Venetsanos, who has been a constant source of knowledge and inspiration. Thank you for your contagious enthusiasm, patience and encouragement. Also, a special thank you to Dr Homa Hadavinia and Dr Ali Heidari for their insightful comments, support and valuable input during this research.

My sincere thanks to the Doctoral Training Alliance (DTA), who provided me with both a scholarship and the resources to complete this project.

Thank you to all my colleagues for the stimulating discussions in the coffee breaks and shared experiences. I would also like to thank Alex, who has been by my side throughout the process of researching and writing this thesis.

And finally, thanks to my family for their unconditional love and support. Each one of you has helped me in your own unique way.

Table of Contents

List of Figures

List of Tables

List of Abbreviations

ABC	Acrylic Bone Cement
ANOVA	Analysis of Variance
ANCOVA	Analysis of Covariance
APDL	Ansys Parametric Design Language
BESO	Bidirectional Evolutionary Structural Optimisation
BMD	Bone Mineral Density
BV	Bone Volume
BVF	Bone Volume Fraction
CT	Computerised Tomography
CPC	Calcium Phosphate Cement
CV	Coefficient of Variation
DXA	Dual-energy X-ray Absorptiometry
DOF	Degrees of Freedom
ESO	Evolutionary Structural Optimisation

FE	Finite Element
FEA	Finite Element Analysis
FRAX	Fracture Risk Assessment Tool
GPC	Glass Polyalkenoate Cement
HU	Hounsfield Unit
MMA	Methyl methacrylate
PDMS	Polydimethylsiloxane
PMMA	Polymethyl methacrylate
ROI	Region of Interest
SD	Standard Deviation
SERM	Selective Estrogen Receptor Modulator
TPM	Theory of Porous Media
WHI	Women's Health Initiative
XFEM	Extended Finite Element Method

List of Symbols

$\boldsymbol{\alpha}$	Transverse load direction
$\boldsymbol{\beta}$	Frontal load direction
$\boldsymbol{\gamma}$	Shear rate
$\boldsymbol{\delta}$	Reduction factor
$\boldsymbol{D}$	Damage
$\boldsymbol{E}$	Modulus of elasticity
$\boldsymbol{\varepsilon_{max}}$	Maximum principal strain
$\boldsymbol{\varepsilon_{min}}$	Minimum principal strain
$\boldsymbol{\varepsilon_0}$	Damage strain threshold
$\boldsymbol{\varepsilon_f}$	Fracture strain
$\boldsymbol{\varepsilon_{thermal}}$	Thermal strain
$\boldsymbol{\varepsilon_{chemical}}$	Chemical strain
$\boldsymbol{k}$	Permeability
$\boldsymbol{\eta}$	Kinematic viscosity

ψ	Bone porosity
ρ_{app}	Apparent density
ρ_{ash}	Ash density
ρ_{tissue}	Bone tissue density
ρ_{QCT}	Radiological density
φ	Volume fraction
p	Polymerisation fraction
R	Radius
S	Heat generation rate
S/N	Signal to Noise ratio
V_{PMMA}	PMMA Volume
YL	Yield load

Chapter 1

Introduction

Osteoporotic hip fractures consist of cracks or breaks in the upper part of the femur due to a load that would not typically fracture a healthy bone. Given their severe consequences and extended recovery times, they are responsible for 47% of the total cost of osteoporotic fractures in the UK (Svedbom et al., 2013). Hence, several preventative treatments including drugs, hip protectors, specific diets and exercises and calcium and vitamin D supplementation have been proposed in the past. However, due to their side effects and lack of patient compliance their efficacy is limited. Femoral augmentation is a preventive treatment against osteoporotic hip fractures that should not present these drawbacks. It involves reinforcing the proximal femur using an injectable bone cement and aims to restore the reduced load-bearing capacity of the bone. Due to the risks associated when injecting large volumes of bone cement, this procedure is not currently applied in clinical practice. Hence, before applying this treatment in vivo, two unknowns need to be addressed: the minimum amount of bone cement required and its distribution to avoid an osteoporotic hip fracture and the risks that the procedure would involve with the minimum amount of bone cement. Given the large number of factors that can affect the outcome of femoral augmentation (degree of osteoporosis, type of bone cement, volume and distribution of bone cement, type of fall), a numerical study is

an efficient approach to find answers to the aforementioned unknowns. In more detail, the aims and objectives of the present numerical investigation are detailed below.

1.1 Aims and Objectives

The aim of this research was to numerically investigate the feasibility and consequences of the femoral augmentation procedure. To this end, the following objectives were set:

- Develop a computational model to study the biomechanical effect of femoral augmentation including accurately modelling the mechanical properties of augmented tissue.
- Investigate how the degree of osteoporosis affects the requirements and biomechanical outcome of femoral augmentation.
- Propose and study a range of generalised and patient-specific augmentation approaches.
- Identify optimal bone cement volume and placement for the proposed femoral augmentation strategies.
- Develop a computational model to investigate the risk of bone thermal necrosis and debonding between bone tissue and bone cement during the augmentation procedure.

1.2 Thesis Overview

This thesis presents a numerical study of femoral augmentation and is structured as follows:

- Chapter 2 presents an introduction to osteoporosis and osteoporotic hip fractures, a review of current risk assessment strategies and existing preventative treatments for these fractures. From all preventative treatments, a literature review of femoral augmentation is presented, including the advantages and disadvantages that the procedure can entail.

- In Chapter 3, the ideal locations where bone cement should be placed to prevent an osteoporotic hip fracture are found. To achieve this, femur Finite Element (FE) models with different levels of osteoporosis and osteopenia were developed based on a CT scan. FE analyses of the femora under lateral fall conditions were conducted and an Evolutionary Structural Optimisation (ESO) algorithm was applied to find the ideal distribution of bone cement. However, the obtained ideal distribution of bone cement is not constrained to be realistic and injectable in practice.

- In Chapter 4, a set of modifications that could improve the approach used in Chapter 3 to model the augmented tissue are proposed. These modifications involve the use of a rule of mixtures, consideration of bone volume fraction per element and bone cement porosity. Five different modelling approaches are proposed and a statistical analysis is performed to find if they are significantly different from each other. Additionally, the effect of fall direction and bone cement porosity on the femoral augmentation requirements is investigated through a sensitivity analysis.

- In Chapter 5, an important limitation of Chapters 3 and 4 is addressed: the lack of realistic augmentation strategies. To do so, several realistic femoral augmentation strategies are proposed based on the ideal bone cement distribution found in previous chapters. These augmentation strategies are based on injecting cement in one or two pre-drilled paths or injecting cement in up to three spheres. The different augmentation approaches are studied through the use of FE and Taguchi analyses and their placement is optimised using a *patternsearch* algorithm.

- Chapter 6 studies the possible changes in fracture patterns that can occur due to the femoral augmentation procedure. Based on the realistic, optimised

augmentation strategies found in Chapter 5, a fracture analysis is performed in augmented and non-augmented femora using FEA and a nonlocal damage model. Changes in fracture patterns are studied to determine if augmentation with PMMA bone cement can lead to more complicated fractures.

- Chapter 7 investigates the risks involved in the femoral augmentation procedure due to the injection and solidification of bone cement inside the femur. Using the augmentation strategies proposed in previous chapters, a 2D computational framework is applied to simulate the bone cement injection and curing processes in femoral augmentation. Intraosseous pressure, temperature fields and stresses are studied to evaluate the risks of leakage, thermal necrosis and debonding.

- Chapter 8 presents a summary of the obtained results, limitations of the current study and recommendations for future work.

Chapter 2

Background

2.1 Osteoporosis

Bone is a dynamic tissue that develops in three main stages: growth, modelling and remodelling. During childhood and adolescence bone tissue grows with accompanying changes to shape and thickness influenced by environmental factors. For men and women of normal body weight, total skeletal mass reaches its peak at the end of the growth period, a few years after the fusion of the long bone epiphyses. Bone mass of an individual in later life will depend on the peak attained during growth and subsequent rate of bone loss. The remodelling phase occurs during adulthood and continues throughout life when tissue is lost by resorption and rebuilt by formation. In normal bone remodelling, a balance between bone resorption and bone formation is maintained to ensure that bone mass and mechanical strength remain the same after each cycle (Feng and McDonald, 2011). However, an imbalance between bone formation and resorption can lead to bone loss and the development of bone disorders such as osteoporosis.

Osteoporosis is a disease characterized by low bone mass, deterioration of bone tissue and disruption of bone microarchitecture (NIH Consensus Development Panel on

Osteoporosis Prevention, 2001) that can lead to compromised bone strength and increased risk of fractures. This disease can be divided into two subtypes: type I and type II (Riggs et al., 1982, 2001). Type I osteoporosis appears solely in postmenopausal women and is mainly caused by oestrogen deficiency resulting from menopause, whereas type II osteoporosis is associated primarily with aging in both women and men. In both types of osteoporosis, the condition is directly related to the decrease of bone mineral density (BMD). This decrease affects the microstructure of the bone and explains the lowering of bone strength and higher risk of fracture. Currently, the diagnosis of osteoporosis is based on the BMD of the femoral neck, measured using dual-energy x-ray absorptiometry (DXA). According to the World Health Organization, osteoporosis is defined as having a BMD below 2.5 standard deviations of the young adult average value (T-Score equal or less than -2.5). Table 2.1 shows the diagnostic criteria in detail (Kanis, 2002):

Table 2.1: Osteoporosis levels based on T-Score.

Condition	**T-Score**
Normal	-1.0 or higher
Osteopenia	Between -1.0 and -2.5
Osteoporosis	-2.5 or lower
Severe Osteoporosis	-2.5 or lower and personal history of fragility fractures

Osteoporotic fractures commonly occur in the distal radius, proximal humerus, vertebral bodies, pelvis and the proximal femur (Compston et al., 2017). Each year in the UK, approximately 536,000 new fragility fractures occur, including 79,000 hip fractures, 66,000 vertebral fractures and 69,000 forearm fractures (Svedbom et al., 2013). These fractures constitute a major burden to the health care system and the economy due to hospitalisation costs, disability, loss of independence and increase of early mortality levels. Moreover, the increased longevity of the world population will lead to a significant rise in fragility fractures if improvements are not made to bone health awareness and elderly healthcare practice (Gullberg et al., 1997; Kanis, 2002; Svedbom

et al., 2013). Therefore, the early identification of patients at high risk of fracture and the development of new preventative strategies will be crucial for more effective management of patients with osteoporosis.

2.2 Hip Fractures

The present study is focused on hip fractures, which are defined as a partial or complete break in the proximal region of the femur, close to the hip joint. Despite representing less than 15% of the total fragility fractures occurring annually in the UK, they account for 47% of the total cost of osteoporotic fractures due to their severe consequences and associated extended recovery times (Svedbom et al., 2013). Additionally, hip fractures are associated with significant morbidity, mortality and lack of independence (Cummings and Melton, 2002). Approximately 53% of patients suffering a hip fracture can no longer live independently (Neuburger et al., 2015) and the risk of mortality increases by 20% in the year following a hip fracture (Leibson et al., 2002). Furthermore, due to the ageing of the world's population the incidence of hip fractures is increasing by 1-3% per year in most areas of the world (Cummings and Melton, 2002).

2.2.1 Femur Anatomy

In order to better understand the types and risk of hip fractures, a brief description of the proximal femoral anatomy is provided. The femur is the longest bone in the human body, connecting the hip and knee and transmitting forces from the tibia to the hip joint. The proximal femur forms the hip joint with the pelvis, and it is comprised of the head, the neck, and two trochanters (Figure 2.1). The femoral head is a half-spherical region covered by cartilage, which connects with the pelvis through the acetabulum, forming the hip joint. The femoral neck constitutes the main support of the femoral head, connecting it to the femoral shaft. The greater and lesser trochanters are located in the lateral region

of the femur and have a complex geometry due to the presence of muscle, ligament and tendon connections. Both cortical and trabecular bone are present in different regions of the femur. Trabecular bone is a porous tissue, with 50 to 90% porosity, while cortical bone is solid, strong and denser than trabecular bone, with only 5 to 10% porosity. The femoral shaft has a thick layer of cortical tissue, which decreases progressively towards the neck area until becoming a very thin layer in the proximal femur.

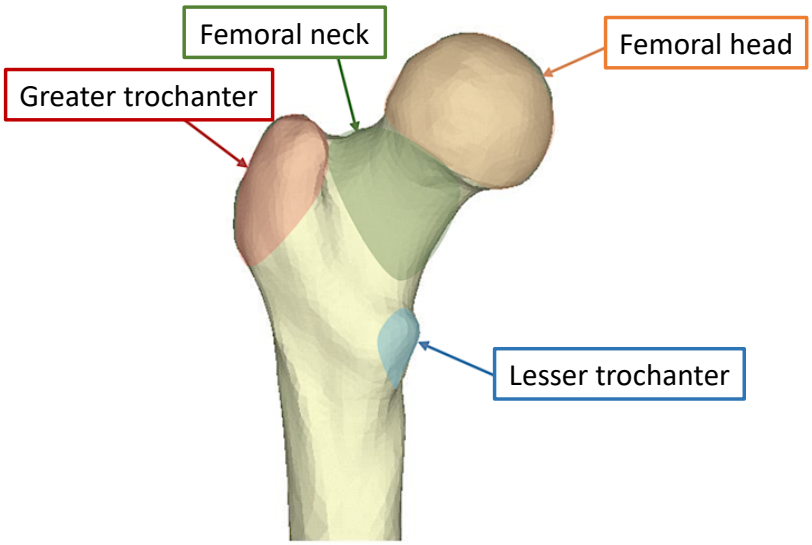

Figure 2.1: Proximal femur anatomy.

Fractures of the femur will occur when the force acting in the bone exceeds its capacity to dissipate the related energy without suffering damage (Nobile and Nobile, 2019). This energy to failure is shown in Figure 2.2 as the area under the stress-strain curve limited by the maximum stress (ultimate strength) and strain (ultimate strain) that the bone can sustain. Additionally, this curve is formed of an elastic strain region and a plastic strain region, separated by the yield point (Turner, 2006). Stresses above the yield point (forces higher than the bone yield load) would cause permanent damage to the bone.

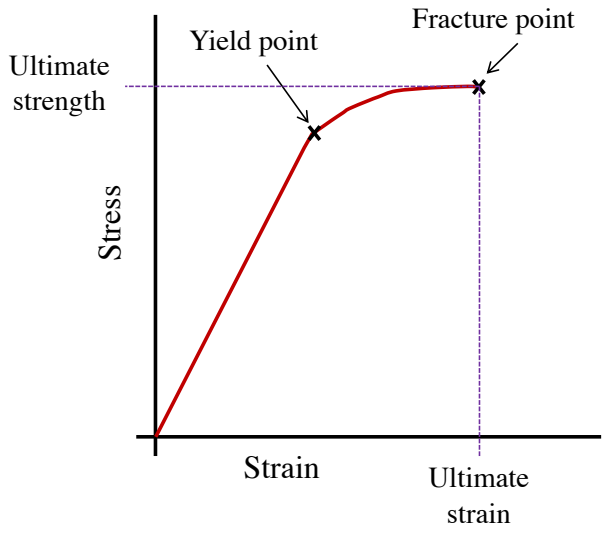

Figure 2.2: Typical stress-strain curve for bone (Turner, 2006).

2.2.2 Hip Fracture Classification

The proximal femur carries a variety of loads during daily activities and subsequently presents different fracture configurations which are strongly affected by hip geometry, environmental factors, and health conditions such as osteoporosis (Gomez-Alonso et al., 2000; Kaptoge et al., 2008; Marks, 2010). Depending on fracture location, hip fractures are classified into three types: femoral neck, trochanteric and femoral head fractures.

Femoral neck fractures occur in the region of the upper femur located between the femoral head and the trochanters. These fractures can be classified according to their location in subcapital, transcervical or basicervical and can be displaced or non-displaced (Figure 2.3). The blood supply to the femoral head depends on several arteries that pass through the femoral neck region. Hence, displacement of the femoral neck can restrict blood supply to the femoral head and lead to necrosis (Fox et al., 2000). Elderly individuals with reduced BMD tend to present subcapital femoral neck fractures from low-energy falls (Parkkari et al., 1999), while young adults often present vertically oriented distal neck fractures associated with high-energy trauma (Riggs et al., 2001; Winter et al., 2016).

Femoral neck fractures have also been associated with Parkinson's disease (Fisher et al., 2010), oestrogenic therapy (Fox et al., 1999) and variations in hip morphology (Pulkkinen et al., 2011).

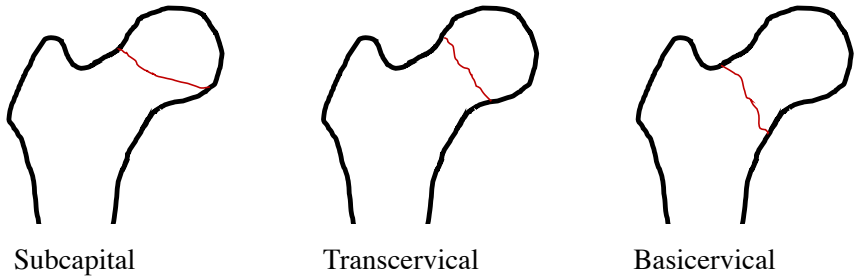

Figure 2.3: Classification of femoral neck fractures.

Trochanteric fractures occur out of the joint capsule (extracapsular), in the area between the greater and lesser trochanters. Depending on their location, they can be classified as pertrochanteric or intertrochanteric fractures (Figure 2.4). These areas involve bone with good local blood supply, reducing the possibility of bone necrosis. However, they contain numerous muscle attachments, which may exert forces capable of pulling bone segments out of alignment. Fractures of the trochanter are usually associated with elderly patients with a previous fracture history (Fox et al., 1999), low BMD, and vitamin D deficiency (Pulkkinen et al., 2011).

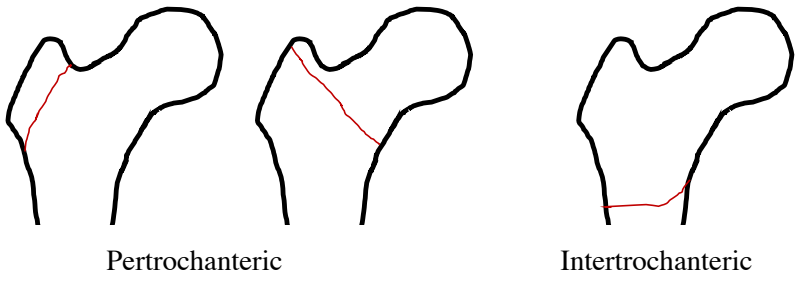

Figure 2.4: Classification of trochanteric femoral fractures.

Finally, fractures of the femoral head are classified into split fractures and depression fractures (Figure 2.5). Femoral head fractures are rare and normally occur in young adults as the result of a high-energy traumatic hip dislocation (Alonso et al., 2000).

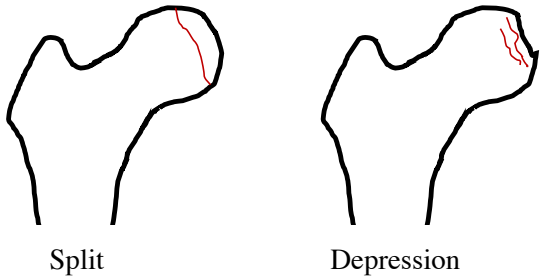

Figure 2.5: Classification of femoral head fractures.

2.2.3 Risk Assessment

Epidemiological evidence suggests most osteoporotic hip fractures occur due to a lateral fall on the greater trochanter from standing height or lower (Parkkari et al., 1999; Turner, 2002). However, despite falls in the elderly being frequent (Sanders et al., 2017), only about 5% of falls are reported to result in a fracture (Nachreiner et al., 2007). Therefore, the risk of suffering a hip fracture due to a fall can be defined as the femur's ability to resist the force that it encounters in case of a fall.

Multiple factors such as advancing age, family history of fracture, personal history of previous fractures and/or falls, sex, excessive bone loss, low BMD, low body weight, and smoking habits have been associated with fracture risk (Cummings et al., 1995). From these, the most robust predictors are low BMD and existence of previous fractures (LaFleur et al., 2008; Klotzbuecher et al., 2000), although they are unable to account for all fracture cases on their own. For instance, among those aged over 50 years old, more than 50% of women and up to 70% of men who sustained a fracture had not had osteoporosis as defined by the BMD criteria (Nguyen et al., 2007a). For this reason, a number of models for fracture risk assessment have been developed based on the idea of incorporating data from multiple factors. To date, the most common models used in clinical practice are FRAX (Kanis et al., 2008) and the Garvan Fracture Risk Calculator (Nguyen et al., 2007b). FRAX uses 12 risk factors such as femoral neck BMD, anthropometric and

lifestyle factors, and comorbidities. The Garvan Fracture Risk Calculator uses 5 risk factors: age, sex, femoral neck BMD, prior fracture, and history of falls. Unfortunately, these tools are limited in their ability to accurately detect patients at risk due to their ethnic specificity and not taking into account the magnitude of the fall-induced impact force (Watts et al., 2009; Geusens et al., 2010; Järvinen et al., 2014). However, recent advances in statistical modelling and machine learning have opened new opportunities for improving this type of fracture prediction models (Kruse et al., 2017; Ferizi et al., 2019).

A different approach to predict the risk of hip fractures consists of simulating falls onto soft protective surfaces with human volunteers (Svedbom et al., 2013; Laing and Robinovitch, 2010). Using the soft protective surfaces reduces the load acting on the volunteers' femur, so in order to predict the real forces at impact conditions these models rely on extrapolation beyond the force range for which they were validated. Ex-vivo models, using cadaveric or synthetic femora and following the same methodology can replicate a fall up to the fracture point (Gilchrist et al., 2014; Fleps et al., 2018). However, most systems fail to accurately represent the patient-specific fracture loads or the soft tissue and pelvis surrounding the bone.

Subject-specific finite element (FE) models show potential as a tool to improve the accuracy of fracture risk prediction. These models may estimate bone strength and characterise the bone mechanical behaviour under different loading conditions. Several FE studies have examined the differences in femoral strength under various load configurations such as single stance (Cody et al., 1999; Keyak, 2001; Keyak and Falkinstein, 2003) or fall in different directions (Ford et al., 1996; Pinilla et al., 1996; Majumder et al., 2007; Grassi et al., 2012). Moreover, FE models have proven to be better predictors of femoral strength than BMD based on DXA images (Cody et al., 1999). However, despite a few studies attempting to show their applicability in clinical settings (Floerkemeier et al., 2011; Eggermont et al., 2018; Benca et al., 2019), there are still several reasons as to why FE models are not widely used in clinical practice. One concern is the reproducibility of FE models, since the procedure to generate such models

involves several steps like image segmentation, meshing, materials and boundary conditions assignment. The execution of each one of these steps varies between published studies in terms of different input parameters and level of detail implemented (van den Munckhof and Zadpoor, 2014). Another concern is related to the fact that the majority of proposed FE modelling techniques are based on computed tomography (CT) datasets. When compared with DXA, performing a CT scan involves higher operational costs and subjects patients to a higher radiation dose (Kanis, 2002; Engelke et al., 2015). Subject-specific FE models from DXA images have the potential to overcome some of these issues. The process to build these models consists of using statistical tools to reconstruct 3D shape and BMD distribution from a planar DXA image (Langton et al., 2009). Their accuracy predicting femoral strength has been reported to be only slightly inferior to those obtained with state-of-the-art CT-based models (Grassi et al., 2017), suggesting such models could potentially be used in clinical settings to improve hip fracture risk assessment.

2.3 Prevention of Hip Fractures

Due to the serious consequences of osteoporotic hip fractures and the world's ageing population, numerous methods for the prevention of such fractures have been developed over the past years. These include specific weight-bearing exercises to stimulate bone growth, calcium and vitamin D supplementation, pharmacological treatments to prevent or treat osteoporosis and interventions to reduce the risk and consequences of falling.

2.3.1 Pharmacological Prevention

Pharmacological treatment of osteoporosis plays an important role in the prevention of osteoporotic fractures and have been shown to reduce risk of vertebral and hip fractures (Kanis et al., 2013). However, the majority of drugs are limited by side effects and the

long time taken to restore bone properties. Besides this, due to the slow and progressive nature of osteoporosis it is difficult to maintain patient compliance with scheduled dosing (Kothawala et al., 2007). To date, most pharmacological treatments for osteoporosis are based either on inhibiting bone resorption (antiresorptive agents) or stimulating bone formation (osteoanabolic agents). However, use of antiresoptives such as calcium, vitamin D, bisphosphonates, selective oestrogen receptor modulators, and oestrogen is usually followed by a decrease in bone formation, limiting their efficacy. Similarly, use of osteoanabolics increases bone formation but also increases bone resorption. Therefore, attempts are currently being made to develop molecules that can overcome this issue and achieve uncoupling of bone formation from bone resorption (Makras et al., 2015). The current most common pharmacological treatments for the prevention of osteoporotic fractures are detailed below:

- **Calcium and vitamin D**

The effect of calcium and vitamin D supplements on osteoporosis and fracture risk depends on several factors which include dosing, combinations of calcium and vitamin D and type of ingestion (van der Velde et al., 2014). It has been proved that mono-supplements with calcium have no effect on the development of osteoporosis (Abrahamsen, 2017) but mono-supplementation with vitamin D can reduce the risk of osteoporotic fractures in subjects with a high vitamin D deficiency (Bischoff-Ferrari et al., 2018). In the case of supplements combining calcium and vitamin D, it has been shown that these measures can decrease the risk of hip fracture in elderly institutionalized adults (Chapuy et al., 1992), as well as the risk of non-vertebral fractures in men and women over the age of 65 (Trivedi et al., 2003; Bischoff-Ferrari et al., 2009). Therefore, evidence suggests that providing calcium and vitamin D supplements to individuals at high risk of deficiencies or patients receiving anti-osteoporosis drugs could help prevent osteoporotic fractures (Harvey et al., 2017). A range of side effects such as gastrointestinal intolerance, kidney stones and cardiovascular problems (Bolland et al., 2015) have been reported due to calcium and/or vitamin D supplementation. Hence, despite these two supplements demonstrating strong

benefits against osteoporotic fractures, they also entail a renal and cardiovascular risk (Abrahamsen, 2017).

- **Bisphosphonates**

Bisphosphonates have been the most commonly used treatment for osteoporosis since the late 1960s. They are antiresorptive agents that inhibit the resorption of bone and try to restore the balance between bone loss and formation. Alendronate and risedronate are the most commonly used bisphosphonates due to their efficacy and low cost. A randomized placebo-controlled trial of alendronate showed a 47% reduction in hip fractures after 12 months of continuous dosing (Black et al., 2000). Similarly, a trial of risedronate demonstrated a significant reduction in hip fracture risk after 24 months of therapy (McClung et al., 2001). Bisphosphonates are well tolerated by most people, but side effects such as hypocalcemia, severe muscular pain, and ocular inflammation are likely to occur in calcium and vitamin D deficient patients. However, the main concern with this treatment is that prolonged use may result in suppression of osteoclasts and osteoblasts which may cause reduced bone remodelling, impairing the repair of micro-cracks in bone and leading to atypical femoral fractures (Dell et al., 2012).

- **Hormone replacement therapy**

Hormone replacement therapy (oestrogen) is an antiresorptive treatment that inhibits bone resorption and maintains bone formation. Oestrogen treatment was formerly the primary choice for prevention of osteoporosis in menopausal women. A study developed by the Women's Health Initiative (WHI) proved the effectiveness of this treatment in the reduction of hip fracture risk, but also reported increases in breast cancer risk, cardiovascular disease and venous thromboembolic events (Rossouw et al., 2002). Hence, despite this treatment proving beneficial to post-menopausal women, due to its severe adverse effects, this therapy is no longer recommended in the elderly population.

- **Selective oestrogen receptor modulators**

Selective oestrogen receptor modulators (SERMs) were developed to maintain the benefits of oestrogen therapy but avoid its potential side effects. SERMs such as raloxifene and bazedoxifene act like oestrogen on bone processes (decreasing bone resorption) but exhibit the effects of an anti-oestrogen on uterus, breast and brain tissue. A meta-analysis of seven randomized trials in postmenopausal women with osteoporosis following a raloxifene treatment showed a reduction of 30% in vertebral fractures but no risk reduction for non-vertebral fractures (Cranney et al., 2002). In a different study, therapy with bazedoxifene and raloxifene was studied, showing a significant effect on maintaining BMD and reducing the incidence of new vertebral fractures (Kaufman et al., 2013). Further trials examining various SERM preparations have shown that BMD can be maintained and incidence of vertebral fractures reduced, yet risk of non-vertebral fractures did not decrease. All these studies indicate that the benefits of SERMs might be anatomically limited and their effectiveness is curtailed once the medication is suspended. The side effects of SERMs include increased risk of venous thromboembolic events and incidence of hot flashes.

2.3.2 Non-pharmacological Prevention

Non-pharmacological osteoporosis management is a broad concept that includes nutrition, physical exercise and wider lifestyle changes. It has been shown that lifestyle habits can contribute up to 20% of the variation in peak bone mass attainment, as well as to the rate of bone loss in adults (Rubin et al., 1999; Drake et al., 2004). For this reason, healthy lifestyle habits such as adequate calcium intake and weight-bearing exercise should be part of the long-term approach for the prevention of fragility fractures, for all sexes and ages.

Falls are the major health concern for people with diagnosed osteoporosis. Between 28% and 35% of community-living adults over 65 years old experience at least one fall each year

(Campbell et al., 1981; Blake et al., 1988), and the likelihood of suffering falls increases with ageing (Masud and Morris, 2001). For those living in nursing care facilities, the annual risk of falls increases to up to 70% (Cameron et al., 2010). Therefore, due to the severe impacts of some fragility fractures, fall prevention and hip protectors are key preventative measures. Physical therapy and exercise such as Tai Chi, and gait and strength training have been thoroughly investigated as methods to prevent falls in the elderly (Chang et al., 2004; Gillespie et al., 2012). These activities have been effective in reducing the fear of falling in older people (Zijlstra et al., 2007) and have shown a 35% reduction in the number of falls and fall-related injuries in adults over 65 years old (Robertson et al., 2002). In some cases, fall prevention requires home safety assessment and environmental modifications, which have proven to significantly reduce the number of falls in adults with fall history or severe visual impairment (Gillespie et al., 2012).

Since the majority of osteoporotic hip fractures occur due to a sideways fall with impact on the greater trochanter (Parkkari et al., 1999), a proposed preventative measure is to use a device to protect the hip. A hip protector is a plastic shell that fits around the hip and is generally fixed to specialised undergarments. They are designed to absorb the energy from a fall, decreasing the force on the trochanter and avoiding the fracture. Numerous trials have examined the effect of external hip protectors on the incidence of hip fractures, but findings have been conflicting. In a number of studies, hip protectors did significantly reduce the incidence of hip fractures (Lauritzen et al., 1993; Kannus et al., 2000; Chan et al., 2000), while in others it did not show statistical significance (Cameron et al., 2001; Schoor et al., 2003; Kiel et al., 2007). In addition to the inconsistency of the results, the main concerns with external hip protectors are discomfort and poor patient compliance (Zimmerman et al., 2010).

2.4 Femoral Augmentation

Femoral augmentation (also known as femoroplasty) is a procedure that may prevent osteoporotic hip fractures and involves the reinforcement of the proximal femur using injectable bone cement. The procedure consists of drilling a path into the proximal femur and then filling the drilled cavity and inner bone with bone cement. Initially the bone cement is in the form of a viscous dough, and a few minutes after being injected inside the bone it polymerises and solidifies. The solid bone cement should help restore the strength of the osteoporotic femur, improving its ability to withstand physiological loading conditions and low-impact falls. From a biomechanical perspective, properties such as fracture load, yield load and energy to fracture are expected to increase after the procedure. Moreover, given that it is a minimally invasive surgery, femoral augmentation should require low hospitalization costs and a short recovery time.

However, there are risks associated with this treatment that must be addressed before proceeding to in vivo application. First, if PMMA (polymethylmethacrylate) is used as the reinforcing agent, there is risk of thermal necrosis due to the exothermic reaction generated during the polymerisation stage. The maximum temperature reached in the process is directly related to the volume and distribution of bone cement. Thermal necrosis may occur in the tissues surrounding the PMMA if they are exposed to a temperature of 56°C for over 10 seconds (Pearce et al., 2005). Given the toxic nature of the monomer in PMMA there is also risk of infection and allergic reaction to the augmentation material. Additionally, injecting bone cement into the trabecular tissue might have an adverse effect on the blood supply of bone and adjacent soft tissues, as well as increasing the intraosseous pressure. Further, if bone cement leaks into the blood vessels, it can lead to fat embolisms (Geraci et al., 2013). Finally, patients with osteoporosis who have undergone femoral augmentation may develop a fracture as a result of the stiffness discontinuity between the augmented and the non-augmented regions of the femur. In this case, femoral augmentation might change the location of

the fracture or damage the areas near the bone cement but not avoid the fracture.

2.4.1 Augmentation Strategies

Most experimental studies of femoral augmentation have been performed in vitro using paired cadaveric femora. One of the femora is randomly chosen as the control and the contralateral as the specimen for augmentation. Mechanical tests are then performed under two main loading conditions: single-leg stance or lateral fall onto the greater trochanter, with the latter being most common. In this scenario, there is a significant variation amongst studies regarding the inclination to the horizontal plane and the load displacement rate. However, the factor dividing experiments into two main categories (first-generation and second-generation) is the injected volume of bone cement.

First-generation studies tend to inject large amounts of cement (30 to 50ml) into the bone, with the primary aim being to fill most of the proximal femur and stopping the injection if leakage occurs (Heini et al., 2004; Beckmann et al., 2007; van der Steenhoven et al., 2009; Sutter et al., 2010a). Most of these studies support the hypothesis that femoral augmentation strengthens the bone, although results depend to a large extent on the augmentation material. Using on average 36ml of PMMA, Heini et al. (2004) achieved an increase of 188% in the energy to failure of the augmented femur and of 82% in the fracture load. However, the significant improvement in biomechanical properties also involved a femoral surface temperature rise of 22.1°C.

In order to avoid the high temperatures reached in the curing process of PMMA, Beckmann et al. (2007) used Cortoss®, which is a composite-cement with a reduced exothermic curing process, to reinforce 9 pairs of osteoporotic femora. Results after injecting 40ml of the composite showed a lower surface temperature rise compared to augmentation with PMMA (temperature increase of approximately 11°C) and significant improvement in the femur mechanical properties (187% increase in the energy to fracture and 43% in the fracture load). Similar results were obtained by Sutter et al.

(2010a), who used 47ml of PMMA and achieved a gain of 154% in the energy to fracture and of 37% in the ultimate load. van der Steenhoven et al. (2009) also attempted to overcome PMMA high temperatures during polymerisation through the use of a silicone rubber that cures without exothermic heat (polydimethylsiloxane; PDMS) as the reinforcing agent. Using PDMS reduced the fracture displacement, but since it is not a stiff material the femur fracture load decreased after augmentation.

Second-generation experiments take into account cement placement and inject a reduced volume (8 to 15ml) of cement (Sutter et al., 2010b; Beckmann et al., 2011; Steenhoven et al., 2011; Fliri et al., 2013; Springorum et al., 2014; Basafa et al., 2015; Raas et al., 2016). The optimum cement distribution inside the bone and augmentation technique remain unclear, so studies continue to use a variety of approaches. The majority of authors agree that it is necessary to drill at least one channel into the bone to facilitate cement injection. However, Beckmann et al. (2011) found that drilling two paths into the proximal femur weakened too much the cortical bone and led to decreased bone strength after the augmentation procedure. Moreover, Steenhoven et al. (2011) studied the difference between creating the cavity in the femoral neck with a drill or with and inflatable balloon. The balloon technique required an additional 4ml of bone cement compared to the conventional drilling technique but there were no significant differences in the augmented femur biomechanical properties. Also, in order to have more control over the procedure, some studies use fluoroscopic guidance while injecting the cement (Sutter et al., 2010b; Steenhoven et al., 2011; Springorum et al., 2014) or a navigation system to drill the injection paths accurately (Basafa et al., 2015).

Regarding bone cement placement, Sutter et al. (2010b) injected 15ml of cement and studied the difference between cementing the femoral neck or the greater trochanter. Augmentation of the femoral neck achieved slightly better results, although no techniques substantially increased the ultimate load or the energy to fracture. A different approach is V-Shaped augmentation, which consists on reinforcing the femur through two channels parallel to the superior and inferior femoral neck. Fliri et al. (2013) used this augmentation

technique and replicated a lateral fall onto the greater trochanter. On average, 10.8ml of PMMA were injected into the femur, leading to an increase in energy absorption of 124% but no change in the fracture or yield load. In a more recent study, Raas et al. (2016) injected 13ml of bone cement in a V-shaped augmentation but tested the femora using single leg stance configuration. The outcome of the study showed that the resistance to fracture did not increase significantly. Beckmann et al. (2011) tested four different cementing techniques and concluded that the optimum approach was injecting 12ml of PMMA into a single centrodorsal drilled cavity in the femoral neck. This technique managed to increase the energy to fracture by 164% and the ultimate load by 35%. The same technique was applied by Springorum et al. (2014), who recorded a rise of energy to failure by 117% and fracture load by 33% using 8-15ml of cement. In a recent in vitro study, Stroncek et al. (2019) investigated the injection of a resorbable triphasic calcium sulphate/calcium phosphate material (AGN1) into the proximal femur. This material is designed to be resorbed and replaced by new bone and its exothermic reaction does not exceed 35°C. After injecting 19ml of AGN1 from the greater trochanter to the femoral neck and replicating a lateral fall onto the greater trochanter, the ultimate load of the studied femora increased on average by 20.5%. Work to failure also increased significantly but stiffness did not change. However, since this material would be resorbed by the bone and disappear over time, its applicability to prevent osteoporotic fractures in highly osteoporotic bones is questionable.

Besides experimental testing, computational work has also been applied in this field to plan and analyse the effect of the femoral augmentation procedure. Basafa and Armand (2013, 2014) used Finite Element Analysis (FEA) to optimise the PMMA volume and distribution in 8 pairs of osteoporotic femora prior to the experiment. Numerically, using on average 13.4ml of bone cement, an increase of 100% in the femur yield load could be achieved. The cement distribution primarily depended on the material properties of each bone, but in most femora the injection pattern was directed from the supero-anterior aspect of the neck to the posterior zone of the greater trochanter. In order to perform their experiments, this optimal distribution was converted into a feasible injection

pattern (Basafa et al., 2015). Using 9.5ml of bone cement, the fracture load increased by 30% and the energy to failure by 124%. Using a similar strategy, Farvardin et al. (2019) conducted a computational study highlighting the importance of preoperative planning in femoral augmentation. Three generalized augmentation strategies were studied and compared against a customised pattern based on matching spheroids to the optimal distribution (Basafa and Armand, 2014). Using 9.2ml of bone cement, the customised pattern resulted in a 79.6% yield load increase and 199% yield energy increase while the generalized strategies reached a maximum of 32.7% and 139.9% yield load and yield energy increase respectively. Based on the principles of bone remodelling, Varga et al. (2017) designed an augmentation strategy that would protect the femur against a lateral fall with approximately 12ml of bone cement. Nonlinear FE simulations were used to evaluate the mechanical properties, and augmentation resulted in a 64% increase in the yield force. Using FEA, Ramos-Infante and Pérez (2019) compared augmentations with low viscosity and high viscosity bone cement. In their study, the elastic modulus of each augmented element increased by a percentage, dependent on the element volume, bone cement viscosity and minimum density associated with the femoral area where the element is located (Ramos-Infante et al., 2018). This improvement factor was determined to be approximately 37% for high viscosity bone cement and 224% for low viscosity bone cement. Therefore, their results suggest that when using lower amounts of bone cement (3ml), low viscosity bone cement led to a greater improvement in fracture load (29% increase) than high viscosity (10% increase).

2.4.2 Augmentation Materials

Given the risks associated with femoral augmentation, a crucial aspect to consider is the augmentation material. The desirable properties of bone cement for femoral augmentation comprise ease of preparation and handling, suitable working and setting time, and adequate viscosity. Another necessary characteristic is radiopacity, to allow cement visibility in X-rays. Additionally, in order to avoid thermal necrosis and other

potential side effects, the material should present a low curing temperature after injection and not be toxic. After the curing process, the bone cement should have mechanical properties that are adequate for withstanding the loads acting on a femur during normal activities and low-impact falls. Ideally, bone cement should be osteoinductive (promote bone formation) and osteoconductive (promote bone apposition along its surface). It is also essential that it is biocompatible and non-resorbable. The main types of injectable bone cements are Acrylic Bone Cements (ABCs), Calcium Phosphate Cements (CPCs), Glass Polyalkenoate Cements (GPCs) and Composite materials.

- **Acrylic Bone Cements (ABCs)**

Acrylic bone cements are composed of polymethyl methacrylate (PMMA) and methyl methacrylate (MMA). In the compound, an activator-initiator and radiopaque agents are also present. The mixing of the polymer powder with the liquid monomer forms a highly viscous material that can be easily injected into bone cavities (Vazquez et al., 1998). PMMA-based acrylic bone cement is a self-curing material that polymerises and solidifies rapidly at room or body temperatures.

Despite a large number of PMMA bone cement brands being commercially available, their compositions only vary slightly and have essentially remained unaltered over the past 50 years. This is due to the good performance of PMMA in terms of biomechanical strength, stiffness and ease of handling, the familiarity for orthopaedic surgeons and the fact that it is a cost-effective solution (Lieberman et al., 2005). This type of bone cement presents in vitro compressive strengths between 70 and 100MPa (Heini and Berlemann, 2001). Given the characteristics of this material, it is expected that most femoral augmentation experiments use commercial PMMA cement as the reinforcing agent (Heini et al., 2004; Sutter et al., 2010a,b; Beckmann et al., 2011; Fliri et al., 2013; Springorum et al., 2014; Basafa et al., 2015; Raas et al., 2016). However, although the use of PMMA bone cements is widespread, they present several disadvantages.

Depending on the amount of PMMA and the cement composition, the polymerisation temperature can be higher than 65°C and cause thermal necrosis in the surrounding tissues. Another concern is the monomer toxicity: MMA is not biocompatible and can cause chemical necrosis in the surrounding tissues if polymerisation is incomplete (Feith, 1975; Albrektsson and Linder, 1984; Lu et al., 2002). Additionally, over exposure to its fumes during mixing and injection may cause asthmatic reactions and/or lachrymation. Also, PMMA bone cement is not osteoinductive or osteoconductive and does not remodel. There is no chemical bonding between PMMA based cements and bone tissue; loads are transmitted by contact and mechanical interlocking (Kinzl et al., 2012). Thus, the fact that PMMA shrinks (from 2% to 6% in volume) due to polymerisation (Muller et al., 2002) contributes to the development of gaps between the two materials and residual stresses in the trabecular bone.

- **Calcium Phosphate Cements (CPCs)**

Calcium Phosphate Cements (CPCs) are produced by a chemical reaction between a solid and a liquid phase which, when mixed, form a paste that progressively sets and hardens into a solid mass (Zhang et al., 2014). The solid phase comprises one or several calcium phosphate (CaP) compounds and the liquid phase is water or an aqueous solution. The CPC reaction can generate two possible final products: brushite or apatite (such as hydroxyapatite or calcium-deficient hydroxyapatite) (Bohner, 2007). In general, apatite cements have higher strengths than brushite cements. Unlike PMMA based cements, calcium phosphate cements are osteoconductive and progressively remodel with time (Frankenburg et al., 1998; Larsson and Bauer, 2002). CPCs harden at body temperature and do not produce a highly exothermic reaction, which increases the possibility of incorporating drugs or biological molecules in the cement (Ginebra et al., 2006, 2012; Verron et al., 2012). Additionally, CPCs do not shrink during the hardening process, avoiding the generation of residual stresses in the trabecular tissue.

The handling characteristics of calcium phosphate cements also differ from those of

PMMA. In general, CPCs need to be modified to reduce their setting time and improve their cohesion and injectability (Bohner et al., 2006). CPCs with long setting times or weak cohesion are not adequate for bone augmentation and can cause a number of medical issues (Ueyama et al., 2001). Therefore, the composition and preparation of CPCs are often altered in order to improve these properties but not compromise others such as strength or fracture toughness. Further disadvantages of this type of cement are their high cost and poor mechanical properties, with compressive strengths ranging from 0.34 to 80MPa depending on the powder composition (He et al., 2015). Additionally, CPCs present brittle behaviour and low fracture toughness (Morgan et al., 1997; Harmata et al., 2015) which makes them unsuitable for usage in load-bearing applications. In addition, they can be resorbed and substituted by new bone, with a resorption rate depending on their composition and microstructure.

- **Glass polyalkenoate cements (GPCs)**

Glass polyalkenoate cements (GPCs) are materials formed by the reaction of an acid degradable alumino–silicate glass with an aqueous solution of polyalkenoic acid. As bone cements, they have the advantages of setting without a significant heat generation, adhering to the bone and presenting high compressive strengths of up to 200MPa (Higgs et al., 2001; Boyd et al., 2008a). Due to these reasons, they have been used in dental applications but the presence of aluminium (Al) in all commercial formulations has restricted their use in orthopaedics (the release of the Al3+ ion causes defective bone mineralization and is involved in the development of degenerative brain diseases (Polizzi et al., 2002)).

Aluminium-free GPCs have been developed for consideration in skeletal applications (Darling and Hill, 1994; Wren et al., 2008), based on calcium-zinc-silicate or calcium-strontium-zinc-silicate glasses. Zinc has the ability to increase bone mass (Ovesen et al., 2001) and is antibacterial (Boyd et al., 2006), but zinc-based GPCs present either setting times that are too short or a considerable drop in strength

(Clarkin et al., 2009). Recently, Magnesium has been included in Al-free GPCs in order to improve their handling characteristics without deteriorating their strength (Khader et al., 2018). However, Al-free GPCs for orthopaedic applications are still not widely commercially available.

- **Composite Materials**

Composite materials like Cortoss® (Orthovita, Malvern, USA) are currently being studied as alternatives to PMMA bone cements. Cortoss® is a glass-ceramic reinforced polymer composite designed to mimic cortical bone. It is supplemented with different materials to stimulate bone apposition along its surface, obtain a suitable viscosity and increase radiopacity and strength (Erbe et al., 2001). In vitro tests have shown a compressive strength between 91 and 179MPa (Boyd et al., 2008b) and a lower curing temperature than that of conventional PMMA. This material has proven to be bioactive and biocompatible. It also benefits from a higher degree of monomer conversion compared to PMMA bone cements (Pomrink et al., 2003), decreasing the possibility of toxic MMA leakage.

Femoral augmentation may be considered in the future as treatment option for the prevention of osteoporotic hip fractures. However, due the serious risks involved in the treatment, further research must be carried to evaluate its safety before applying it in vivo. Additionally, femoral strength improvement following augmentation is highly dependent on bone cement location and volume, original bone material properties, augmentation material and type of fall. Given all the sources of variability involved in femoral augmentation, the use of computational models to study the procedure seems more efficient than carrying experimental work. Therefore, it could be beneficial to use such models to plan the femoral augmentation procedure, study its biomechanical effects and evaluate its risks. Through the use of numerical simulations. the following chapters explore the requirements of femoral augmentation, its side effects and its limitations.

Chapter 3

Heuristic Optimisation of Bone Cement Volume and Placement in Femoral Augmentation

3.1 Introduction

Femoral augmentation involves the mechanical reinforcement of osteoporotic femora using an injectable bone cement, commonly PMMA. The biomechanical effect of this treatment is patient-specific and related to the augmentation material, its volume and distribution inside the femur. Additionally, side effects such as bone thermal necrosis and embolism (Jefferiss et al., 1975; Belkoff et al., 2001; Geraci et al., 2013) are risks involved in the procedure and are related to the injection of large volumes of bone cement. Therefore, it is of importance to achieve the best possible compromise between maximising the strength enhancement of the osteoporotic femur, through the injection of bone cement, and minimising the side effects of the procedure. Finding the optimum bone cement distribution through experiments would require a very large sample size, and it would

not be possible to compare how different augmentation strategies affect the same femur. Applying numerical optimisation techniques to computational models of the femur is a more efficient approach that could provide valuable information.

The first objective in this chapter was to develop seven computational models of the same femur with different osteoporotic levels. Numerically imposing several degrees of osteoporosis to the model allows for direct comparison in results with respect to the same bone morphology. The second objective was to calculate the yield load of the femur models and compare them with existing experimental and computational data to evaluate the model's response. The third objective was to identify the optimum bone cement volume and distribution required in those osteoporotic femora to achieve certain level of reinforcement. Therefore, bone augmentation was stated as a topology optimisation problem given a specific set of loads, boundary conditions and constraints related to the mechanical strength of the augmented bone. The fourth objective was to identify the correlation between level of osteoporosis and optimum volume of bone cement, as the latter is proven to be an important factor both for the biomechanical properties of bone after an augmentation procedure (Chevalier et al., 2008; Varga et al., 2017) and the long-term behaviour of bone after augmentation (Badilatti et al., 2017).

3.2 Methods

3.2.1 Model Development

One inherent element to bone augmentation research is the fact that cadaveric osteoporotic femora, based on which researchers develop their computational models, are of varied morphology. Consequently, the respective conclusions are not always directly comparable. For this reason, in experimental studies of femoral augmentation the control group comprises of the non-augmented native contralateral femora (Heini

et al., 2004; Beckmann et al., 2007; Sutter et al., 2010a,b; Beckmann et al., 2011; Fliri et al., 2013). In this scenario, the ideal case would involve having a set of different bones and, for each bone, its material properties for different T-Score levels (ranging from a healthy condition to severe osteoporosis). As an attempt to mimic this ideal case and for the needs of the present study, a healthy femur was used as a reference model and different degrees of osteoporosis were virtually introduced by appropriately changing the modulus of elasticity of the bone tissue. The advantage of this approach is that all numerical results, related to a specific degree of osteoporosis, refer to the same bone and allow direct comparison.

One femoral CT dataset was obtained from the OsiriX open access repository (available at www.osirixviewer.com) and segmented using InVesalius 3.1 (CTI, Sao Paulo, Brazil). The model was then imported to SolidWorks 2017 in order to obtain a 3D solid bone model. This model was imported into ANSYS Mechanical APDL v.17.0 (Ansys Inc, Pennsylvania, USA), where an unstructured mesh was generated using 4-node tetrahedral elements. Inhomogeneous isotropic bone properties were mapped from the CT images to the mesh using BoneMat v.3.1 software (available at http://www.bonemat.org/). Typically, radiological density (ρ_{QCT}) is obtained from the CT calibration phantom. However, as no scanner calibration was available for the files used in the present study, each Hounsfield Unit (HU) was converted into radiological density (ρ_{QCT}) using information from the images and the literature. In greater detail, Equation 3.1 was used to convert HU into radiological density for the healthy tissue:

$$\rho_{QCT(H)} = 0.109 + 0.001086 \cdot HU \tag{3.1}$$

This equation was derived by taking into account the range of the HU, as given by the software InVesalius during the development of the model and supported by literature data on material properties of typical healthy bone tissue. For the latter, a Young's modulus of 17GPa and 2.5GPa was considered for the cortical and trabecular tissue, respectively (Falcinelli et al., 2014; Chen et al., 2015).

In order to develop several osteoporotic femur models, the following relationship between T-Score and BMD was defined according to the World Health Organization definition of osteoporosis:

$$T - Score = \frac{BMD_{osteo} - 1.02}{0.144} \tag{3.2}$$

Where BMD_{osteo} stands for the Bone Mineral Density of an osteoporotic femur and the normalisation has taken place with respect to a young, normal adult population (Bone Mineral Density (BMD) of the femoral neck: 1.02g/cm^2; Standard Deviation: 0.144g/cm^2 (Looker et al., 2012)).

The values for BMD_{osteo} were calculated by rearranging Equation 3.2 and selecting discrete values for the T-Score. These values were then compared to the reference BMD (i.e. 1.02g/cm^2), yielding the reduction of the reference BMD. This percentage (referred in this study as reduction factor δ) was used to virtually introduce osteoporosis in the models. The elastic modulus of both the cortical and trabecular tissue were reduced by the same percentage, which is representative of senile (Type 2) osteoporosis, especially for men (Riggs et al., 1982; Khosla and Riggs, 2005). Table 3.1 summarizes, for a predefined set of T-Scores, the respective values for BMD_{osteo} and the reduction factor δ.

Table 3.1: T-Score, BMD and BMD reduction applied to each femur

	Osteopenia			**Osteoporosis**		
T-Score	-1.0	-1.5	-2.0	-2.5	-3.0	-3.5
$\boldsymbol{BMD_{osteo}}$ **(g/cm^2)**	0.876	0.804	0.732	0.660	0.588	0.516
Reduction Factor $\boldsymbol{\delta}$	14%	21%	28%	35%	42%	49%

Therefore, for the six osteoporotic femur models (which cover the range from mild osteopenia to severe osteoporosis), the radiological density $\rho_{QCT(O)}$ was derived applying a uniform reduction factor δ to $\rho_{QCT(H)}$:

$$\rho_{QCT(O)} = 0.109\delta + 0.001086\delta HU \tag{3.3}$$

After this, the radiological density ($\rho_{QCT(O)}$) was converted to ash density (ρ_{ash}) according to Schileo et al. (2008a):

$$\rho_{ash} = 0.079 + 0.88 \cdot \rho_{QCT(O)} \tag{3.4}$$

Finally, the ash density (ρ_{ash}) was converted into the modulus of elasticity using Equation 3.5 (Keller, 1994):

$$E = 10500 \cdot \rho_{ash}^{2.29} \tag{3.5}$$

For all elements, a Poisson's ratio of 0.3 (Zhang et al., 2013) was assumed. Also, all moduli of elasticity calculated using Equation 3.5 were grouped into intervals of width 100MPa. In this way, a controlled number of material properties groups were created (Figure 3.1).

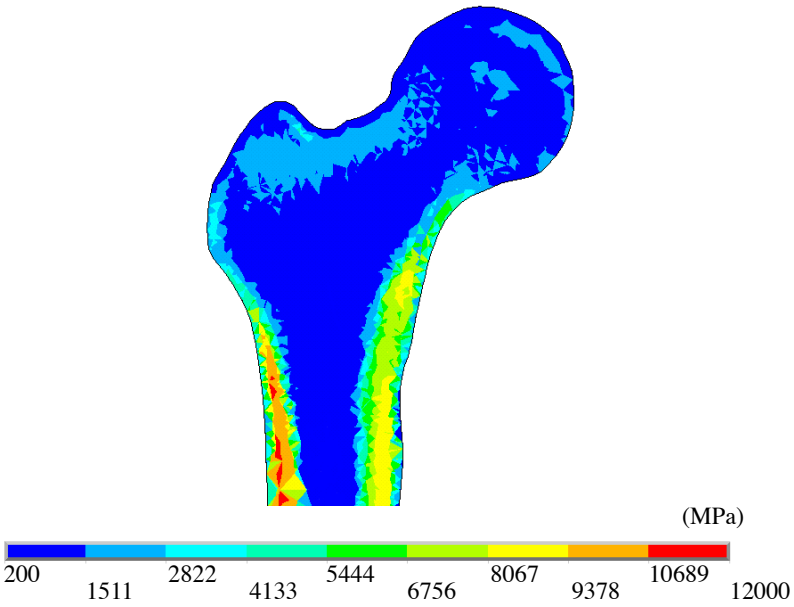

Figure 3.1: Distribution of elastic modulus in a sagittal cross-section of a femur with T-Score -2.5

3.2.2 Load Case

Given that most osteoporotic hip fractures occur as the result of a lateral fall, boundary conditions replicating a lateral fall onto the greater trochanter were applied to the femur models. To this end, the femur was distally fully constrained, while the lateral side of the greater trochanter was restricted to move only in one plane (Schileo et al., 2014). The applied force was tilted by 10° in the transverse plane and 15° in the frontal plane and was uniformly distributed over the medial nodes of the femoral head (Figure 3.2). Similar sets of boundary conditions are commonly used in mechanical tests to replicate lateral falls on the greater trochanter (Beckmann et al., 2007; Sutter et al., 2010a,b; Beckmann et al., 2011; Fliri et al., 2013).

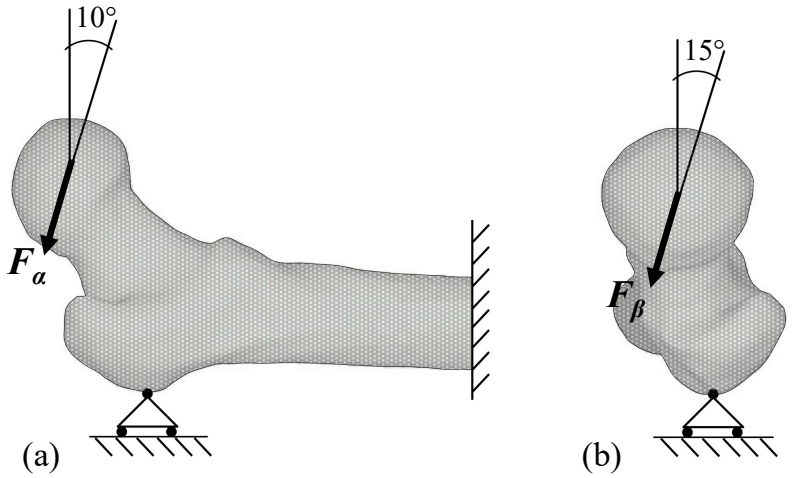

Figure 3.2: Lateral fall boundary conditions

3.2.3 Topology Optimisation

A unidirectional evolutionary scheme was developed to optimise the bone cement volume and placement in the osteoporotic femur. This iterative algorithm concerns a two-level nested conditional loop, where the outer loop controls the magnitude of the externally applied load and the inner loop controls the number of failed elements.

Initially, a small external load is applied and a linear Finite Element (FE) simulation of a lateral fall on the greater trochanter is conducted (applying the boundary conditions detailed in Section 3.2.2). Then, the maximum (ε_{max}) and minimum (ε_{min}) principal strains of each element are computed. If these values are within the range of acceptable strain values (less than 0.73% in tension and 1.04% in compression (Bayraktar et al., 2004)), a new iteration of the outer loop begins with an increased external load (in steps of 52.5N). Otherwise, the inner loop is activated, which calculates the percentage of failed elements in the proximal femur. An element is considered failed if the aforementioned strain constraint is violated. If the percentage of failed elements is equal or higher than 1 (Basafa and Armand, 2014), the yield load of the bone has been reached. The yield load was calculated for the healthy femur and the six osteoporotic and osteopenic models.

When the yield load of the femur is reached, the material properties of the failed elements are changed to the ones of PMMA bone cement (Young's modulus: 2300MPa; Poisson's ratio: 0.3 (Kinzl et al., 2012; Lu et al., 2014)) and the total accumulated volume of bone cement is updated. It is worth noting that in a femoral augmentation procedure, cement is only injected in the trabecular bone, so elements that belong to the cortical will not be replaced by bone cement and will remain intact. Besides, bone cement elements can also fail if their maximum/minimum principal strains are above 0.2% both in tension and compression. This nested loop is repeated until the target value for the external load is reached. In this study, the target load was set to be 15% larger than the load capacity of the reference healthy femur. The obtained accumulated volume of bone cement represents the optimum volume of bone cement.

The algorithm was developed in ANSYS Parametric Design Language (APDL) and applied to the six osteoporotic and osteopenic femur models. The pseudocode is presented below:

Model Setup: Setup the model of the examined osteoporotic bone for a linear static analysis and count the total number of elements ($\text{NEL}_{\text{total}}$) of the proximal femur.

Define the following parameters: Initial Load, Target Load, Load Step, Threshold

Define Region of Interest (ROI): All elements used for the discretisation of the trabecular tissue

Apply Initial Load: Applied Load = Initial Load

While (Applied Load < Target Load) **Do**

FE Linear Static Analysis

Count elements violating the strain constraints (NEL_{fail})

Define: $PERC_{fail} = NEL_{fail} / NEL_{total}$

While $PERC_{fail}$ > Threshold **Do**

Assign bone cement to NEL_{fail} elements in the ROI

Bone Cement Volume (BCV) = BCV + NEL_{fail} elements volume

End ($PERC_{fail}$)

Applied Load = Applied Load + Load Step

End (Applied Load)

A mesh convergence analysis was performed to ensure reliability of obtained results. To this end and for each one of the developed models, six meshes with different element density (from approximately 38,500 to 432,000 DOFs) were studied under the same loading conditions representing a lateral fall on the greater trochanter. The stiffness, strain energy and optimum bone cement volume required to reach a predefined target load were monitored.

3.3 Results

Results of the mesh convergence analysis for the osteoporotic femur with T-Score equal to -2.5 is shown in Figure 3.3. The percentage difference between the results obtained

with the reference mesh (finest mesh) and each one of the other meshes was plotted against the Degrees of Freedom (DOF) of each mesh. Mesh convergence was achieved for a discretisation using 501,1399 4-node tetrahedral elements (i.e. 270,792 DOF). It should be noted that in all examined cases, the metrics for orthogonal quality and aspect ratio were monitored and found to be similar and within an acceptable range across all used meshes.

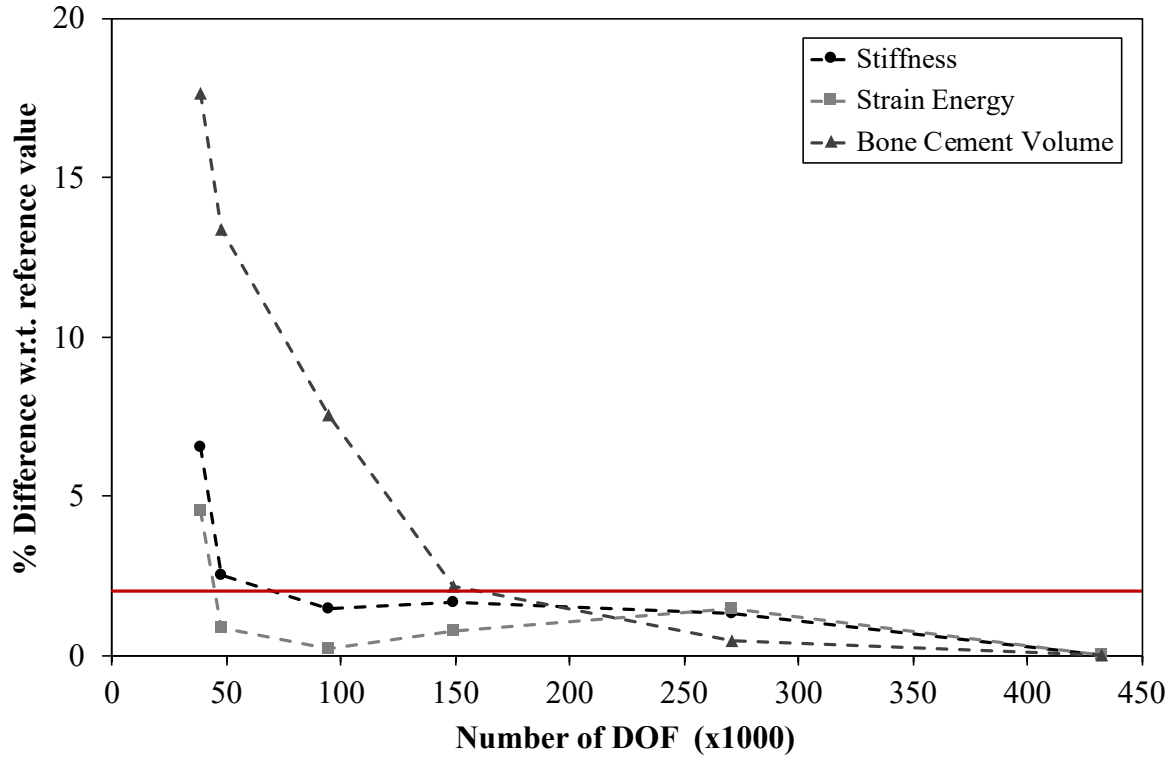

Figure 3.3: Mesh convergence for a T-Score -2.5 femur

The yield load of the healthy femur was calculated as the necessary force to load 1% of the tissue above the principal strain limits and was found to be 5513N. This was also calculated for the rest of models and is plotted in Figure 3.4 according to their T-Score. Results from previous computational (C) or experimental (E) studies that also calculated the femur yield load (YL) or ultimate load (UL) under lateral fall conditions are included in the chart for comparison purposes (corridors based on mean value and Standard Deviation).

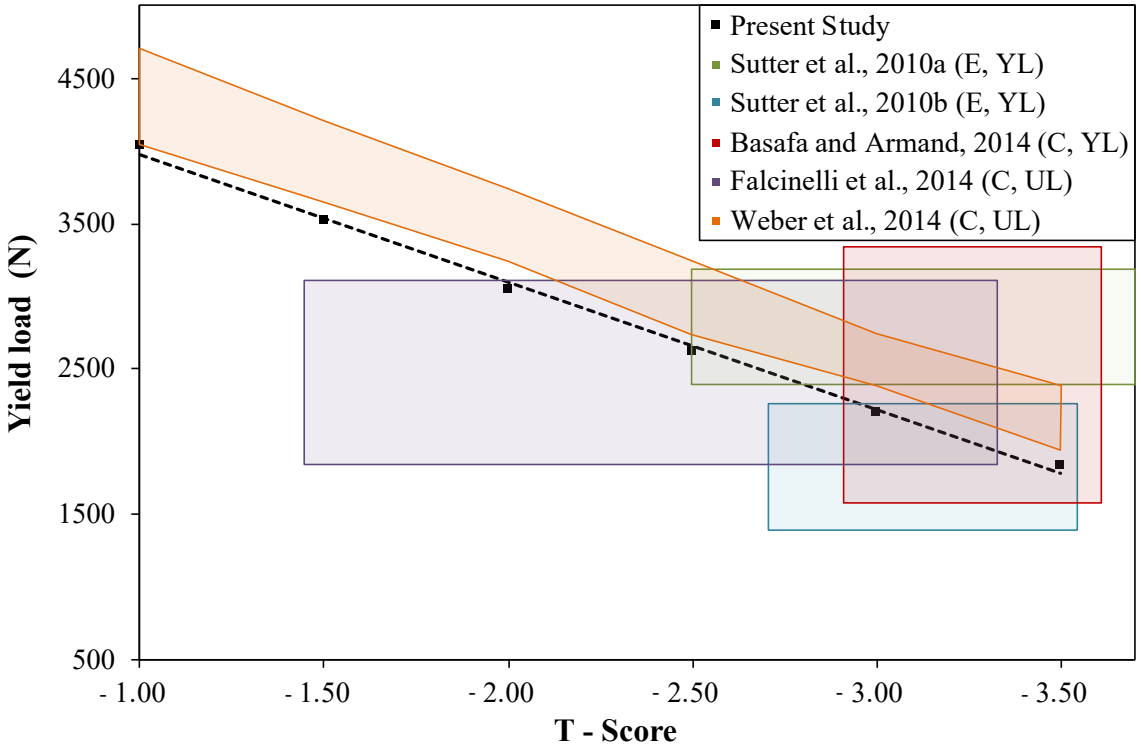

Figure 3.4: Yield load comparison between the present study and previously published studies

The healthy bone yield load value increased by 15% was subsequently used as the target load for the optimisation algorithm. Table 3.2 shows the bone cement volume needed to restore the femur yield load for different levels of osteopenia and osteoporosis. The average optimum bone cement volume was 5.24ml for osteopenic and 14.39ml for osteoporotic femora. As expected, the required bone cement volume was larger in models with high degree of osteoporosis.

Table 3.2: Evolutionary Structural Optimisation results

	Osteopenia			**Osteoporosis**		
T-Score	**-1.0**	**-1.5**	**-2.0**	**-2.5**	**-3.0**	**-3.5**
Original Yield Load (N)	4043	3518	3045	2625	2205	1805
Bone Cement Volume (ml)	2.98	4.75	7.99	10.84	14.24	18.09

The final bone cement distribution for the three osteoporotic models is qualitatively similar (Figure 3.5), requiring bone cement in the greater trochanter, superior area of the femoral neck and ring around the femoral neck. Femur models with low degree of osteoporosis required the largest amount of bone cement in the greater trochanter region.

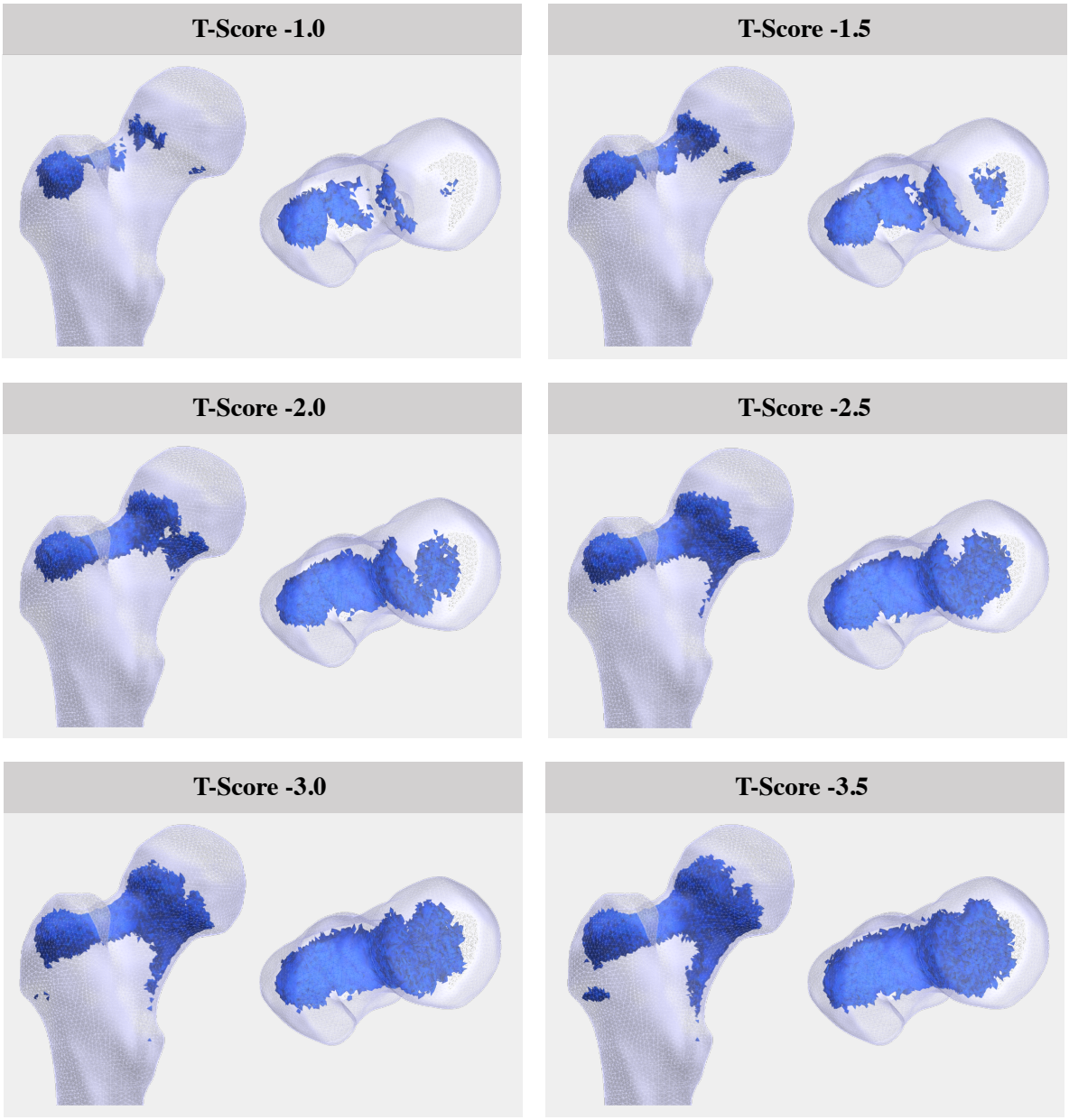

Figure 3.5: Final bone cement distribution for the six developed models

Figure 3.6 illustrates the evolution of failed elements and bone cement volume for the model with T-Score -2.5. During the 88 iterations, the percentage of elements violating the strain constraints exceeds 1% several times (Figure 3.6a). At this point, additional bone cement is introduced in the proximal femur (Figure 3.6b) and the percentage of failed elements is recomputed. Since the elements of the cortical tissue cannot be replaced with bone cement, a small percentage of elements remain failed throughout each cycle despite the continued augmentation.

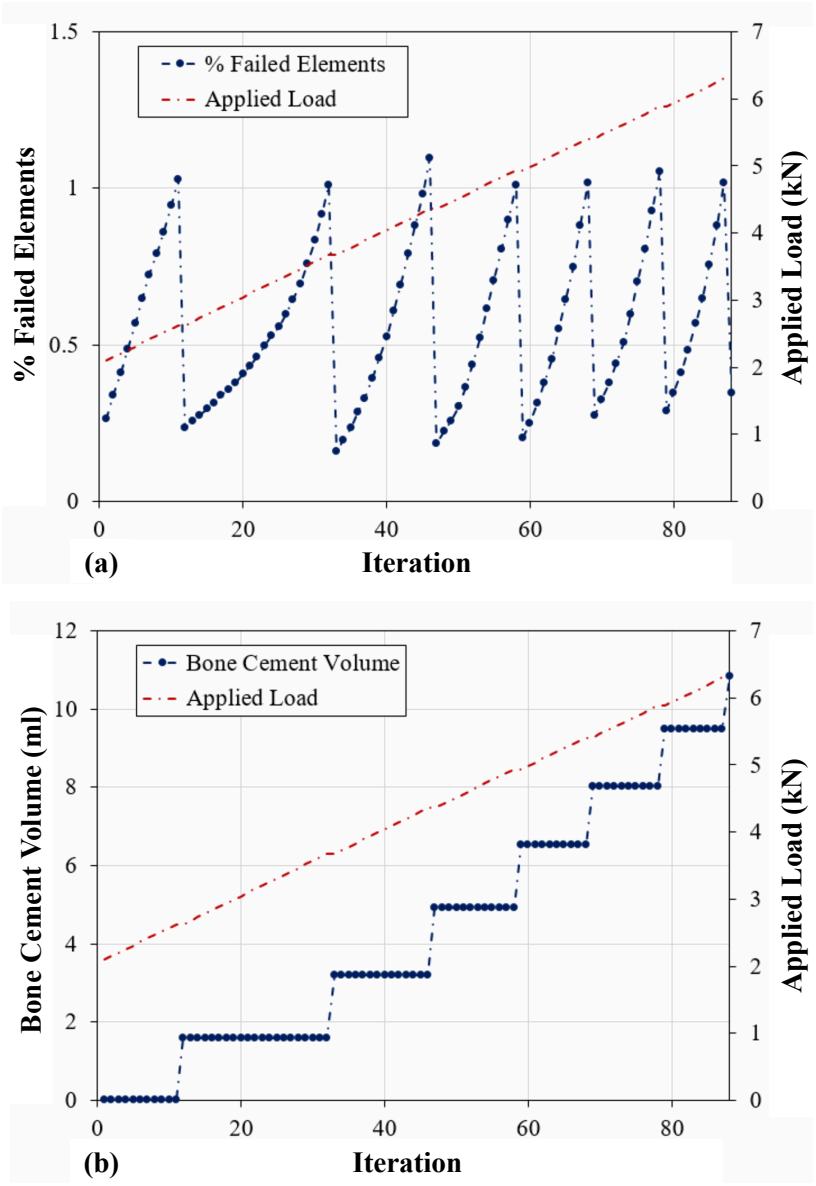

Figure 3.6: Iteration history of (a) % failed elements and (b) bone cement volume for the femur with T-Score -2.5

The progression of bone cement distribution through the evolutionary optimisation of a reference model (T-Score -2.5) is illustrated in Figure 3.7. The algorithm initially reinforced the greater trochanter, where the largest principal strains are located. Then, the superior and inferior part of the femoral neck are augmented independently until they merge forming an incomplete ring around the femoral neck.

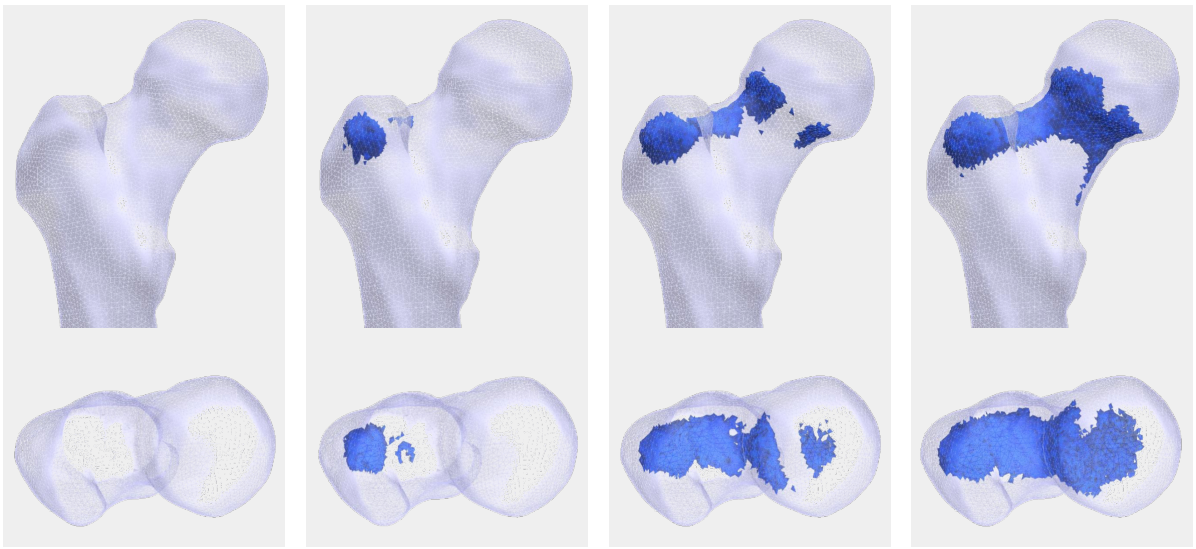

Figure 3.7: Evolution of the bone cement placement for the femur with T-Score -2.5

3.4 Discussion

The yield load of the developed femur models was calculated in this study as part of the topology optimisation algorithm and to achieve this, it was necessary to adopt a yield criterion. Some studies use stress-based yield criterion like von Mises (Keyak et al., 2001; Keyak and Falkinstein, 2003), while others agree that the Drucker-Prager criterion is more suitable in FE models that simulate brittle materials like bone (Bessho et al., 2007). Finally, some others propose that bone fracture is a strain-controlled mechanism (Nalla et al., 2005; Väänänen et al., 2013). In order to prove this, Schileo et al. (2008b) performed a numerical-experimental study comparing a strain criterion with two different stress criteria to determine the femur failure and yield load. Their results, in agreement

with Yosibash et al. (2010) suggest that the failure load would be underestimated when using von Mises or principal stress criteria. Therefore, the criteria adopted in this study to predict the failure of the elements were principal strains, considering that bone reaches its yield point at lower strains in tension than in compression (Bayraktar et al., 2004). The predicted yield loads in this study due to a lateral fall on the greater trochanter ranged from 1805N to 4042.5N (mean 2873N) depending on the femur T-Score.

For the development of the femur 3D models, a power law was used to relate elastic modulus and ash density (Keller, 1994). This relationship was developed based on uniaxial compression tests of human vertebral and femoral bones. Other relationships have been proposed in the past (Carte and Hayes, 1977; Morgan et al., 2003), which could affect the final elastic modulus distribution in the femur. Additionally, osteoporosis was artificially introduced in these models in a homogeneous way. This is representative of senile osteoporosis, where the bone mass loss of cortical and trabecular tissue deteriorate at a similar rate (Riggs et al., 1982; Khosla and Riggs, 2005) but not of postmenopausal osteoporosis, where the rate of loss of cortical bone mass is lower than the rate of loss of trabecular bone mass (O'Flaherty, 2000). Because of the aforementioned reasons, it was necessary to validate our yield load predictions with results from the literature (Figure 3.4). Yield or fracture load predictions in previously published studies are varied, as they depend on several factors such as the applied boundary conditions, bone size and shape and material properties. Despite this, the predicted yield loads for osteoporotic T-Scores (-2.5 to -3.5) in this study were in a reasonable range and corresponded well with fracture load values obtained in studies replicating a lateral fall by Sutter et al. (2010a,b); Falcinelli et al. (2014); Basafa and Armand (2014). Since most studies are performed in osteoporotic models, the yield load of osteopenic models (T-Score -1 to -2.5) was only compared against Weber et al. (2014), limiting its validity. A good correlation was found between the two studies, showing a similar load vs T-Score trend. The healthy femur yield load prediction (5500N) was also similar to the healthy bone yield load found by Verhulp et al. (2008) (5450N) using micro-FE meshes. Comparisons were performed against these studies

because they replicate a fall onto the greater trochanter, with boundary conditions or experimental settings that are similar to the ones applied in the present chapter.

Linear static analyses were conducted to find the femur yield load in order to avoid the complexities related to the simulation of a dynamic event (such as modelling the material properties of bone at high strain rates). A large number of experimental studies of femoral augmentation have been performed using quasi-static tests (load applied at 2mm/s) to determine the augmented and non-augmented femur fracture load (Heini et al., 2004; Beckmann et al., 2007, 2011; van der Steenhoven et al., 2009; Steenhoven et al., 2011; Springorum et al., 2014; Raas et al., 2016). Hence, despite they do not represent accurately the behaviour of bone during an impact, static simulations were considered acceptable to determine augmented and non-augmented yield load and compare with the aforementioned quasi-static tests.

Finding the yield load of the developed models was only part of the optimisation procedure presented in this chapter, that was developed based on the idea of the ESO method presented by Xie and Steven (1996). With the algorithm, the optimum bone cement volume and placement was computed for femora with different levels of osteoporosis and osteopenia. Results suggest that on average, 5.24ml of PMMA for osteopenic and 14.39ml for osteoporotic femora can restore the yield load of the femur models. For the osteoporotic femora, the bone cement pattern generated inside the bone by the optimiser involved augmenting the greater trochanter and creating an incomplete ring of cement around the femoral neck. This PMMA distribution is similar to the one obtained by Basafa and Armand (2013, 2014) when applying their BESO strategy. In their investigation, values ranging from 5.6ml to 26.2ml of PMMA were necessary to obtain an increase of 100% in the femur yield load depending on the size, shape and material properties of each osteoporotic femur. The average T-Score of the osteoporotic femora studied in their research was -3.53 and their pre-augmentation yield load ranged from 1485N to 3905N. The femora with similar yield load to that of the present research (T-Score -3.5, 1805$\pm$500N) were selected for comparison, and required on average 9.36ml of bone cement

to double their yield load. In this current study, 6.21ml of bone cement were necessary to increase the yield load of the T-Score -3.5 femur by 100%. This value can be extrapolated from the iteration history of the optimisation method. Comparing the method presented in the aforementioned research with the one of this study, some significant differences arise. Firstly, the method presented in this chapter is a unidirectional ESO that uses principal strain values as the optimisation criterion, while Basafa and Armand (2013, 2014) applied a Bidirectional ESO and considered strain energy density. Moreover, in the proposed algorithm the applied load increases by a constant value (52.5N) at each iteration, while Basafa and Armand (2013, 2014) applied a constant load and scaled the strains assuming linearity.

Other computational studies have been developed recently, focusing on bone cement distributions that, as opposed to the ones presented in this chapter, are easy to inject in practice. Varga et al. (2017) studied five different augmentation strategies and attempted to find the most advantageous one through numerical simulations. They concluded that approximately 12ml of PMMA can result in an average increase of 64% in the femur yield load when augmenting with a cylinder from the greater trochanter to the end of the femoral head. In contrast to this generalised approach to femoral augmentation, Farvardin et al. (2019) reported that subject-specific planning of femoroplasty can result in a 79.6% yield load increase using 9.2ml of bone cement. In a more recent study, Ramos-Infante and Pérez (2019) reduced bone cement injection to only 3ml in the weakest locations of the femur, leading to a 29% increase in the yield load. Interpolating our results to obtain the yield load increase reported by the aforementioned studies shows that 5ml of bone cement would be required to obtain a 64% increase in the yield load, 6ml to obtain a 79.6% increase and 2ml to obtain a 29% increase. This shows that the ideal bone cement distribution presented in this chapter is more effective at improving the bone strength, although this is expected due to the use of realistic bone cement geometries in their studies. Therefore, it is still unclear if adapting the ideal bone cement distributions presented in this chapter to become feasible augmentation strategies will lead to better results than the ones of the

previously mentioned studies or not.

Several parameters in the applied optimisation method could be changed in order to adapt it to different needs. One of these parameters is the target load, which in the present work was set to be 15% larger than the yield load of the healthy femur. However, the optimiser provides sufficient versatility to allow a target load of any desired value and finding the optimum cement volume and distribution for partial restoration of bone properties could also be an application of this algorithm. Furthermore, the reported predictions were made considering that the femur yield load was achieved if 1% of the elements of the proximal femur were above the strain limit values. This value was also adopted by Pistoia et al. (2002); Basafa and Armand (2014). However, different approaches have been presented in the literature as in the case of Falcinelli et al. (2014) who averaged the principal strains on a circle of 3mm radius and Yosibash et al. (2010), who focused their analysis on the 10 elements most susceptible to failure. Results of both yield load and optimum bone cement volume are susceptible to change if different criteria are adopted. However, since the values chosen in this chapter have been used in the past in experimentally validated studies, they were considered appropriate for the simulations.

In this chapter, six osteoporotic and one healthy model were developed. Their yield load under lateral fall conditions were calculated and compared against existing experimental and computational data, showing a good agreement. After this, a topology optimisation algorithm was applied to each model in order to find the ideal distribution of bone cement in the femur that would protect them against a lateral fall. To achieve this, specific simplifications were applied. The time-dependent bone cement injection process was not simulated, nor was the solidification of the injected bone cement. Consequently, the influence of the gravitational field on the liquid state of the bone cement as well as partial filling of voids and shrinkage of the bone cement after solidification were not considered. Additionally, given that bone cement is embedded in trabecular tissue, assuming that bone tissue can be directly replaced by bone cement is not physiologically realistic. The distribution of elastic modulus in the osteoporotic models should affect the behaviour

of the augmentation material, which is a limitation addressed in Chapter 4. Another simplification of this study concerns the assumption that bone cement may be injected independently and separately into any location. In theory, that might be achieved through minimally invasive surgical techniques and miniaturization (Bergeles et al., 2015; Gultepe et al., 2015) but, to the best knowledge of the author, this has not yet been applied in femoroplasty. For this reason, feasible injection strategies will be studied in Chapter 5.

Chapter 4

Effect of Bone Cement Porosity on Femoral Augmentation

4.1 Introduction

Computational studies such as the one presented in Chapter 3 have been conducted to minimise the required amount of bone cement and optimise the injection locations while providing a significant net benefit to femoral mechanical properties (Basafa and Armand, 2014; Varga et al., 2017). However, results from numerical simulations depend on a variety of factors such as the bone morphology, the degree of osteoporosis, the imposed boundary conditions and the material properties of the augmented bone (Rohlmann et al., 2010; Wijayathunga et al., 2013). The bone geometry, degree of osteoporosis and the respective material properties are often obtained from a CT scan. Similarly, the most commonly used boundary conditions in the experimental and computational study of femoroplasty replicate a lateral fall on the greater trochanter (Sutter et al., 2010a,b; Beckmann et al., 2011; Fliri et al., 2013; Springorum et al., 2014; Basafa and Armand, 2014; Basafa et al., 2015; Varga et al., 2017), although different fall directions have not been compared. While

all these factors remain significant topics of ongoing computational analysis research, the present chapter is focused on two of them: the material properties of the augmented bone and the direction of the fall.

Some studies consider the material properties of augmented bone as those of pure PMMA without any porosity (Basafa and Armand, 2014), while other studies make use of the concept of PMMA porosity (Varga et al., 2017; Kinzl et al., 2012). The mixing and injection technique, as well as the shrinkage of the cement contribute to the porosity in the solidified cement. More complex schemes have also been proposed, including PMMA porosity, bone volume fraction and change of PMMA material properties with temperature (Soyka et al., 2016). Consequently, the first objective is to determine whether PMMA porosity has a statistically important impact when predicting the optimal volume of bone cement required to achieve a specific level of bone augmentation. Additionally, the second objective is to compare different approaches used to model the modulus of elasticity of augmented bone. Finally, the importance of fall direction in the femur fracture load has been previously studied (Pinilla et al., 1996; Falcinelli et al., 2014), but not applied to determine bone cement requirements in femoral augmentation. Therefore, the third objective is to quantify the sensitivity of the optimum volume of bone cement on two essential design variables of the examined problem, namely grade of porosity of PMMA and direction of the external load, which resembles variations of the fall direction.

4.2 Methods

4.2.1 Modelling the Material Properties of Augmented Regions

The six osteoporotic models developed in Section 3.2.1 were used throughout the analyses performed in this chapter. In these models, ash density was calculated for each mesh element from the femur CT scan. The ratio between ash density (ρ_{ash}) and apparent

density (ρ_{app}) was considered to be constant and equal to 0.6. Therefore, the Bone Volume Fraction (BVF) per element, defined as the ratio of the Bone Volume (BV) over the Total Volume (TV), is equal to:

$$BVF = \frac{\rho_{app}}{\rho_{tissue}} \tag{4.1}$$

Where the density of bone tissue (ρ_{tissue}) was considered to be equal to 1.81g/cm^3 (Nazarian et al., 2008).

The optimum volume of bone cement and its distribution within the femur was computed for each model following the optimisation algorithm presented in Chapter 3, but the material properties of the augmented regions were modelled following the five different approaches shown below:

A. Pure PMMA ($E_{PMMA} = 2300MPa$) according to Lu et al. (2014).

B. Pure PMMA considering cement porosity as per Equation 4.2 and according to Kinzl et al. (2013).

$$E_{POROUS-PMMA} = E_{PMMA} - (k_E \cdot pv) \tag{4.2}$$

Where E_{PMMA} is the elastic modulus of pure PMMA (2300MPa), k_E is the decreasing constant (6314MPa) and pv is the pore volume fraction (10%).

C. Bone cement composite applying the Voigt-Reuss-Hill average based on the Bone Volume Fraction (BVF). The composite elastic modulus E_{COMP} was computed (Equation 4.3) as the average of the Voigt upper bound E_V (Equation 4.4) and the Reuss lower bound E_R (Equation 4.5).

$$E_{COMP} = \frac{E_V + E_R}{2} \tag{4.3}$$

$$E_V = E_{BONE} \cdot BVF + E_{PMMA} \cdot (1 - BVF) \tag{4.4}$$

$$E_R = \left(\frac{BVF}{E_{BONE}} + \frac{1 - BVF}{E_{PMMA}} \right)^{-1} \tag{4.5}$$

The Voigt bound yields from an isostrain consideration and the application of a rule of mixtures to the stiffness of the involved materials, while the Reuss bound yields from an isostress consideration and the application of a rule of mixtures to the compliance of the involved phases.

D. Bone cement composite applying the Voigt-Reuss-Hill average (Equation 4.3) but replacing the elastic modulus of pure PMMA (E_{PMMA}) in Equations 4.4 and 4.5 with the elastic modulus of pure PMMA including cement porosity $E_{POROUS-PMMA}$, as per Equation 4.2.

$$E_{POROUS-COMP} = \frac{E_{V-POR} + E_{R-POR}}{2} \tag{4.6}$$

$$E_{V-POR} = E_{BONE} \cdot BVF + E_{POROUS-PMMA} \cdot (1 - BVF) \tag{4.7}$$

$$E_{R-POR} = \left(\frac{BVF}{E_{BONE}} + \frac{1 - BVF}{E_{POROUS-PMMA}} \right)^{-1} \tag{4.8}$$

E. Bone cement composite considering only the Voigt bound (Equation 4.4) but neglecting the material properties of bone tissue ($E_{BONE} = 0$) in the respective rule of mixtures, as shown in Equation 4.9.

$$E_{V-PMMA} = E_{PMMA} \cdot (1 - BVF) \tag{4.9}$$

The difference between methods A and B is the elastic modulus of PMMA, which is reduced by a constant in approach B. Method A was applied in Chapter 3 to compute the optimum bone cement volume and placement but to the best knowledge of the author,

the application of approaches C, D and E in femoral augmentation were firstly introduced in this chapter.

The five defined modelling approaches for the modulus of elasticity of the bone cement composite were investigated for six different levels of virtual osteoporosis, totalling 30 different cases. In all cases, bone cement was considered as a homogeneous and isotropic material, with Poisson's ratio equal to 0.3. It is worth clarifying that the available void per element ($V_{(ELE/PMMA)}$) that could be filled-in by bone cement was computed according to Equation 4.10, where the element-specific BVF value is provided by Equation 4.1 and the total element volume ($V_{(ELE/TOTAL)}$) is retrieved from the mesh:

$$V_{(ELE/PMMA)} = (1 - BVF) \cdot V_{(ELE/TOTAL)} \tag{4.10}$$

Based on these 30 cases, a one-way Analysis of Covariance (ANCOVA), using the software package SPSS Statistics v.17 (IBM Corporation, USA) was conducted to investigate whether the different five modelling approaches provided results significantly different to each other. To this end, within the SPSS environment, a post hoc Bonferroni test was used to compare the influence of the different factors. For the statistical analysis, values of $p<0.05$ were considered to be statistically significant.

4.2.2 Impact of Design Variables on the Optimum Volume of Bone Cement

A sensitivity analysis was conducted using ANSYS Mechanical APDL in order to investigate the sensitivity of the optimum volume of bone cement with respect to 3 design variables, namely the frontal and transverse direction of the applied load (Figure 4.1), and the bone cement porosity. In total, 1452 FEA were performed in a femur with T-Score -2.5, based on all the combinations of the three parameters shown in Table 4.1 (α can have 11 different values, β can have 11 different values and pv can have 12

different values).

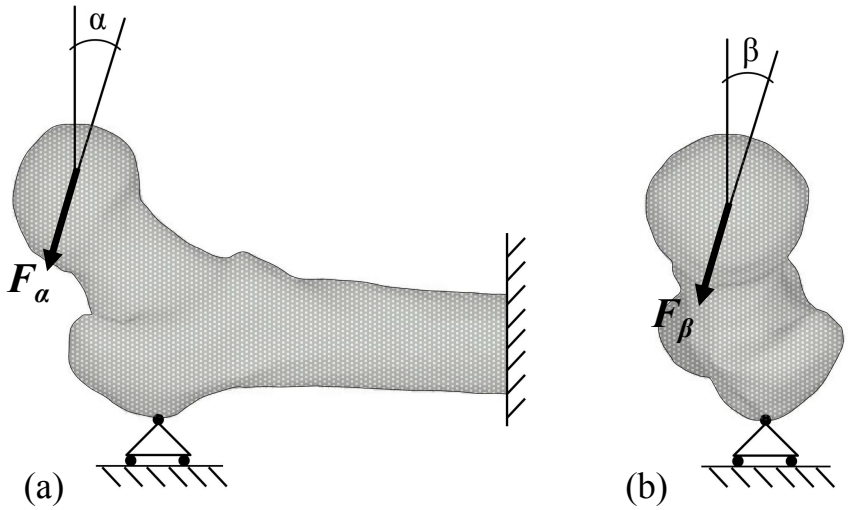

Figure 4.1: Direction of the applied load: transverse (α) and frontal (β).

Table 4.1: Input parameters, step size and range for the sensitivity analysis

Input parameter	**Step size**	**Minimum**	**Maximum**
Transverse load direction (α)	2.5°	0°	25°
Frontal load direction (β)	2.5°	0°	25°
Pore volume fraction (pv)	2%	0%	22%

4.3 Results

The optimum volume of bone cement is plotted against the respective T-Score for all the modelling approaches in Figure 4.2, showing that in order to reach the same target load, the required PMMA volume increased with the degree of osteoporosis. This is anticipated due to the femur yield load reduction as the degree of osteoporosis increases. Both the mean value and the standard deviation increased as the degree of osteoporosis increased, ranging from 3ml (SD=0.017) to 19.62ml (SD=2.25), as shown in Table 4.2. For femora with a T-Score between -1.5 and -3.0, the Coefficient of Variation (CV) for the optimum

volume of bone cement remains within the interval 13.53% - 14.61%. Additionally, Figure 4.2 shows that regardless the modelling method for estimating the modulus of elasticity of the augmented bone, there is a strong linear correlation between the T-Score and the optimum volume of bone cement ($R^2 > 0.9721$ in all cases). It is because of this strong linear correlation that an ANCOVA was applicable.

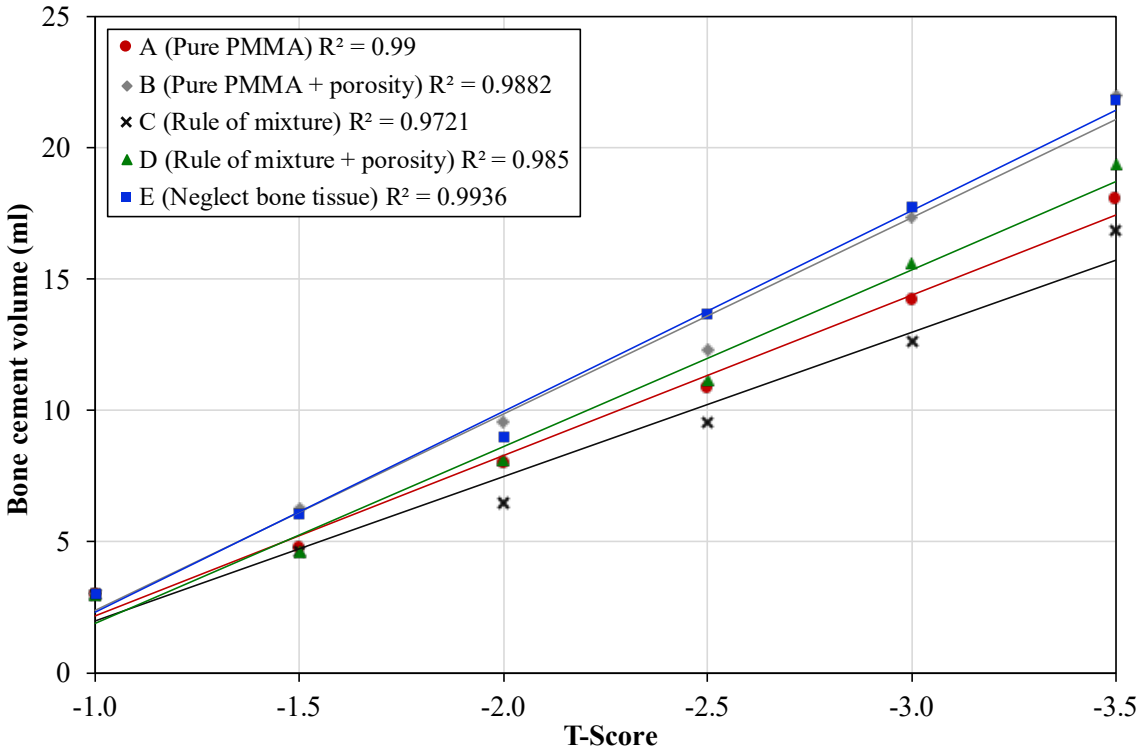

Figure 4.2: Degree of osteoporosis vs optimum bone cement volume for the different modelling approaches, including trend lines and correlation coefficient.

The ANCOVA test conducted across the modelling techniques defined in Section 4.2.1 evidenced no relevant differences between the pure PMMA approach and the rule of mixture when bone cement porosity is not considered (pair A-C, p=1). The same applied when bone cement porosity is considered (pair B-D, p=0.137). However, statistically significant differences appeared between techniques A-B (p=0.048), A-E (p=0.027), C-B (p=0.001) and C-E (p=0.001). This indicates that modelling without porosity is statistically different to neglecting bone tissue or modelling with pure PMMA and porosity. However, the ANCOVA test also showed that there was one modelling

Table 4.2: Optimum volume of bone cement for the different modelling approaches and grades of osteoporosis.

	Osteopenia			**Osteoporosis**		
T-Score	**-1.0**	**-1.5**	**-2.0**	**-2.5**	**-3.0**	**-3.5**
(A) Pure PMMA	2.98	4.75	7.99	10.84	14.24	18.09
(B) Pure PMMA + porosity	3.01	6.25	9.53	12.33	17.33	21.97
(C) Rule of mixture	3.00	4.75	6.62	9.57	12.81	16.89
(D) Rule of mixture + porosity	2.99	4.72	7.99	11.19	14.32	19.34
(E) Neglect bone tissue	3.03	6.04	8.98	13.69	17.73	21.83
Mean value	3.00	5.30	8.23	11.52	15.29	19.62
Standard Deviation	0.02	0.77	1.12	1.56	2.14	2.25
Coefficient of Variation (%)	0.6%	14.6%	13.6%	13.5%	14.0%	11.5%

approach, i.e. the newly introduced approach D (rule of mixture considering porous PMMA) for which there was no statistically significant difference against any of the other examined modelling methods. For this reason, approach D will be used as the preferable modelling technique in this research. It is also highlighted that the approaches A and B, which were found to be significantly different to each other, are two approaches widely used in the literature (Basafa and Armand, 2014; Varga et al., 2017).

The aforementioned statistical findings are shown in Figure 4.3, where the five modelling approaches are plotted as vertical bars, the height of which denotes the respective optimum volume of bone cement. Bars with the same letter at their top correspond to modelling approaches which were found not to be significantly different to each other. Noted that for approach D there are two letters, where W indicates similarity between approach D and approaches A and C, while X indicates similarity between approach D and approaches B and E. Approaches A,C are statistically different to approaches B,E.

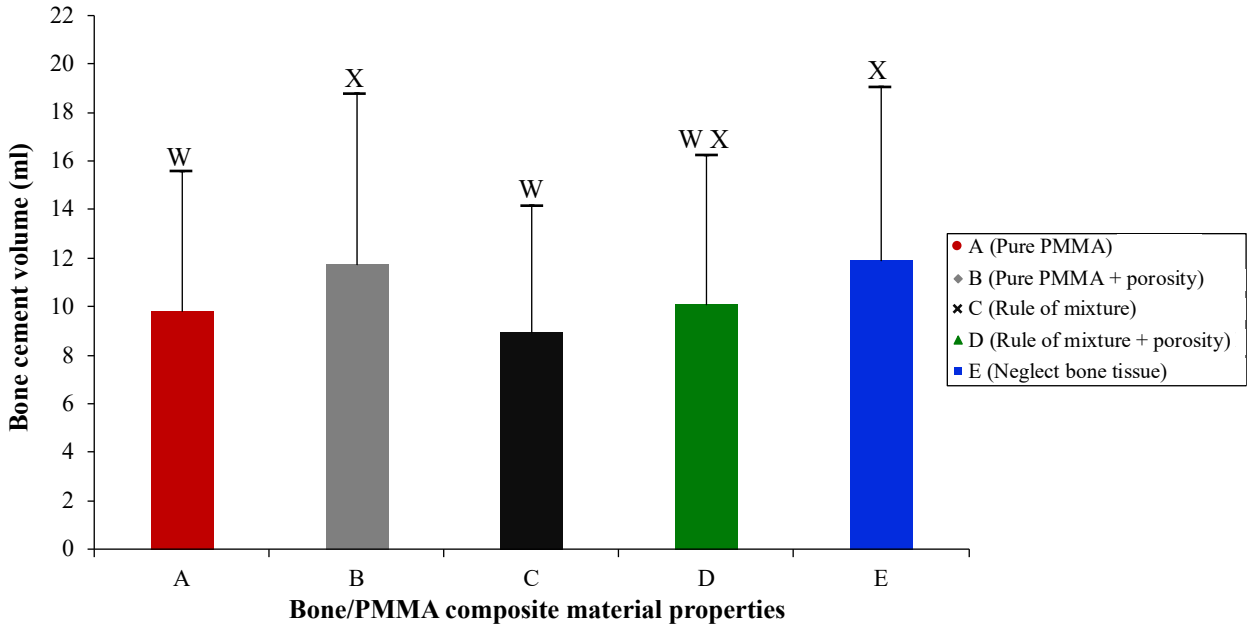

Figure 4.3: Effect of the modelling approach on the final bone cement volume. Means with different letters (W, X) are significantly different (Bonferroni procedure, $p<0.05$).

The optimum distributions of bone cement for one of the models (T-Score -2.5) are depicted in Figure 4.4. Despite the different modelling approaches, bone cement placement is very similar in all cases: reinforcing the femoral neck, superior part of the proximal femur and greater trochanter.

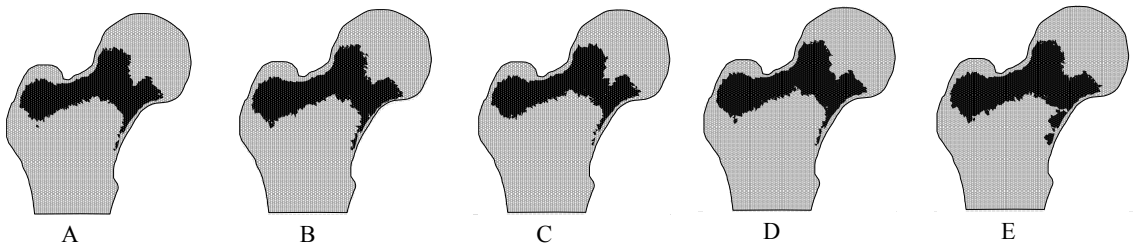

Figure 4.4: Bone cement volume in a femur with T-Score -2.5 and for the five different modelling approaches (A to E).

Figure 4.5 shows the upper and lower bounds of the rule of mixture applied in approaches C and D. It can be seen that when porosity is not considered (case C, Figure 4.5(a)), the maximum difference between the two bounds is approximately 8.5%, found for a T-Score of -3.5. However, when porosity is considered (case D, case C, Figure 4.5(b)), the

maximum difference occurs in the femur with a T-Score of -1.0, and it is approximately 15%. Therefore, for approach D, the effect of bone cement porosity yields in Voigt and Reuss bounds becoming more distinctive. For case C and up to a T-Score of -2.0, the composite elastic modulus increases as the BVF increases, while for case D this observation holds up to a T-Score of -2.5.

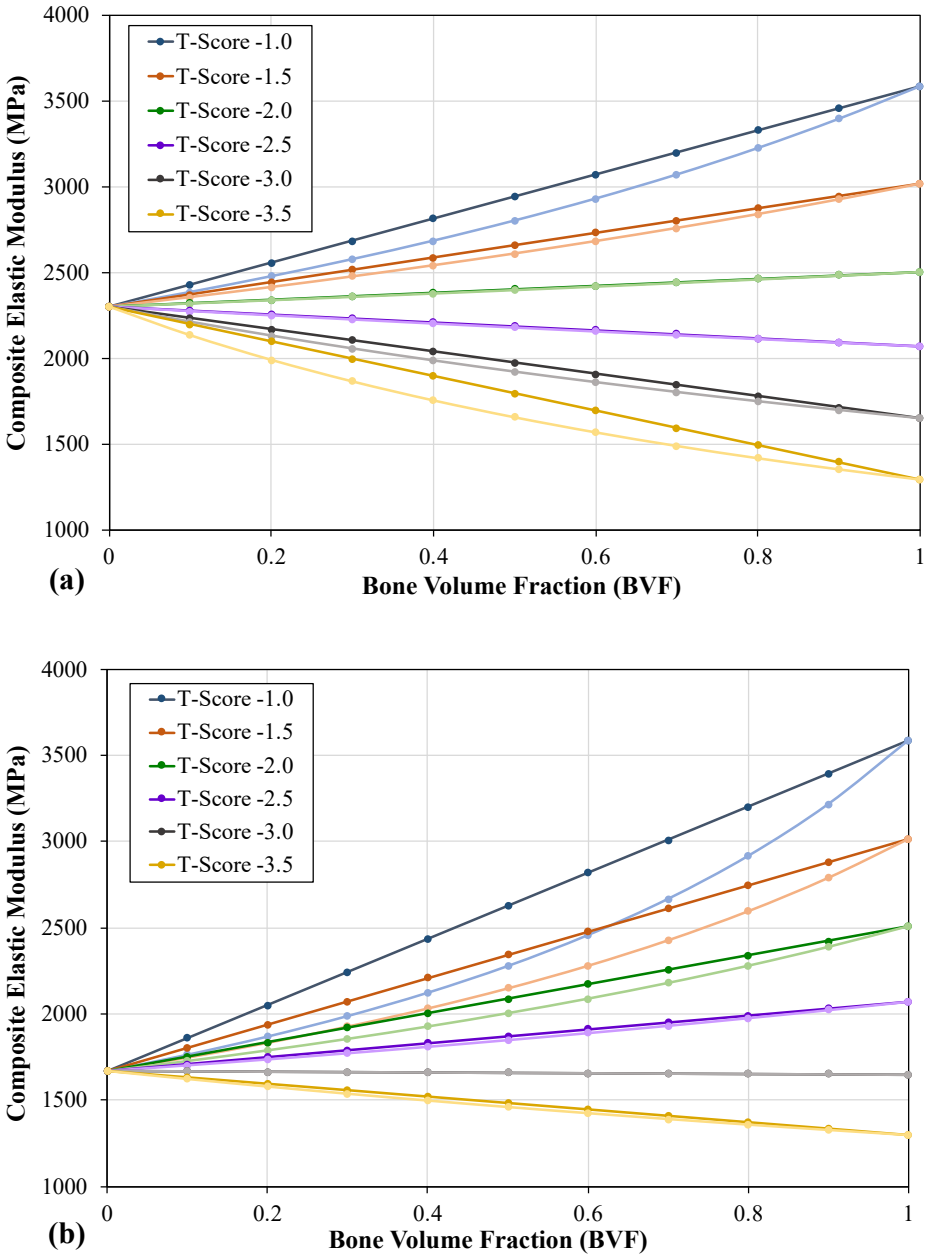

Figure 4.5: Voigt and Reuss bounds for cases C (a) and D (b) and for different values of bone volume fraction. Dark colour represents Voigt bound and light colour represents Reuss bound.

Figure 4.6 shows the optimum volume of bone cement for all combinations of the input parameters, namely the frontal angle, the transverse angle and the bone cement porosity, when approach D is implemented. The PMMA volume increases when any of the three inputs increases. This effect is more significant when the frontal angle increases than when the transverse angle increases and therefore, more reinforcement would be required to prevent a fracture if a fall were to occur under conditions characterised by high rotation in the frontal plane.

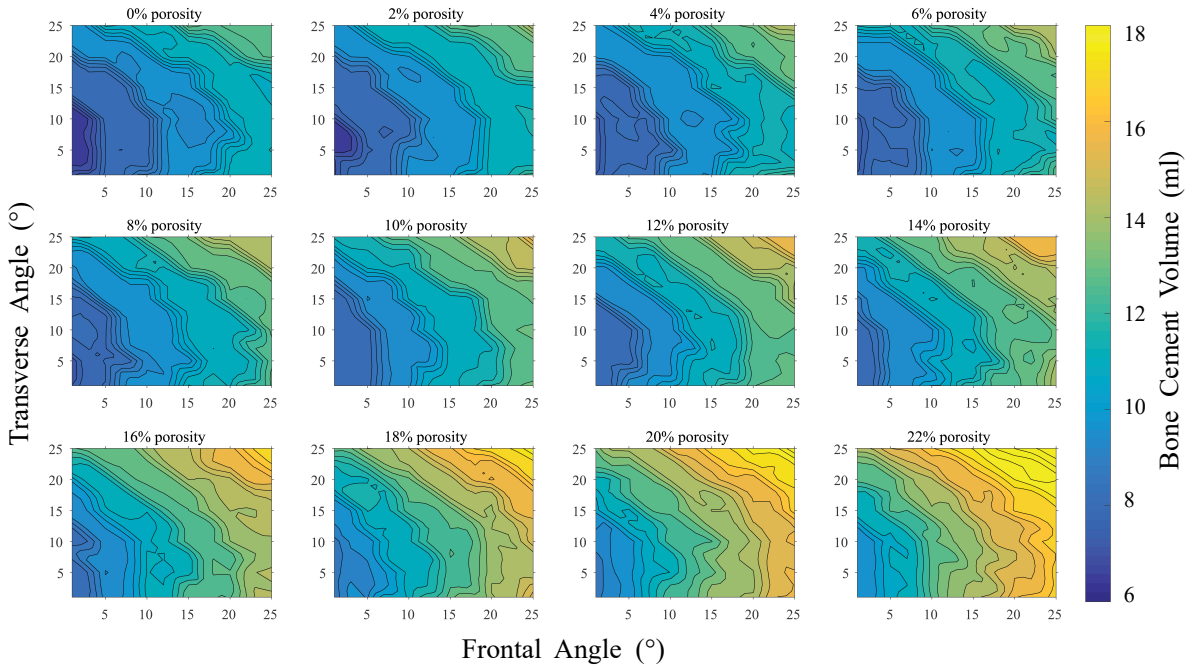

Figure 4.6: Contours of required PMMA volume for the combination of all the input parameters: frontal angle, transverse angle and bone cement porosity.

The porosity of PMMA also influences the distribution of the optimisation results, as Figure 4.7 illustrates. This figure shows the relative frequency distribution of the optimum volumes from the 1452 examined combinations. In total, eight classes were used of width equal to 2 and ranging from [6,8) up to and including [20,22]. For porosity levels up to 4%, almost 50% of the combinations of frontal and transverse angles would require a volume of bone cement within the class of (8, 10]. For porosity levels up to 8%, there is one class (i.e. ([8,10)) which prevails with a relative frequency of at least 40%. For porosity levels between 10% and 16%, the relative distribution becomes more uniform

with a decreasing maximum peak value per class, as the porosity increases. For porosity levels between 18%-22%, the class [14,16) clearly prevails over the other classes, with a relative frequency of 35%, while the second highest relative frequency is at least 10% lower. Lastly, no strong linear correlation was found between any of the three design variables and the optimum volume of bone cement.

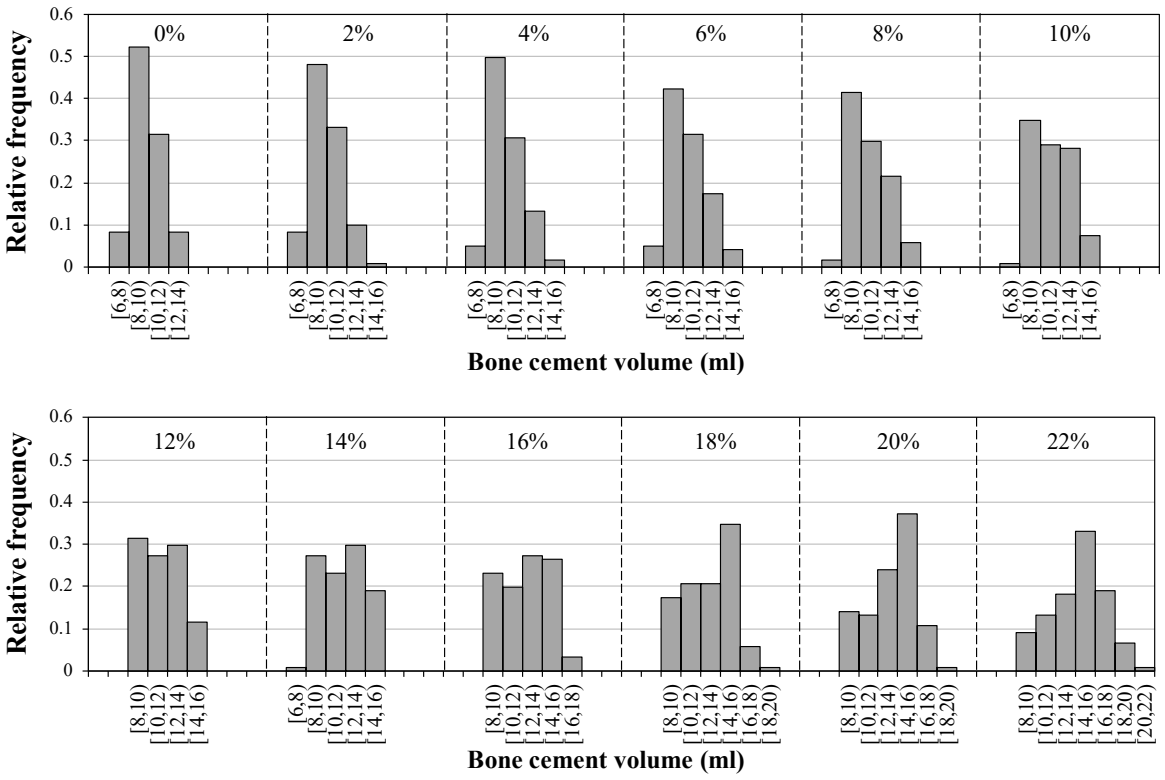

Figure 4.7: Distribution of bone cement volume (relative frequency) for each level of porosity.

4.4 Discussion

The first research question that this chapter aimed to address was whether the bone cement porosity has a statistically significant impact on the prediction of the optimal bone cement volume required to achieve a specific level of augmentation. In Chapter 3, the volume of bone cement was considered to be numerically equal to the volume of a finite element which represents augmented bone (Basafa and Armand, 2014; Varga et al.,

2017). This is not always a valid assumption, as injected bone cement may only fill-in voids and not replace existing bone tissue. To overcome this problem, a more accurate approach to determine the bone cement volume that is embedded in trabecular tissue based the bone volume fraction was used in this chapter. However, in order to perform femoral augmentation in practice it is necessary to pre-drill a channel in the bone, which will eventually only be filled with bone cement. Therefore, once the length and radius of the channel(s) are known, the bone volume fraction of the channel(s) elements should be set to zero to accurately compute the required bone cement volume.

Five different approaches were used to model the modulus of elasticity of the bone cement composite. Approach A was applied in Chapter 3 and considered that cemented elements had the material properties of pure PMMA, as presented by Basafa and Armand (2014). For different levels of osteoporosis and osteopenia, the required bone cement volume varied from approximately 3 to 18ml (mean 9.82ml, SD=5.74). Given that the goal of the optimisation was to increase the yield load of the different femora to a predefined target load, the range of required bone cement volume is wide and highly dependent on the degree of osteoporosis. Using approach, A, it has been reported (Basafa and Armand, 2014) that for an increase of 100% in the osteoporotic femur yield load (T-Score -3.53) volumes between 5.6ml and 26.2ml of bone cement were needed. Following the same method, a recent numerical study with four femur models of average T-Score -3.2 (Farvardin et al., 2019) showed a 79.6% average yield load increase with 9.2ml of bone cement. Using the modelling approach proposed in case A for a femur with T-Score -3.5, 6.21ml of bone cement were required to double the yield load. Results of the present study align with those of Basafa and Armand (2014) regarding bone cement placement, i.e. superior part of the femoral neck and greater trochanter. Varga et al. (2017) considered homogeneous material properties for all the cemented elements and assumed 10% pore volume fraction for the PMMA (similar to case B). In their study, after performing several non-linear FE analyses placing a cylinder of bone cement in different locations they concluded that approximately 12ml of PMMA result in an average increase of 64% in the femur yield load. Following the approach presented in case B, using the average from all femur models,

approximately 9.6ml of bone cement would be necessary to increase the yield force by 64%, suggesting a more efficient placement of bone cement. However, as discussed in Chapter 3 this is may be due to the use of unrealistic augmentation patterns in the bone.

No statistically significant differences were found between cases A-C or B-D, which indicates that using a rule of mixtures did not affect the optimisation result. However, significant differences arise when introducing bone cement porosity (pairs A-B and B-C). This is in agreement with Kinzl et al. (2011), who demonstrated that mechanical properties of augmented tissue (in vertebroplasty) depend mainly on the bone cement porosity and material properties. Despite constant porosity was assumed in this chapter, additional factors such as bone damage due to shrinkage or detailed behaviour at the bone-PMMA interface have been proposed to simulate augmented vertebrae (Kinzl et al., 2012) on micro-FE models. The inclusion of those elements could help develop a more accurate representation of the bone cement composite in the framework of femoral augmentation, but would also increase the computational cost of the simulations.

Despite the statistically significant differences between some of the presented modelling approaches, when bringing the problem to a practical scenario, it is necessary to contextualise these differences. The maximum variation amongst the modelling techniques occurred in the femur with T-Score -3.5 and was 5.1ml. In previous experimental studies of femoral augmentation with PMMA, the reported injected volumes of bone cement were between 9-18ml (Beckmann et al., 2011), 8-14ml (Varga et al., 2016), 8-15ml (Springorum et al., 2014) and 11-15ml (Raas et al., 2016) depending on the femur size and bone cement location. However, in other investigations focused on the study of bone cement placement, the variation of injected PMMA in different femora is much smaller, such as 15.2ml (SD=1.5) and 15.1ml (SD=1.6) (Sutter et al., 2010a) and 9.5ml (SD=1.7) (Basafa et al., 2015). Hence, a variation of 5.1ml of bone cement in the same femur is significant and may have an effect on the risks involved in the augmentation procedure.

In this study, and for the cases C and D, the elastic modulus of augmented elements

was computed using the Voigt-Reuss-Hill average as a function of bone volume fraction. Given that the upper and lower bounds of the rule of mixture were sufficiently close, it was not considered necessary to apply more complex formulations such as the Hashin-Shtrikman. Case E aimed at investigating an extreme case where the bone tissue was so deteriorated that it could be neglected. The long-term behaviour of the bone present in the augmented region is unclear (Badilatti et al., 2017), so results obtained with method E are a representation of one of the worst possible cases. It is also worth noticing the similarity between approaches E (bone tissue is neglected) and B (pure porous PMMA). In both cases the elastic modulus of the pure PMMA is reduced by a factor, controlled either by the bone volume fraction or the porosity.

In the conducted sensitivity analysis, the required volume of bone cement was monitored for various combinations of three design variables: frontal angle and transverse angle of the applied load and bone cement porosity. Under lateral fall conditions, a reduction of the femur yield load for high values of internal rotation (frontal angle) have been reported by Bessho et al. (2009); Falcinelli et al. (2014); Zani et al. (2015); Pinilla et al. (1996). This corroborates the findings of the conducted sensitivity analysis, since significantly larger volumes of PMMA were required in cases with higher frontal angles due to the reduction of the yield load. Results also show that the effect of increasing the transverse load direction is not as significant. Both these findings are in accordance with the fact that bone is capable of adapting to mechanical stimuli (Mullender and Huiskes, 1995) such as loads occurring in normal body activities. Such loading conditions in the femur usually comprise axial load and bending moment. This affects the femoral trabecular architecture, which follows patterns suggesting the directions of principle compressive and tensile stresses (Brand, 2011) and makes the bone more suitable to carry bending than torsion (which occurs with high internal rotation).

The presence of porosity in the PMMA was modelled by reducing the elastic modulus of the bone cement composite, which increases the necessary amount of PMMA to reach certain augmentation level. For a low pore volume fraction, regardless the load direction,

the optimum amount of bone cement for over 70% of cases was found to be between 8-12ml. However, when porosity is greater than 8% the maximum relative frequency of optimum bone cement decreases to less than 40% and the histogram (Figure 4.7) becomes more uniform. Hence, as the bone cement porosity increases, load direction becomes a more significant factor in the optimisation result.

In this chapter, five different approaches were employed to calculate the elastic modulus of the augmented bone, of which two are widely used in the literature. One of the proposed schemes, which combined the Voigt-Reuss-Hill average with bone cement porosity was the only one providing results that were not statistically different to the rest of all other approaches and represented the most physiologically realistic case. Furthermore, a strong linear correlation between the T-Score and the optimum volume of bone cement required to restore the load capacity of the examined femora was demonstrated. Lastly, the importance of the femur rotation in the frontal and transverse plane in case of a lateral fall was quantified in terms of required bone cement volume to avoid a fracture. Similar simplifications to the ones described in Chapter 3 apply to this study, in addition to considering bone cement porosity constant and not modelling in detail the bone-PMMA interface. Despite the results of the present chapter may be useful to identify the weakest locations of the femur under lateral fall conditions and the importance of bone cement porosity, they do not provide any solutions that are directly applicable in the planning of femoral augmentation. For this reason, the outcomes of this chapter will be used as a starting point in Chapter 5 to propose and optimise several augmentation strategies that can be executed in real life.

Chapter 5

Study of Generalised, Feasible Bone Cement Distributions

5.1 Introduction

The primary objective of femoral augmentation is to increase bone strength to a level that significantly reduces the risk of suffering a fracture spontaneously or due to a low-energy fall. Optimisation studies such as the one presented in Chapter 3 have been conducted towards the joint aims of increasing femur strength and minimising the bone cement volume (Basafa and Armand, 2013). In these studies, the bone cement optimum distribution is patient-specific and generally has a complex shape that is not easily achievable in practice. These customised treatments would require detailed preoperative planning and equipment that is not widely available. Additionally, due to the architecture of trabecular bone tissue it is not realistic to assume such complex injection strategies could be executed without error. A further limitation is the need for pre-drilled channels to inject the bone cement, as well as the limitation in the number of channels that can be drilled before excessively damaging the cortical bone (Beckmann

et al., 2011). Furthermore, during the injection, PMMA bone cement spreads irregularly inside the bone and during the solidification process it generates an exothermic reaction and shrinks (Muller et al., 2002; Gilbert, 2006).

Due to the aforementioned limitations, a more generalised approach with realistic injection patterns could be beneficial for the procedure. To this end, Basafa et al. (2015) proposed an augmentation strategy which matched three spheroids to the patient-specific optimum bone cement distribution. Therefore, bone cement was injected in the bone in three separate injections, requiring a navigation system to control each injection location. An alternate augmentation approach was defined by Varga et al. (2017) based on the principles of Wolff's law. In their study, bone cement was placed in a cylindrical channel from the greater trochanter to the femoral head and five different injection strategies were tested by modifying the location of the cylinders. This strategy, injecting bone cement in a previously drilled channel is the most common augmentation method in experimental studies (Beckmann et al., 2011; Steenhoven et al., 2011, 2012; Springorum et al., 2014). All these studies agree that the location of bone cement is highly influential in the augmentation result, although the effect of minor variations in the bone cement placement remains unclear.

In the past, femoral augmentation methods have been divided in to two main categories: injecting bone cement as spheroids in different locations or drilling a path and filling it with bone cement. Hence, one research question that this chapter aims to address is to what extent these different augmentation techniques affect the augmented femoral strength. To do so, six feasible distributions were proposed and studied based on the optimum bone cement distribution found in Chapter 4. These feasible distributions considered certain limitations of the femoral augmentation procedure such as the radius of the pre-drilled path or the maximum number of paths that can be drilled. A second research topic is to quantify the effect that different parameters in each distribution have on the augmented yield load. Therefore, a sensitivity analysis using the Taguchi method and an ANOVA analysis to determine the most influencing factors were performed for each distribution.

Finally, the third research question is to identify the optimum placement and volume of the proposed distributions which maximise the yield load after augmentation and minimise the bone cement volume. To this end, a multiobjective optimisation was performed using the *patternsearch* algorithm.

5.2 Methods

5.2.1 Feasible Bone Cement Distributions

The optimum and ideal distribution of bone cement inside an osteoporotic femur was found in Chapter 4 using the heuristic optimisation algorithm presented in Chapter 3 and considering the augmented regions as a composite formed of bone and porous PMMA. After this, the next step is to transform the identified volume into a distribution of bone cement that could be easily reproduced in practice. To this aim, two different augmentation strategies were explored in this chapter: placing spheres of bone cement in specific locations and placing bone cement into cylindrical drilled channels. These two types of augmentation are feasible to inject in practice, have been previously tested in experimental studies and are able to create bone cement distributions similar to the ideal one. The ideal distribution of bone cement for a femur with T-Score -2.5 was divided in four regions (Figure 5.1) and the centroids of these regions were used as reference points. These points were A, B, C, D and CD, which is the centroid of the regions C and D combined (Figure 5.1).

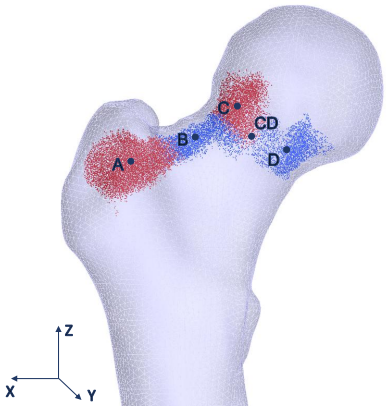

Figure 5.1: Centroids of regions in which the ideal bone cement distribution was divided.

The proposed distributions are the following:

a. Spheres of bone cement

1. **Three spheres located in a straight line:** centroids of the spheres were located at point A, CD and the midpoint of the line joining those points.

2. **Three spheres located in a curve:** centroids of the spheres were located at point A, B and D.

b. Channels filled with bone cement

1. **One straight drilled channel:** straight line from point A to CD.

2. **Two straight drilled channels:** one straight line from point A to C and one straight line from point A to D.

3. **One curved drilled channel:** arc passing through points A, B, CD.

4. **Two curved drilled channels:** one arc passing through points A, B, C and one arc passing through points A, B, D.

In all cases, the paths were extended laterally from point A until they reached the cortical bone. In order to investigate the effect of different volumes of bone cement, three different sphere radiii (5mm, 7mm, 9mm) and channel radii (3mm, 4mm, 5mm) were studied for each distribution. One FE analysis was conducted for each case to calculate the increase in the femur yield load after augmentation. To calculate the femur yield force, an initial small load was applied and increased gradually until 1% of the elements in the proximal femur failed, using boundary conditions that replicated a lateral fall onto the greater trochanter (as described in Section 3.2.2). Analyses were conducted in ANSYS Mechanical APDL.

5.2.2 Sensitivity Analysis Using the Taguchi Method

For each one of the distributions presented in Section 5.2.1, a sensitivity analysis was performed using the Taguchi orthogonal array. With this, the influence of each parameter in the different distributions could be determined while considering the variation of the remaining variables. The following design parameters were studied:

a. Spheres of bone cement

1. **Three spheres located in a straight line:** Taguchi L27 orthogonal array (27 runs of FEA). Three levels were studied for the radius of each sphere (R_i for $i = 1, 2, 3$) and centroid of spheres 1 and 3 (PX_i, PY_i, PZ_i for $i = 1, 3$). Sphere 2 was located at the midpoint of the line joining these points.

2. **Three spheres located in a curve:** Taguchi L27 orthogonal array (27 runs of FEA). Three levels were studied for the radius of each sphere (R_i for $i = 1, 2, 3$) and centroid of each sphere (PX_i, PYi, PZi for $i = 1, 2, 3$).

In the cases explained above, the sphere radius varied from 5mm to 9mm and the centroid of each sphere varied ±10mm from the region centroid location.

b. Channels filled with bone cement

1. **One straight drilled channel:** Taguchi L54 orthogonal array (54 runs of FEA). Two levels were studied for the radius of the channel (R) and three levels for the location of the line start and end points ($PX_i, PY_i, PZ_i \ for \ i = 1, 2$).

2. **Two straight drilled channels:** Taguchi L54 orthogonal array (54 runs of FEA). Two levels were studied for the radius of the first channel and three levels for the radius of the second channel ($R_j \ for \ j = m, n$). Three levels were studied for the location of each line start and end points ($PX_{ij}, PY_{ij}, PZ_{ij} \ for \ i = 1, 2 \ and \ j = m, n$).

3. **One curved drilled channel:** Taguchi L54 orthogonal array (54 runs of FEA). Two levels were studied for the radius of the channel (R) and three levels for the length of the arc (L) and location of the three points defining the circular curve ($PX_i, PY_i, PZ_i \ for \ i = 1, 2, 3$).

4. **Two curved drilled channels:** Taguchi L54 orthogonal array (54 runs of FEA). Two levels were studied for the radius of the first channel and three levels for the radius of the second channel ($R_j \ for \ j = m, n$). Three levels were studied for the length of each arc ($L_j \ for \ j = m, n$) and location of the three points defining each circular curve ($PX_{ij}, PY_{ij}, PZ_{ij} \ for \ i = 1, 2, 3 \ and \ j = m, n$).

In the cases described above, the channel radius varied from 3mm to 5mm, the channel length varied from 50mm to 150mm and the points varied $\pm$10mm from the region centroid location.

For each distribution, a FE analysis was conducted to find the femur yield load after augmentation. Given that the objective was to find the parameters that maximise the percentage increase in the femur yield load, results were analysed using the larger-the-better Signal to Noise (S/N) ratio. The S/N ratio (measured in dB) was calculated

according to Equation 5.1.

$$\frac{S}{N} = -10log\frac{1}{y_i^2} \tag{5.1}$$

Where y_i is the value of the yield load obtained from each simulation. After this, an analysis of the variance (ANOVA) was performed to investigate the significance of each parameter in the augmented femur yield load for each case. To do so, the total sum of squares due to the variation of the overall mean (SS_T) is calculated according to Equation 5.2:

$$SS_T = \sum_{i=1}^{n} \left(S/N_i - \overline{S/N}\right)^2 \tag{5.2}$$

Where n is the total number of FE analyses, S/N_i is the S/N of the ith study and $\overline{S/N}$ is the overall mean of S/N. Then, the sum of the squares due to the variation of the mean was computed for each parameter (SS_P) as per Equation 5.3:

$$SS_P = \sum_{j=1}^{m} \left(S/N_{Pj} - \overline{S/N}\right)^2 \tag{5.3}$$

Where P refers to each design parameter, m is the number of discrete levels for each parameter and S/N_{Pj} is the S/N at each level for each parameter. Finally, the percentage contribution of each design parameter ($Contribution_P$) was determined according to Equation 5.4:

$$Contribution_P = \frac{SS_P}{SS_T} \tag{5.4}$$

5.2.3 Optimisation of Feasible Bone Cement Distribution

After studying the effect different bone cement distribution and associated parameters had on the augmented femur yield load, it remained unclear which combination of values would create the optimum augmentation strategy. For this reason, a further step was taken to identify the optimum location and volume of bone cement for each one of the

proposed distributions. The optimisation variables for each case are detailed below:

a. Spheres of bone cement

1. **Three spheres located in a straight line:** radius of each sphere (R_i for $i = 1, 2, 3$) and centroid of spheres 1 and 3 ($PX_i, PY_i, PZ)i$ for $i = 1, 3$). Sphere 2 was located at the midpoint of the line joining these points.

2. **Three spheres located in a curve:** radius of each sphere (R_i for $i = 1, 2, 3$) and centroid of each sphere (PX_i, PY_i, PZ_i for $i = 1, 2, 3$).

b. Channels filled with bone cement

1. **One straight drilled channel:** radius of the channel (R) and location of the line start and end points (PX_i, PY_i, PZ_i for $i = 1, 2$).

2. **Two straight drilled channels:** radius of each channel (R_j for $j = m, n$) and location of each line start and end points ($PX_{ij}, PY_{ij}, PZ_{ij}$ for $i = 1, 2$ and $j = m, n$).

3. **One curved drilled channel:** radius of the channel (R), length of the arc (L) and location of the three points defining the circular curve (PX_i, PY_i, PZ_i for $i = 1, 2, 3$).

4. **Two curved drilled channels:** radius of each channel (R_j for $j = m, n$), length of each arc (L_j for $j = m, n$) and location of the three points defining each circular curve ($PX_{ij}, PY_{ij}, PZ_{ij}$ for $i = 1, 2, 3$ and $j = m, n$).

The lower and upper bounds of the spheres and channel radius were retained from the sensitivity analysis (Section 5.2.2): 5-9mm for the spheres and 3-5mm for the cylindrical channels. The regions in which ideal distribution of bone cement was divided (Figure 5.1)

were used to define the upper and lower bounds of the possible point locations, as well as the maximum arc length.

The objective function (f) was the same for all modelled cases and aimed to minimise the volume of bone cement (V_{PMMA}) and maximise the augmented yield load (YL_{AUG}). The only constraint applied to the optimisation was that the bone cement volume (V_{PMMA}) had to be smaller than 12ml. Both objective variables (V_{PMMA}, YL_{AUG}) were normalised as detailed in Equations 5.5, 5.6:

$$V_{PERC} = \left(\frac{V_{PMMA}}{V_{MAX}}\right) \cdot 100 \tag{5.5}$$

$$YL_{INC} = \left(\frac{YL_{AUG} - YL_{N/AUG}}{YL_{N/AUG}}\right) \cdot 100 \tag{5.6}$$

Where V_{MAX} (12ml) is the maximum volume of bone cement allowed for the optimisation and $YL_{N/AUG}$ (2625N) is the yield load of the non-augmented femur. The multiobjective optimisation problem was solved using scalarisation, giving a larger weight to the yield load increase function (Equation 5.7):

$$f = (0.2 \cdot V_{PERC}) - (0.8 \cdot YL_{INC}) \tag{5.7}$$

Optimisations were performed using *patternseach* in MatLab 2018 (The MathWorks, Inc., Natick, Massachusetts, United States). The function evaluation to calculate the volume of bone cement and percentage increase in the femur yield load was conducted using the lateral fall boundary conditions described in Section 3.2.2 with ANSYS in batch mode.

5.3 Results

Small differences were found in the augmented yield load when reinforcing the femur with three spheres of bone cement in a straight-line or in a curve (Table 5.1). On average, a 4% difference was found between the two strategies, with placing spheres in a straight-line outperforming placing them in a curve. In all cases, increasing the spheres radii resulted in a higher volume of PMMA and hence, higher augmented yield load. The maximum increase in the yield load was 54% when using 10ml of PMMA.

Table 5.1: Yield load increase (YL_{INC}) after augmentation with spheres of bone cement (V_{PMMA}, volume of PMMA)

	Spheres in Straight Line		**Spheres in Curve**	
	$\mathbf{YL_{INC}}$	$\mathbf{V_{PMMA}}$ **(ml)**	$\mathbf{YL_{INC}}$	$\mathbf{V_{PMMA}}$ **(ml)**
R=5mm	22%	1.6	20%	1.6
R=7mm	38%	4.7	35%	4.5
R=9mm	54%	10	46%	9.4

When placing bone cement in a single cylindrical channel, curved distributions displayed higher improvements to the yield load (Table 5.2). As the channel radius increased, the difference in augmented yield load between a single straight and curved channel became higher, reaching up to 6%. When using two paths, curved channels performed better than straight as the radius of the channel increased. The maximum obtained yield load increase was 60% and 74% for one and two curved channels respectively. Using two channels implied in all cases a significantly higher volume of bone cement than augmenting with one channel, so it was expected to find a larger augmented yield load when compared to the single channel equivalent. However, the ratio of yield load increase over PMMA volume was always higher with one channel, suggesting a more efficient use of the bone cement.

Table 5.2: Yield load increase (YL_{INC}) after augmentation with bone cement channels (V_{PMMA}, volume of PMMA)

	One straight channel		**One curved channel**	
	YL_{INC}	**V_{PMMA} (ml)**	**YL_{INC}**	**V_{PMMA} (ml)**
R=3mm	28%	2.7	32%	3.0
R=4mm	42%	4.9	46%	5.4
R=5mm	54%	7.7	60%	8.1
	Two straight channels		**Two curved channels**	
	YL_{INC}	**V_{PMMA} (ml)**	**YL_{INC}**	**V_{PMMA} (ml)**
R=3mm	40%	5.1	30%	4.5
R=4mm	56%	8.4	54%	7.8
R=5mm	72%	13.0	74%	11.5

When comparing all the different augmentation strategies (Figure 5.2), it can be seen that for bone cement volumes of up to 8ml, the single curved channel strategy outperformed all other approaches. However, since drilled paths with large radii can excessively damage the cortical tissue, larger bone cement volumes required the use of two paths. In this case, for bone cement volumes larger than 8ml, curved channels also performed better than straight channels. Overall, the augmentation performance when reinforcing the femur with three spheres of bone cement was lower than when filling a pre-drilled cylindrical path with bone cement.

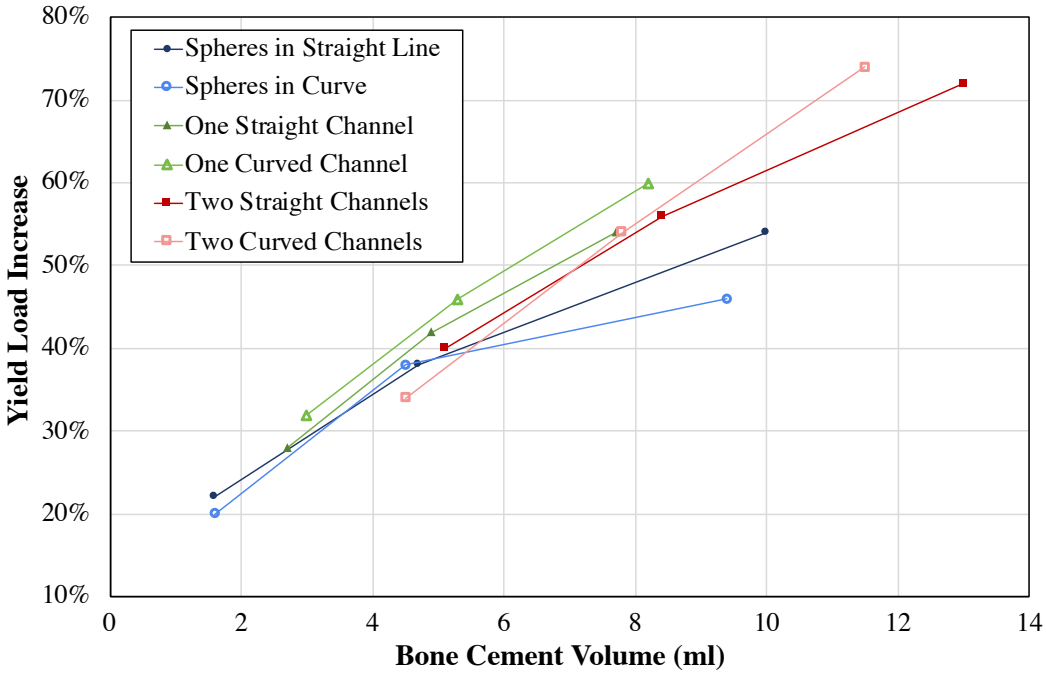

Figure 5.2: Yield load increase vs bone cement volume for all studied bone cement distributions.

After studying the aforementioned bone cement distributions, a sensitivity analysis was performed in order to understand the effect of each parameter in the augmentation result. The S/N response curves shown in Figure 5.3 depict the change in the result (augmented yield load, as a S/N ratio) with variations in the three most significant design parameters. In these plots, Level 2 represents the value from the original region centroids (Section 5.2.1) and Levels 1 and 3 represent the variations explained in Section 5.2.2. Taguchi analyses showed that when spheres were placed in a straight or curved line, the three factors that contributed the most to the increase of the femur yield load were the X, Y coordinates of the first sphere centroid and the radius of the first sphere (PX_1, PY_1, R_1). As expected, increasing the radius of the first sphere resulted in a larger augmented yield load. However, changing PX_1, PY_1 from their original level (Level 2) did not lead to any improvements in the yield load.

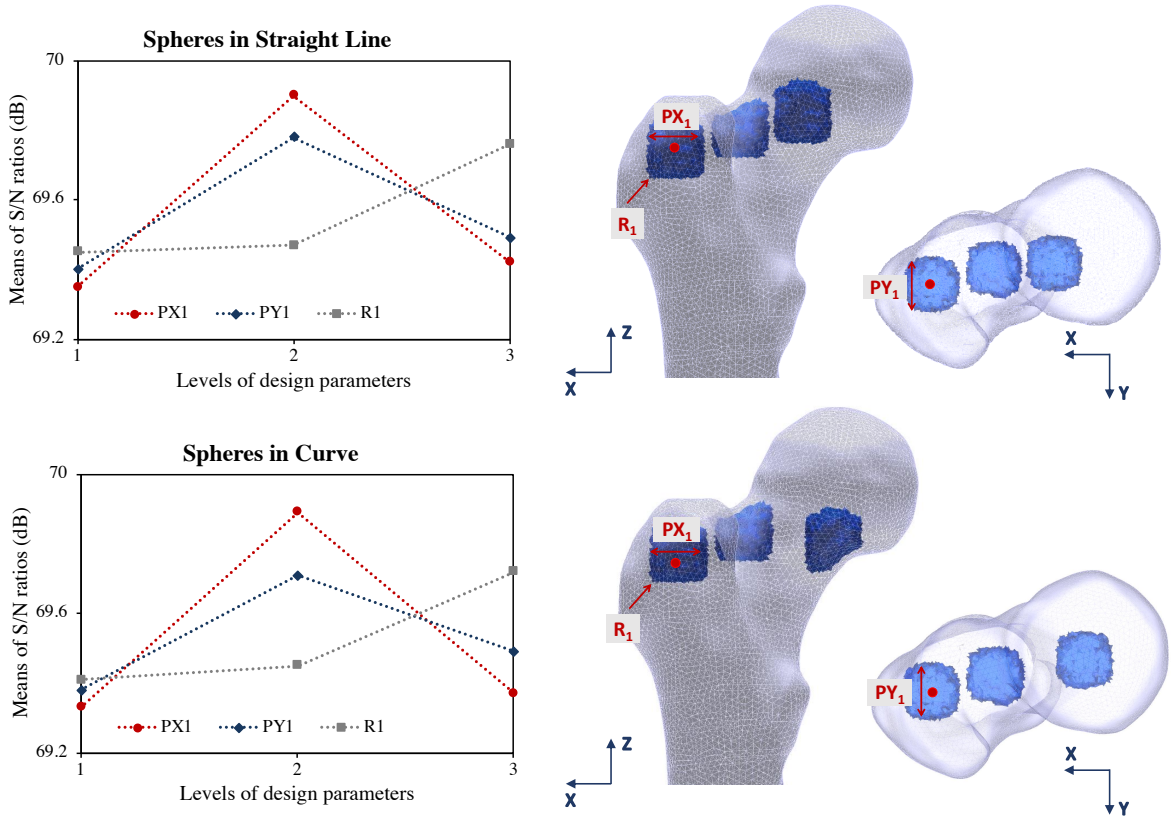

Figure 5.3: Taguchi S/N response curves for augmentation with three spheres of bone cement.

The three factors which displayed the highest contribution to changes in augmented femur yield load when placing bone cement in three spheres are shown in Table 5.3. Similar results were found when placing the spheres in a straight line and in a curve. For both cases, parameters related to the first sphere were of greatest significance. The location of the centroid of the first sphere showed the highest contribution to the augmentation result (between 54% and 55%), while the radius of the first sphere was only responsible for 12-13% of the changes.

Table 5.3: Contribution of most relevant parameters in augmentation result with three spheres of bone cement

Spheres in Straight Line		Spheres in Curve	
Parameter	**Contribution (%)**	**Parameter**	**Contribution (%)**
PX_1	39	PX_1	42
PY_1	16	R_1	12
R_1	13	PY_1	12

For one channel of bone cement (straight or curved), Taguchi analyses concluded that the three most relevant factors in the outcome of the simulation were the coordinates X and Z of the fist point and the radius of the channel (PX_1, PZ_1, R). In both cases, as shown in the S/N graph (Figure 5.4), increasing the radius of the channel or moving the Z coordinate of the first point downwards may benefit the femoral strength after augmentation.

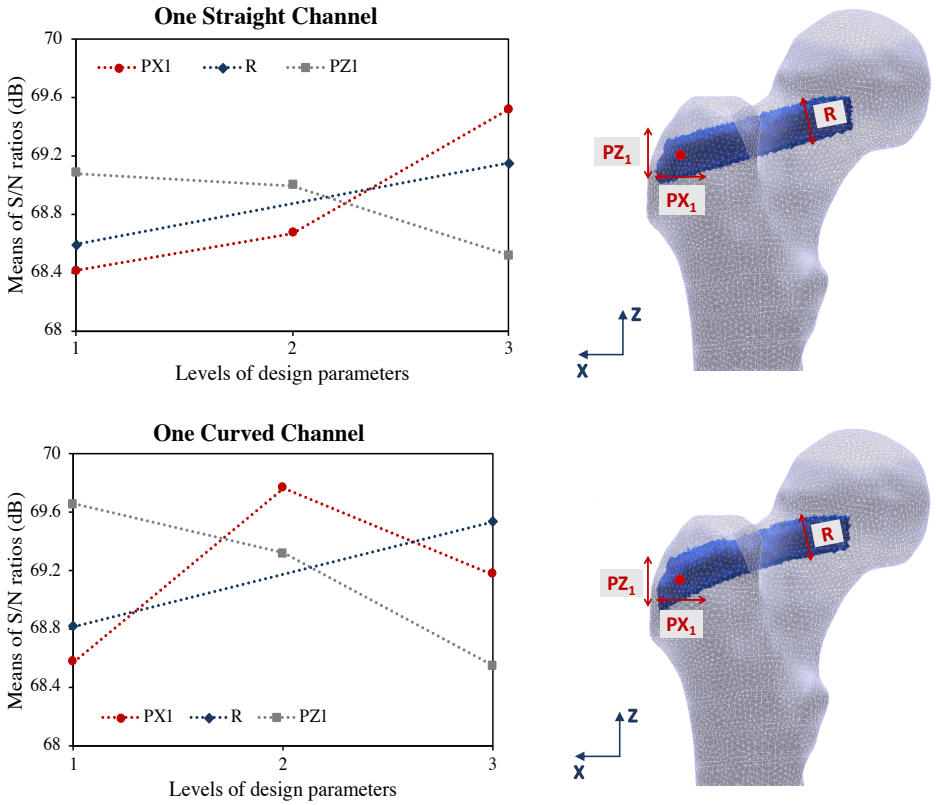

Figure 5.4: Taguchi S/N response curves for augmentation with one channel of bone cement.

The significance of the three most relevant parameters in the augmented femur yield load are shown in Table 5.4. In the straight single-channel distribution, the X coordinate of the first point had the highest contribution to the final yield load (35%), followed by the radius of the channel (12%) and the Z coordinate of the first point (9%). However, in the single curved-channel case both the X and Z coordinate of the first point showed a similar contribution to the femoral strength (30% and 28% respectively). These two factors together with the channel radius accounted for 75% of the total contribution, indicating that they may explain the majority of change to femur yield load after augmentation.

Table 5.4: Contribution of most relevant parameters in augmentation result with one channel of bone cement

One straight channel		**One curved channel**	
Parameter	**Contribution (%)**	**Parameter**	**Contribution (%)**
PX_1	35	PX_1	30
R	12	PZ_1	28
PZ_1	9	R	17

When augmenting with two channels of bone cement (straight or curved), Figure 5.5 shows the S/N ratios for the three most relevant factors. When the bone cement was distributed as two straight channels, those factors were the X, Y and Z coordinates of the first point of the first channel (PX_{1m}, PY_{1m}, PZ_{1m}). For PY_{1m} and PZ_{1m}, increasing or decreasing the original value (Level 2, from the region centroid) did not result in any improvement, suggesting these are approaching optimum values. In the case of two curved channels, the three most important parameters were the X coordinate of the first point of the first and second channels and the Y coordinate of the third point of the second channel (PX_{1m}, PX_{1n}, PY_{3n}). In both straight and curved channels, moving the X coordinate of the first point of the first channel (PX_{1m}) away from the femoral head improved the augmentation. Additionally, in both cases the location of the bone cement cylinder was a more influential factor than the volume of bone cement (radius of each channel).

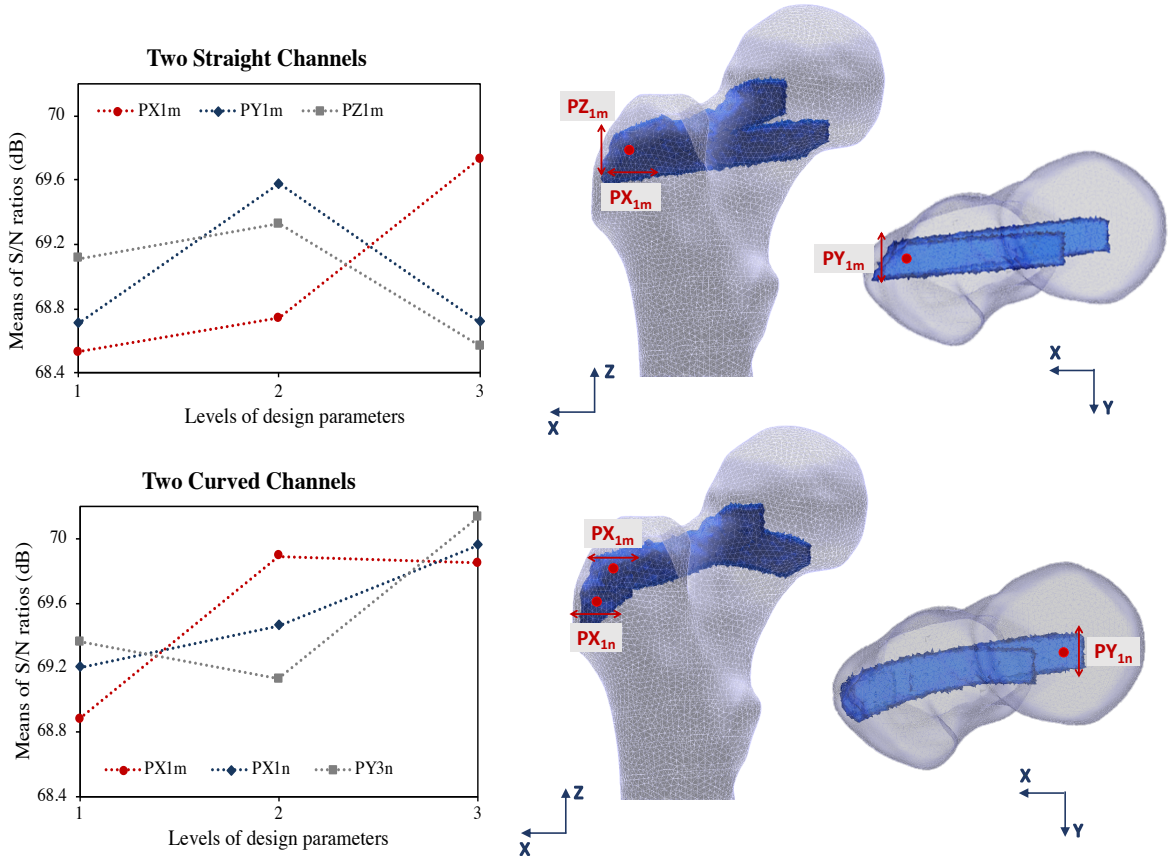

Figure 5.5: Taguchi S/N response curves for augmentation with two channels of bone cement.

As shown in Table 5.5, the three most important factors when augmenting the femur with two channels of bone cement were related to the position of such channels. These three factors account for 56% and 48% of the total contribution for two straight and two curved channels respectively. Furthermore, contribution of the channels' radii in the case of two straight channels is of greater significance (10% first channel, 8% second channel) than in the case of two curved channels (3% first channel, 4% second channel).

Table 5.5: Contribution of most relevant parameters in augmentation result with one channel of bone cement

Two Straight Channels		Two Curved Channels	
Parameter	**Contribution (%)**	**Parameter**	**Contribution (%)**
PX_{1m}	28	PX_{1m}	21
PY_{1m}	17	PY_{3n}	18
PZ_{1m}	11	PY_{1n}	9

The goals of the feasible bone cement distribution optimisation were to maximise yield load and minimise bone cement volume of the augmented femur. A comparison of these two parameters between optimised and non-optimised distributions when using three spheres of bone cement is presented in Figure 5.6. Results show that for both augmentation strategies (spheres in a straight line and in a curve), the optimisation achieved an increase in augmented yield load and a decrease in bone cement volume. Additionally, both strategies performed similarly, obtaining an average increase of 71% in the femur yield load with 8.6ml of bone cement.

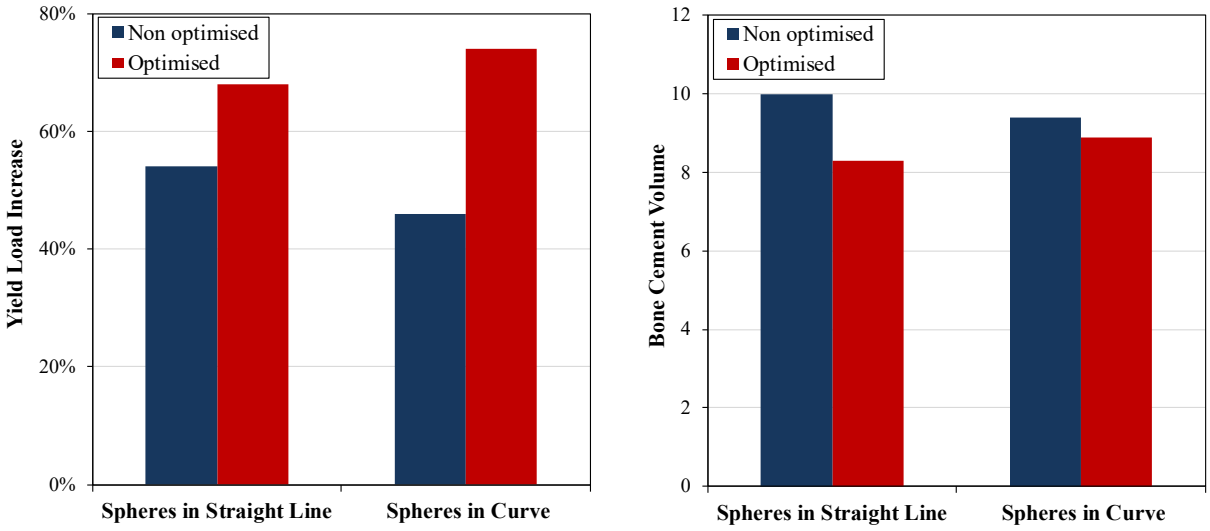

Figure 5.6: Yield load increase and bone cement volume for optimised and non-optimised augmentation with three spheres of bone cement.

The placement and radius of the spheres before and after optimisation is shown in Figure 5.7. The optimised distributions were similar for both strategies and consisted of placing bone cement in the superior aspect of the femoral neck, as close as possible to the cortical bone.

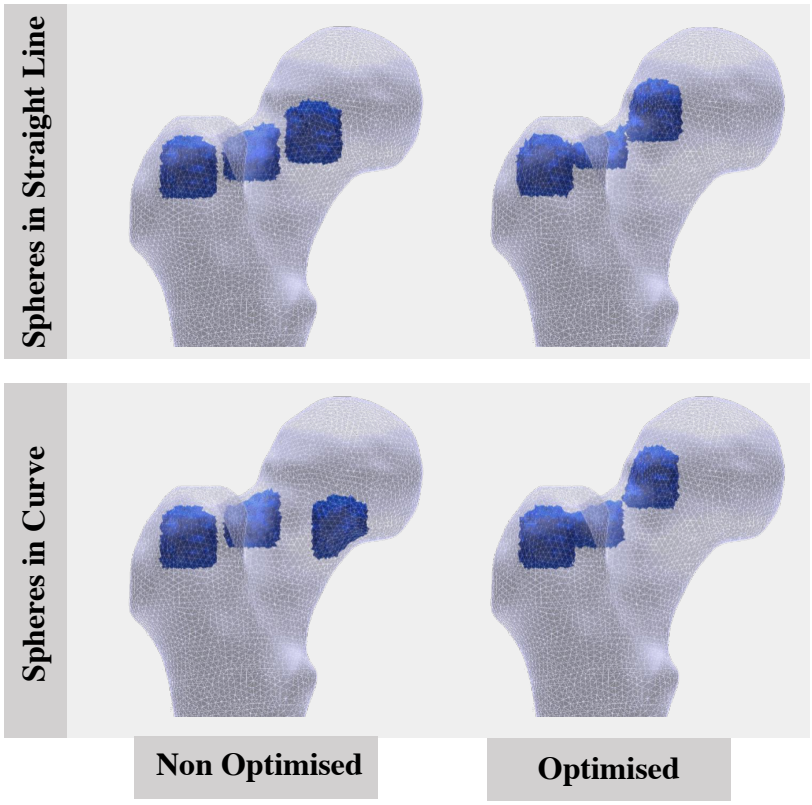

Figure 5.7: Bone cement distribution for optimised and non-optimised augmentation with three spheres of bone cement.

When augmenting the femur with bone cement channels, results show that the yield load increase was always higher in the optimised results compared to the non-optimised ones (Figure 5.8), with a maximum difference of 20%. Similarly, the optimisation reduced the required bone cement volume, especially in the cases involving two channels. Additionally, augmentation with two channels performed marginally better than augmentation with one channel (7% difference on average).

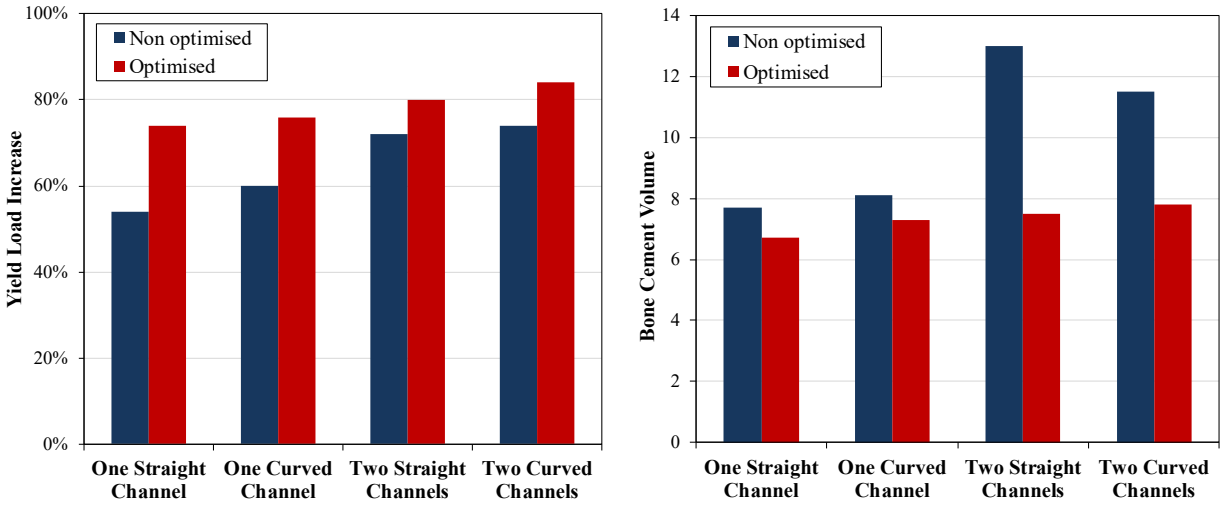

Figure 5.8: Yield load increase and bone cement volume for optimised and non-optimised augmentation with channels of bone cement.

With respect to the distribution of the bone cement inside the femur, Figure 5.9 shows the changes between non-optimised and optimised results. The non-optimised distributions for one straight and one curved channel were similar, although the curved channel was slightly more proximal. For the same cases, in the optimised distribution, the medial end of the bone cement channel was moved upwards. In the case of two straight and curved channels, there are significant differences between the optimised and non-optimised distributions. In the non-optimised distributions, one channel went from the greater trochanter to the superior part of the femoral neck and the other went from the greater trochanter to the inferior part of the femoral neck. However, in the optimised distribution, the main channel was placed from the greater trochanter to the superior part of the femoral neck and the other channel was located as reinforcement in the greater trochanter area. None of the optimised cases involved the reinforcement of the inferior part of the femoral neck.

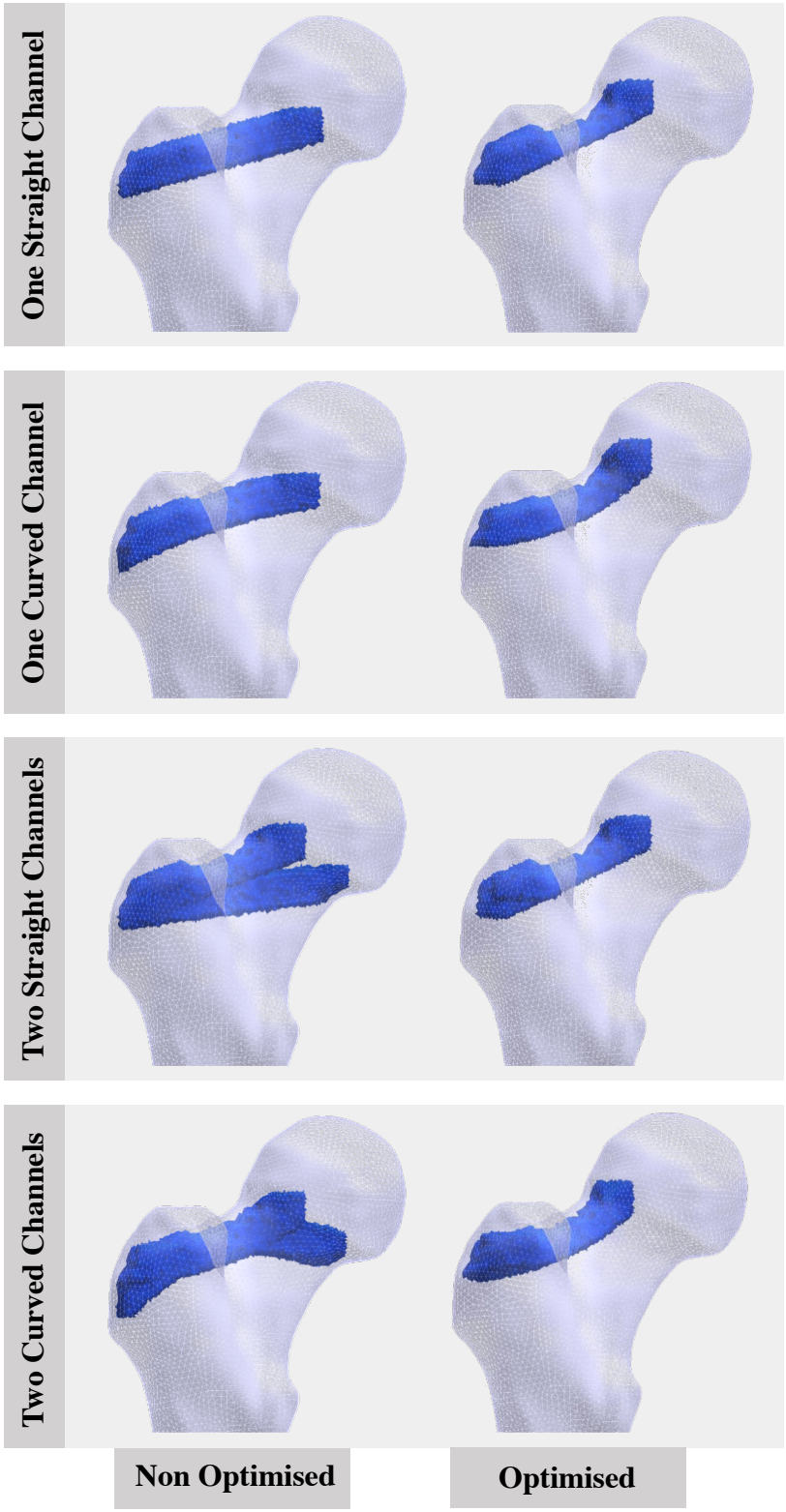

Figure 5.9: Bone cement distribution for optimised and non-optimised augmentation with channels of bone cement.

5.4 Discussion

Different femoral augmentation strategies have been proposed and studied in the past years. The most common ones consist of injecting small amounts of bone cement in specific locations (Basafa et al., 2015; Farvardin et al., 2019) and drilling one or several paths in the bone and filling them with bone cement (Beckmann et al., 2011; Fliri et al., 2013; Raas et al., 2016; Varga et al., 2017). In the present chapter, both approaches with some feasible variations were studied and optimised for a specific case of a femur with T-Score -2.5 under lateral fall boundary conditions.

Only small differences were found when augmenting the proximal femur with three spheres in a straight line or in a curve; the distributions of bone cement, Taguchi analyses and optimisation results were similar in both cases. In both cases, the Taguchi analyses identified the X coordinate, Y coordinate and radius of the first sphere as the main contributing factors to the augmentation result. Additionally, it was found that when these centroid points were moved away from their original location, the augmented yield load decreased. This was also true for the centroids of the other spheres except the X and Z coordinate of the third sphere, suggesting that the original distribution presented in Section 5.2.1 was close to an optimum solution. The *patternsearch* optimisation confirmed this, since in the optimised distributions the centroid of the first two spheres did not move significantly from their original location.

Optimisation results when augmenting the proximal femur with three bone cement spheres denoted the importance of reinforcing the greater trochanter and the superior aspect of the femoral neck. This optimised distribution is consistent with results found with the Evolutionary Structural Optimisation (ESO) algorithm presented by Basafa and Armand (2013). In these studies, the evolution of cement placement with the ESO algorithm showed that the first region to augment was the greater trochanter, followed by the femoral neck. In the present study, the optimised distribution resulted in an

average yield load increase of 71% (V_{PMMA}=8.6ml), while non-optimised cases led to a maximum 54% increase in the yield load (V_{PMMA}=10ml). A similar type of distribution and range of bone cement volumes were studied experimentally by Basafa et al. (2015) (average yield load increase 31.3% with 9.5ml of PMMA) and numerically by Farvardin et al. (2019) (average yield load increase 79.6% with 10ml of PMMA).

Taguchi analyses conducted for one channel of bone cement showed that channel radius was an important augmentation factor, contributing up to 17% to the result. This was expected since increasing the channel radius also increased the bone cement volume. However, the contribution of the X and Z coordinates of the first point of the channel were more significant and added to 44% and 58% for the straight and curved channel respectively. These results suggest that in such cases, bone cement placement played a more important role in femoral augmentation than the amount of bone cement. Similarly, results of Taguchi analyses for two bone cement channels (straight and curved) showed that path placement had a more important effect than path diameter on the augmentation result.

In the cases of augmentation with a single channel of bone cement (straight or curved), optimised results performed better than non-optimised results both in terms of yield load increase and bone cement volume. In these cases, optimised distribution for straight and curved channels was of similar topology and provided a similar augmentation level. This distribution consisted of placing bone cement in a channel in the superior region of the proximal femur that went from the greater trochanter to the femoral neck. Given that most proximal femur fractures due to a lateral fall initiate at the superior aspect of the femoral neck (de Bakker et al., 2009; Nawathe et al., 2014), reinforcing this region might help avoid the fracture. Moreover, results from this optimisation align well with the ones presented by Varga et al. (2017), who decided on the bone cement location through numerical analyses based on Wolff's law. Their results suggest that placing bone cement from the femoral head to the greater trochanter and ensuring cement contact with the superior cortex of the femoral neck provided better augmentation results than placing

bone cement aligned with the femoral neck axis. However, results in this chapter show that the optimum solution does not involve extending bone cement through the femoral head as presented by Varga et al. (2017).

When augmenting the osteoporotic femur using two drilled channels, the distribution of bone cement in the optimised and non-optimised cases are significantly different. The non-optimised distribution consisted of a V-Shape augmentation with the entry point in the greater trochanter area and provided a significant increase (50%) in the femur yield load. This augmentation strategy had already been studied by Raas et al. (2016); Fliri et al. (2013), who did not report significant improvements in the femur yield load. However, the entry point for their augmentation was located in the lateral cortex of the proximal femur, at the extension of the central neck axis. Beckmann et al. (2011) also performed a V-shaped augmentation but using two insertion holes. Their results showed that this strategy weakened the bone, possibly due to the damage to the cortical bone. In the present study, optimisation results for this case consisted of one channel in the superior part of the femoral neck and a second, smaller channel to reinforce the greater trochanter region. The optimised distributions showed higher yield loads than the non-optimised, suggesting that placing bone cement in the inferior part of the femoral neck may not be necessary.

Due to the large number of factors than can influence bone cement distribution for all the proposed approaches, the Taguchi analyses were limited to three levels of design parameters. However, even with this limitation the Taguchi analysis combined with an ANOVA test were a powerful tool to assess relative importance of bone cement volume and location factors in different augmentation strategies. The main conclusion from the Taguchi analyses was that, within the studied variables range, the bone cement location was more important than the bone cement volume in the augmentation result.

In all studied cases, the optimised feasible bone cement distributions provided better results than non-optimised distributions in terms of femur yield load increase and bone cement volume. Therefore, despite the original distributions derived from the centroids

of the ideal bone cement cloud resulted in significant improvements to femur yield load (up to 74% with 11.5ml of PMMA), results could still be improved. Additionally, starting from the ideal bone cement cloud was an important step as it decreased the size of some design variables and the computational time of the *patternsearch* optimiser. The maximum channel or sphere radii were design variables that also had to be limited to avoid potential bone damage when drilling the femur in practice. In the optimisation, the scalarisation method was used to convert a multi-objective function (minimise bone cement volume and maximise yield load) into a single function. To do so, different weights were given to the bone cement volume function and to the yield load function and this determined the performance priority and therefore the solution (Gunantara, 2018). Other approaches, such as the Pareto method or different weight distributions might affect the optimisation result and could be explored in the future.

When comparing all the optimised augmentation strategies (Figure 5.10) it is clear that performance using curved and straight paths is similar. Therefore, despite the slightly better performance of curved bone cement distributions, this is not enough to justify the additional work required to achieve this augmentation in practice. Additionally, given the similarities in bone cement distribution, the performance of augmentation with one or two channels was similar. After the optimisation, the yield load increase when injecting bone cement in the form of spheres or cylinders was also alike. Hence, given the similarity in the results, the choice between methods depends on which one is easiest to replicate in practice and would entail less practical and clinical risks. The main drawbacks of injecting spheres are the need for three injection points and a navigation system to control the location of each injection. Alternately, although injecting bone cement in a single path is easier to achieve in practice, the risk of bone thermal necrosis is potentially higher. While injecting three spheres of bone cement is a procedure that can be done in separate stages (waiting until polymerisation of a sphere finishes before starting the new injection), in the case of a cylinder all the bone cement should be injected at once.

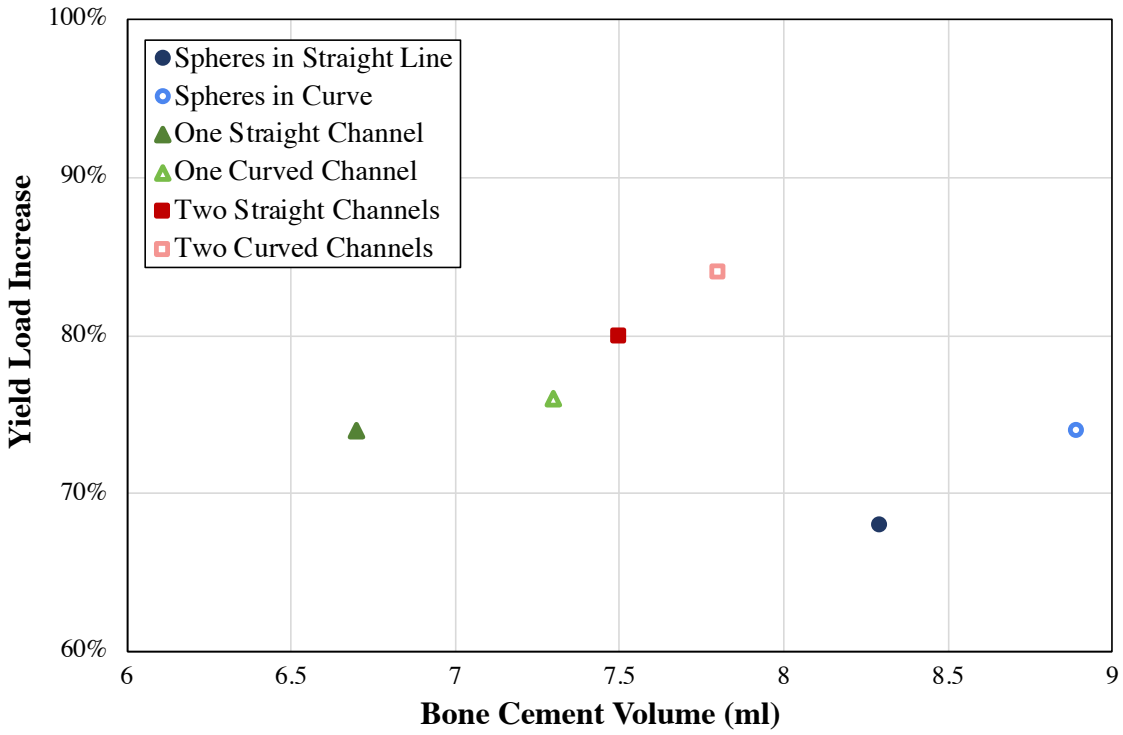

Figure 5.10: Yield load increase vs bone cement volume for all optimised bone cement distributions.

Chapter 6

Augmented and Non-Augmented Femur Fracture Prediction

6.1 Introduction

Several generalised augmentation strategies were proposed in Chapter 5 and tested in one femur with a specific level of osteoporosis (T-Score -2.5), with results suggesting that a significant increase in yield load could be achieved. However, experimental studies (Beckmann et al., 2011; Springorum et al., 2014; Basafa et al., 2015) have proven that the efficacy of femoral augmentation is highly dependent not only on the type, volume and location of bone cement but also on the original bone material properties. Additionally, given that osteoporosis will continue developing with time, it is of interest to understand how the result of the same augmentation strategy will change while the bone material properties degrade. Hence, in this chapter the increase of fracture load and energy to fracture was monitored in femora with different levels of osteoporosis after being augmented using the generalised strategies presented in Chapter 5.

The increase in fracture and/or yield load are the most commonly used parameters to

measure the effectiveness of femoral augmentation. However, it is also important to understand how introducing bone cement into an osteoporotic bone can affect its behaviour in case of a fracture. With this, it would be possible to determine if the augmented femur would present a worse fracture (in terms of ease of fixation and potential complications) than the non-augmented femur. Examining and comparing fracture location and patterns of augmented and non-augmented femora could provide this information. Using numerical approaches, few studies have developed a methodology to predict femur fracture load and crack propagation. Some employed the eXtended Finite Element Method (XFEM) and obtained small fracture paths (Marco et al., 2017; Ali et al., 2014), while others considered that modelling the degradation of material properties through a damage variable could be used to simulate bone fracture (Hambli et al., 2012; Hambli and Allaoui, 2013). Element deletion has also been investigated. (Marco et al., 2018), but presents more convergence problems than other approaches. Recently, Marco et al. (2018) compared different strategies and concluded that the degradation of bone mechanical properties approach presented the best results and performance.

The first objective of this chapter was to determine the increase in fracture load and energy to fracture of femora with different osteoporotic levels augmented with the generalised approaches presented in Chapter 5. The second objective was to study whether augmentation with bone cement changed the fracture pattern in the aforementioned cases, resulting in more complicated fractures. Finally, the third objective was to determine if small modifications applied to a single-cylinder augmentation strategy could improve the augmented fracture load.

6.2 Methods

6.2.1 Prediction of Femoral Fracture Load and Crack Propagation

All the femur FE (Finite Element) models developed in Section 3.2.1, with T-Score ranging from -1.0 to -3.5 were used within the computational studies of this chapter. Each femur mesh was imported to ANSYS Mechanical APDL to perform the Finite Element Analyses (FEA). The augmented tissue was modelled as a composite made of bone and porous bone cement. Material properties were computed by applying the Voigt-Reuss-Hill average and including bone cement porosity, as described in Section 4.2.1. For each femur, three different cases or augmentation strategies (specific volume of bone cement in a predefined location) were studied (Figure 6.1):

V0. Non-augmented femur.

V1. Femur augmented with one cylinder of bone cement. This distribution was the result of the single-path optimisation presented in Section 5.2.3. Bone cement was distributed in a cylinder aligned with the superior part of the femoral neck, starting at the greater trochanter and extending for a length of 7cm. Total volume of bone cement for this augmentation was 6.7ml.

V2. Femur augmented with two cylinders of bone cement. This distribution was the result of the two-path optimisation presented in Section 5.2.3. The first cylinder was aligned with the superior part of the femoral neck, starting at the greater trochanter and extending for a length of 6.5cm and the second cylinder was smaller and only reinforced the trochanter region. Total volume of bone cement for this augmentation was 7.5ml.

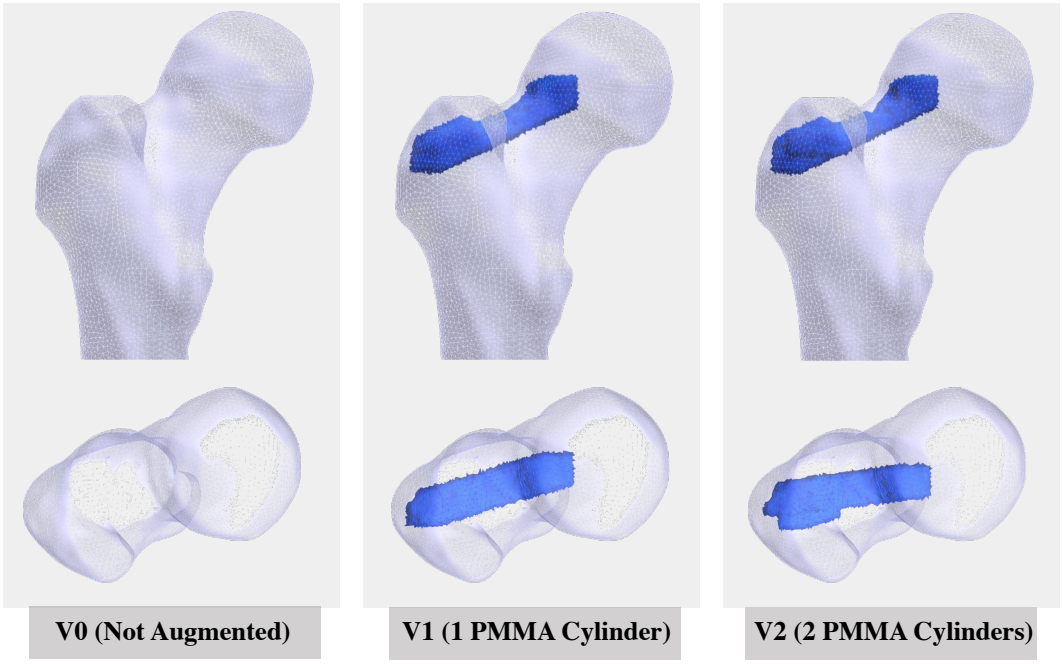

Figure 6.1: Non-augmented (V0) and augmented (V1, V2) cases studied in fracture analysis.

Boundary conditions replicating a lateral fall onto the greater trochanter were applied to each model (Figure 6.2). Surface nodes in the femoral head were coupled with constraint equations to node A, where a displacement was incrementally applied. The displacement was applied in X, Y and Z directions, corresponding to a rotation of the femur of 10° in the transverse plane and 15° in the frontal plane. Surface nodes in the greater trochanter were coupled with constraint equations to node B. In node B, displacement in X and Y directions was set to zero, while displacement in Z direction was unconstrained. Node C was then added to the mesh and attached with rigid beam elements to the distal end of the femur. In this node, all the displacements were constrained except the rotation around the Y axis. This set of boundary conditions is commonly used to replicate a lateral fall onto the greater trochanter in experimental studies (Dragomir-Daescu et al., 2011; Zani et al., 2015; Altai et al., 2019). Therefore, they have been changed from previous chapters to allow comparison between the load-displacement curves, fracture load and fracture patterns found in this chapter and experimental ones.

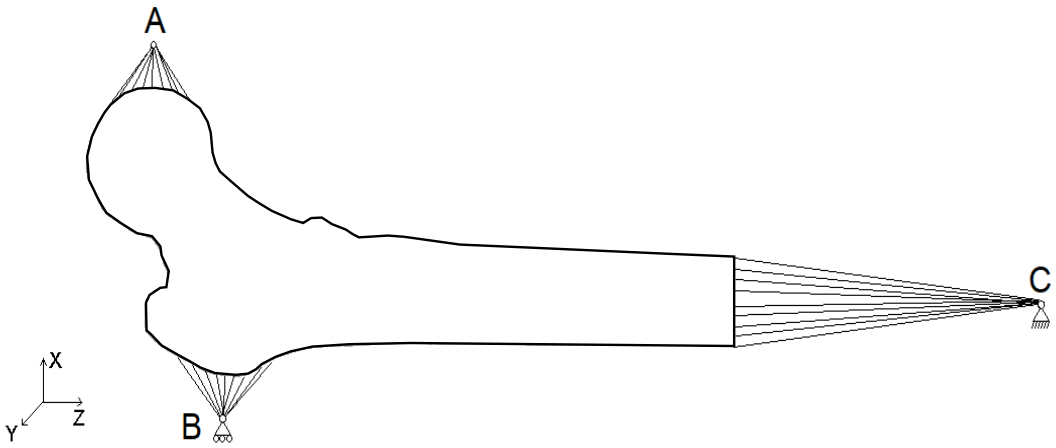

Figure 6.2: Lateral fall boundary conditions applied in fracture analysis.

In order to simulate crack propagation in the femur, a nonlocal damage model based on Continuum Damage Mechanics was included in the simulations (Hambli et al., 2012). An isotropic damage variable (D) was included to represent degradation of the elastic modulus during the loading process:

$$\tilde{E} = (1 - D)E \tag{6.1}$$

Where $\tilde{E}$ is the elastic modulus of the damaged material and E is the original elastic modulus of the material. The damage variable (D) was calculated using a damage law based on the averaged maximum principal strain of each element ($\bar{\varepsilon}_{max}$) at every step of the loading process:

$$D = 0 \quad ; \bar{\varepsilon}_{max} \leq \varepsilon_0 \tag{6.2}$$

$$D = \left(\frac{\bar{\varepsilon}_{max}}{\varepsilon_f} \right)^n \quad ; \bar{\varepsilon}_{max} < \varepsilon_0 < \varepsilon_f \tag{6.3}$$

$$D = 1 \quad ; \bar{\varepsilon}_{max} \geq \varepsilon_f \tag{6.4}$$

Where:

D = damage of each element

$\bar{\varepsilon}_{max}$ = averaged maximum principal strain of each element

Non-local averaging (Equation 6.5) was applied in order to prevent localization and ensure predictions were independent of mesh size. The maximum principal strain of each element was averaged over a neighbourhood of the element (elements located within a 1.5mm radius sphere):

$$\bar{\varepsilon}(x) = \frac{\sum_{i=1}^{n} \varepsilon_i}{n} \tag{6.5}$$

ε_0 = damage strain threshold representing damage start: 0.1% for both bone and bone cement (Wolfram et al., 2011).

ε_f = strain at fracture: 2.605% in tension and 2.1% in compression for the bone (Reilly et al., 1974) and 2.6% for the bone cement (Spierings, 2005).

n = damage exponent: 1.5 (Wolfram et al., 2011).

The crack propagation simulation was performed in ANSYS following an iterative procedure. Initially, a small displacement was applied to node A and using the previously described lateral fall boundary conditions, the FEA was solved. The averaged maximum principal strain (absolute value) and damage variable were computed for each element and the reaction force was calculated in node A. For each element:

- If $D = 0$, nothing was changed from the element.
- If $0 < D < 1$, the elastic modulus of the element was reduced by the value $1 - D$.
- If $D = 1$, the element was *killed* and its mechanical contribution to the stiffness matrix was set to zero.

When the model stiffness was updated, the displacement was increased, and the procedure was repeated until the reaction force in node A was smaller than 500N.

Additionally, this simulation was performed with three different meshes of a representative

femur (T-Score -2.5) (Figure 6.3) in order to verify the mesh independence of the damage law.

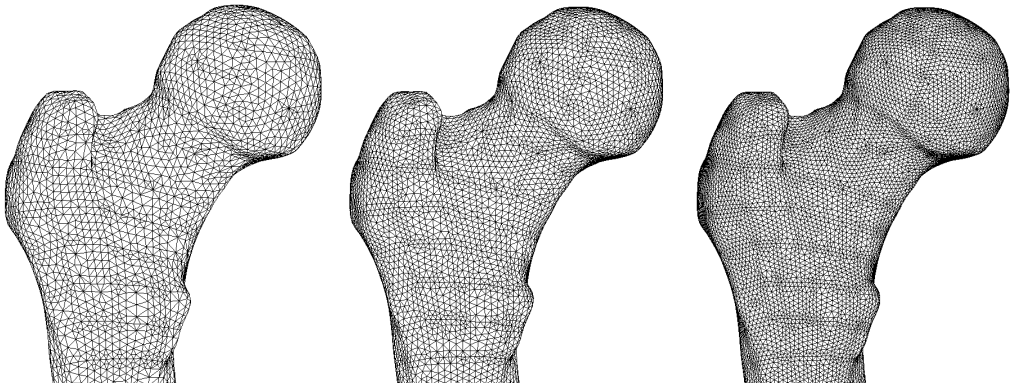

Figure 6.3: Meshes used in the mesh independency analysis for fracture prediction.

6.2.2 Patient-specific Bone Cement Distribution Based on Fracture Prediction

In order to find a patient-specific bone cement distribution for femur augmentation, an algorithm based on the ESO technique was developed. This method used the single-cylinder bone cement distribution (V1) as the initial point for the simulation and, if needed, added bone cement in the regions surrounding the cylinder. The procedure is detailed below:

Define the region of elements that can be augmented: those surrounding the initial bone cement region

Apply initial **displacement** and boundary conditions replicating a sideways fall

While the total PMMA volume is $<$ 12ml:

Run FEA

Apply damage law and find elements that fail

Select failed elements inside the region that can be augmented

Change material properties of those elements to bone cement

Select failed elements outside the region that can be augmented

Kill those elements

Increase the applied displacement and repeat

6.3 Results

Results of the mesh independence analysis performed for a representative femur using three different mesh sizes is shown in Figure 6.4. For each model, fine mesh results were used as reference to compare results generated with other meshes. The percentage difference in ultimate load between meshes remained less than 5% in all cases (4.95% and 2.01% for coarse and normal meshes respectively). Additionally, the shape of the predicted load-displacement curve was similar for all mesh sizes.

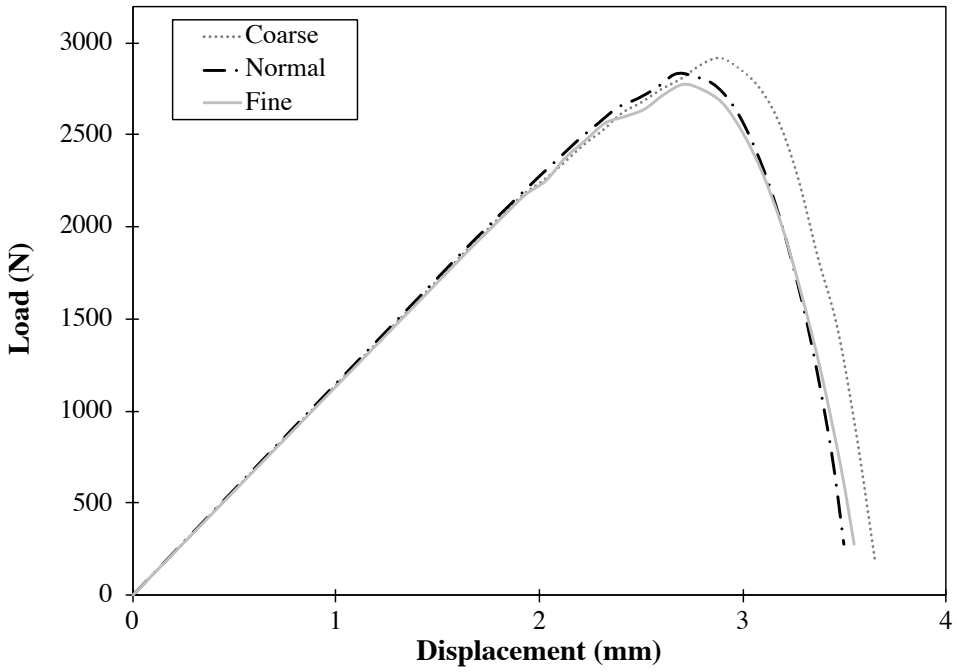

Figure 6.4: Predicted load-displacement curves for three different mesh sizes.

Figure 6.5 shows load-displacement curves for an osteoporotic femur with T-score -2.5 in its non-augmented state (V0) and after being augmented with one (V1) or two (V2) cylinders of bone cement. In all cases, the curves show initial linear behaviour followed by a nonlinear phase, when damage starts and grows. After this, there is a sharp decrease to the load indicating a fracture. The ultimate load of the non-augmented femur was 2778N, which increased by 62% when augmenting with one cylinder of bone cement and by 66% with two cylinders of bone cement.

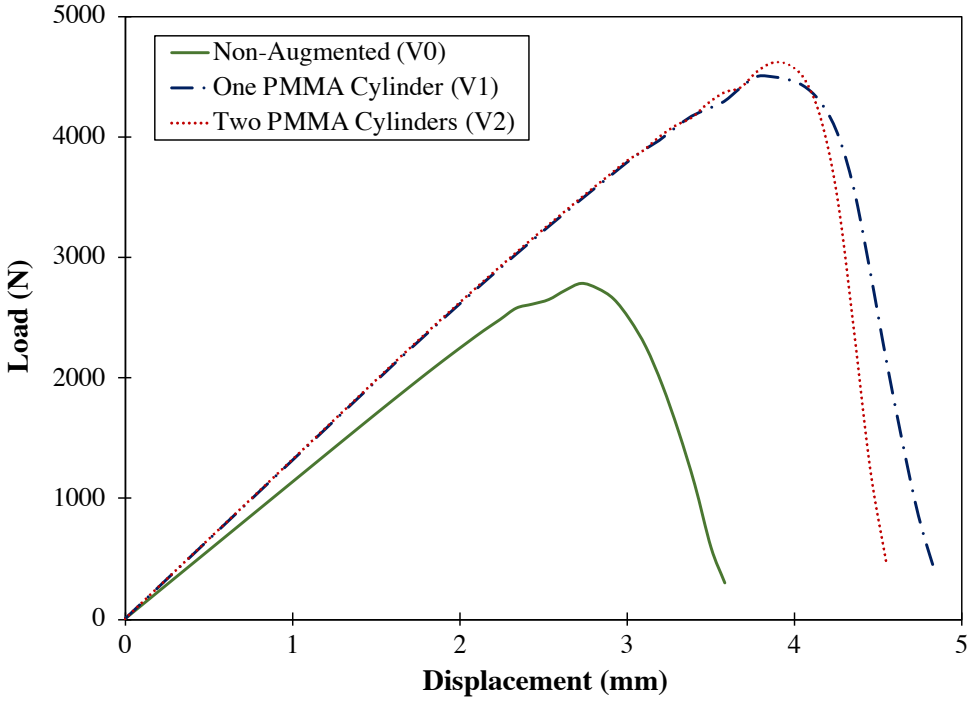

Figure 6.5: Load-displacement curve for augmented and non-augmented femur (T-Score -2.5).

The predicted fracture patterns for the femur with T-Score -2.5 are depicted in Figure 6.6. For the three studied cases, the main crack leading to fracture started in the superior part of the femoral neck, near the greater trochanter. However, the crack propagated differently depending on volume and location of bone cement. In the non-augmented case (V0), a single crack was developed that grew across the femoral neck. In the V1 case (one cylinder of bone cement) the main crack bifurcated, and a second, smaller non-fracture forming crack developed closer to the femoral head. When augmenting with two cylinders of bone cement (V2) the main crack bifurcated, moving the fracture slightly closer to the

femoral neck.

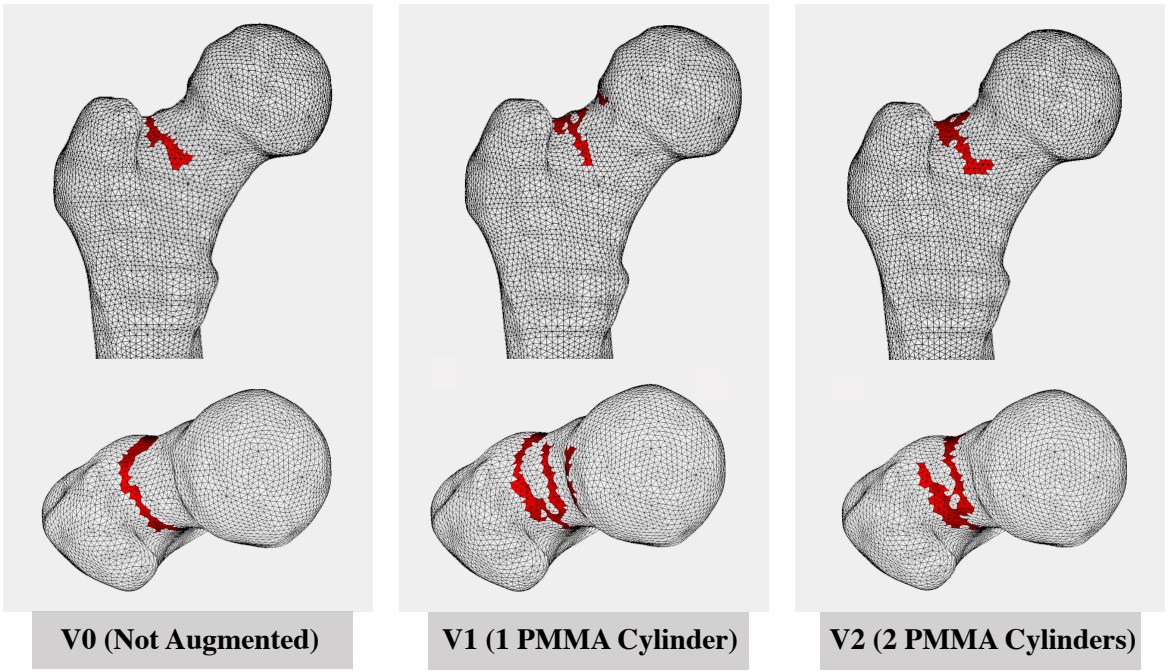

Figure 6.6: Femur fracture patterns in augmented and non-augmented femur model (T-Score -2.5).

Cracks leading to fracture can also be observed in a cross-sectional view of the femur. Final damage distributions of each simulation for three different augmented and non-augmented femora are shown in Figure 6.7, where $D = 1$ represents the failed elements. The main fracture pattern did not change significantly with the degree of osteoporosis or augmentation strategy. In all non-augmented cases (V0) there is a single path that leads to fracture, while in augmented cases (V1, V2) several cracks appeared in the superior cortex of the femoral neck. Despite these smaller cracks propagating less than the primary crack, they could contribute to create a comminuted fracture (fracture with multiple pieces and fracture lines). Furthermore, it can be observed that the differences between augmented and non-augmented fractures increase as the degree of osteoporosis increases.

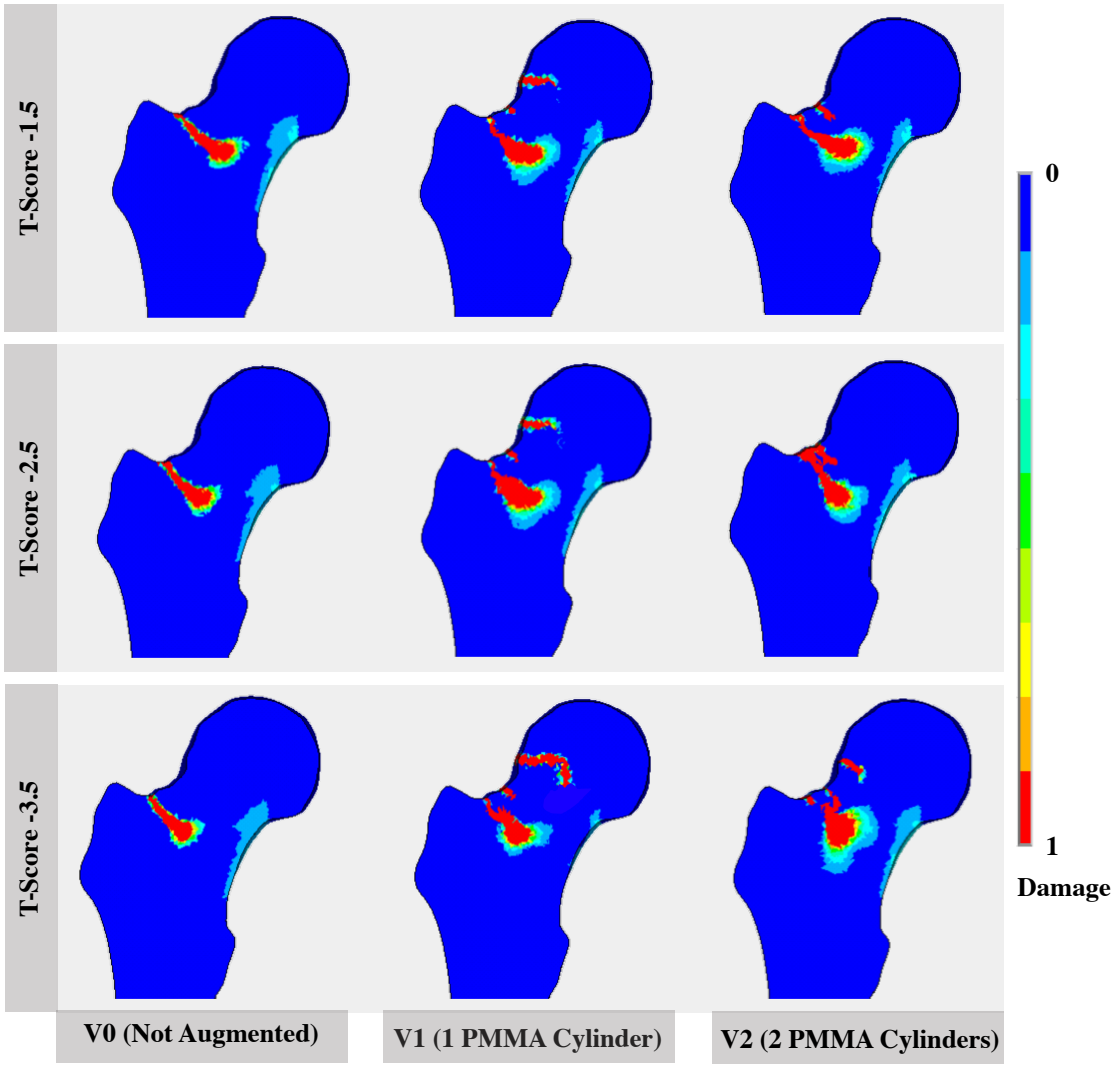

Figure 6.7: Damage at last step of simulation for different augmented and non-augmented femur models.

The fracture load and energy to fracture for all studied osteoporotic levels and augmentation cases are summarised in Table 6.1. For all T-Score levels, using one or two cylinders of bone cement led to a similar increase of the studied biomechanical properties. On average, when using the generalised augmentation strategies, fracture load and energy to fracture were increased by 52% and 81% respectively in osteopenic models (T-Score from -1.0 to -2.0) and by 72% and 126% in osteoporotic models (T-Score from -2.5 to -3.5).

Table 6.1: Fracture load and energy to fracture for all augmented and non-augmented femur models.

	Fracture Load (N)			**Energy to Fracture (J)**		
T-Score	**V0**	**V1**	**V2**	**V0**	**V1**	**V2**
-1.0	4330	6282	6397	9.29	15.56	15.54
-1.5	3752	5618	5789	7.87	14.50	14.62
-2.0	3257	4966	5219	6.74	12.62	13.05
-2.5	2778	4503	4614	5.75	12.47	11.75
-3.0	2283	3863	3929	4.65	10.53	10.11
-3.5	1864	3367	3393	3.70	9.23	8.99

In all studied cases, the relative increase in fracture load and energy to fracture decreased as non-augmented femoral strength increased (Figure 6.8). Hence, when using a constant volume of bone cement weaker bones obtained greater benefits after augmentation.

The relative increase in biomechanical properties when using the patient-specific distribution is shown in Figure 6.9. Results of generalised augmentations are also shown in the figure for comparison. Patient-specific augmentation performed significantly better than generalised distributions, but also required more bone cement (approximately 12ml). On average, when using patient-specific augmentation strategies, fracture load and energy to fracture were increased by 77% and 152% respectively in osteopenic models and by 93% and 203% in osteoporotic models.

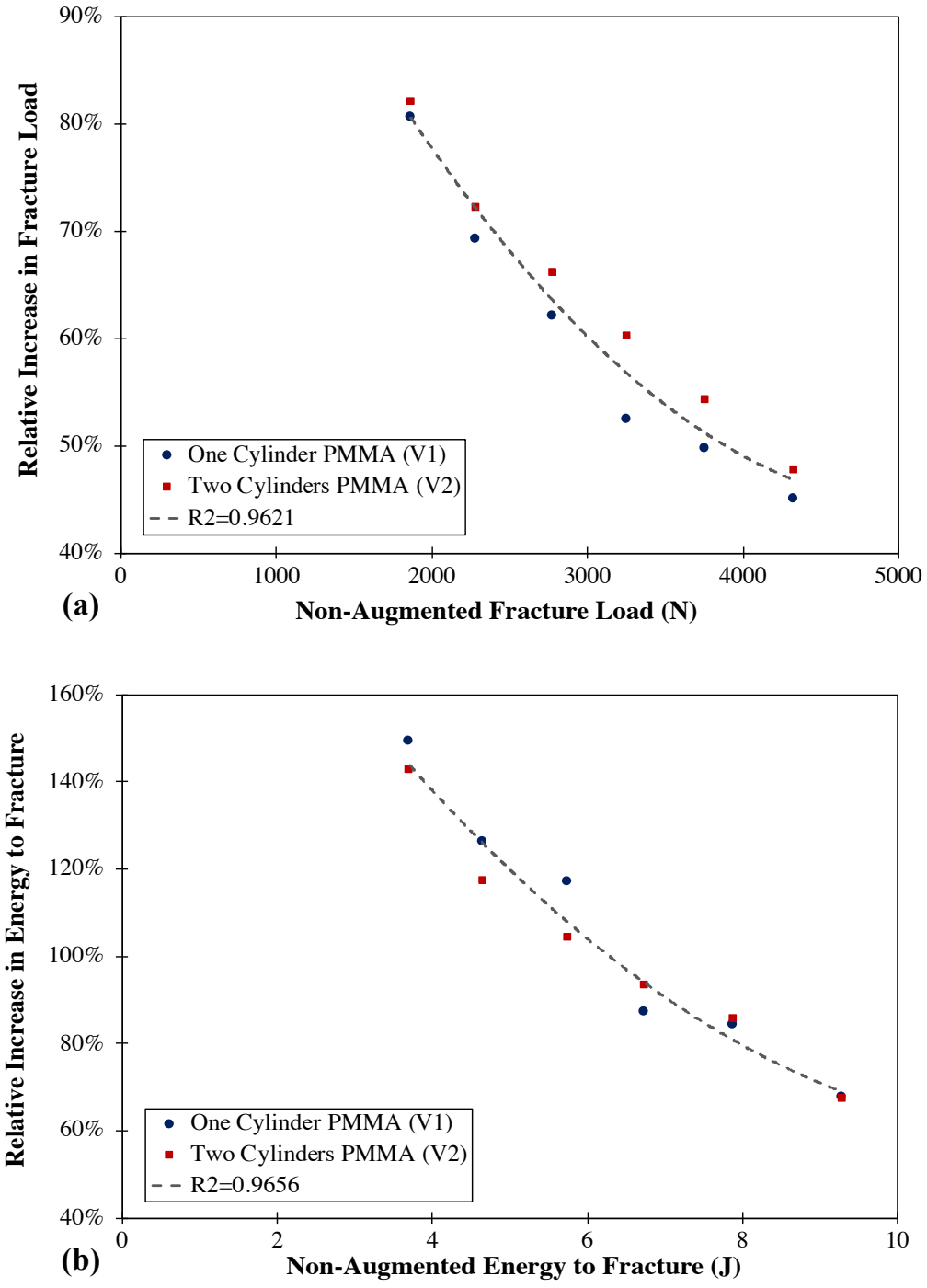

Figure 6.8: Relative changes in fracture load and energy to fracture for augmentation strategies V1 and V2.

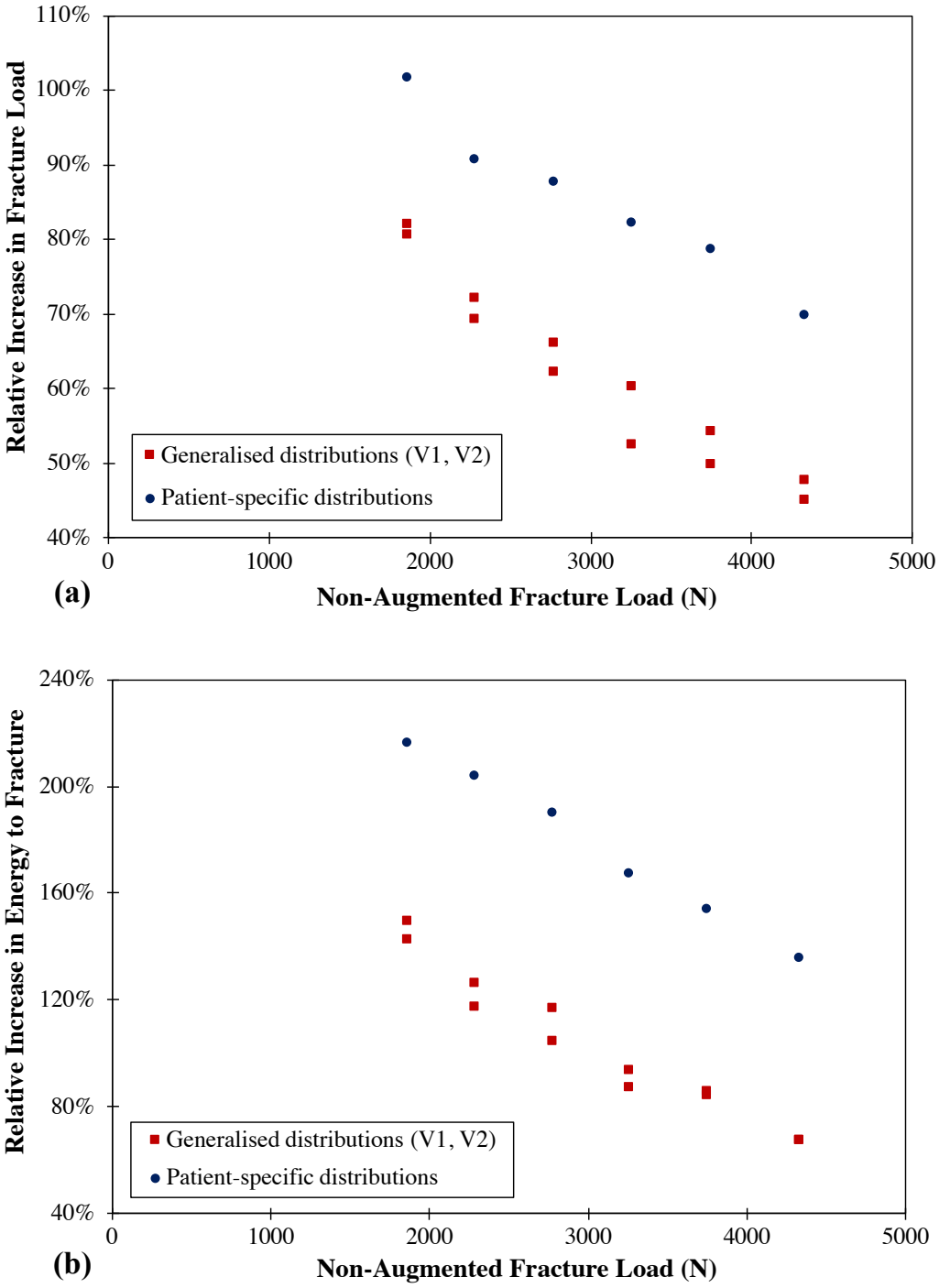

Figure 6.9: Relative changes in fracture load and energy to fracture for patient-specific augmentation.

Patient-specific bone cement distribution in the femur (for a T-Score of -2.5) is shown in Figure 6.10. The primary regions where bone cement was added were the medial part of the original cylinder and the superior aspect of the femoral neck. Similar distributions were created for all models with different T-Score levels.

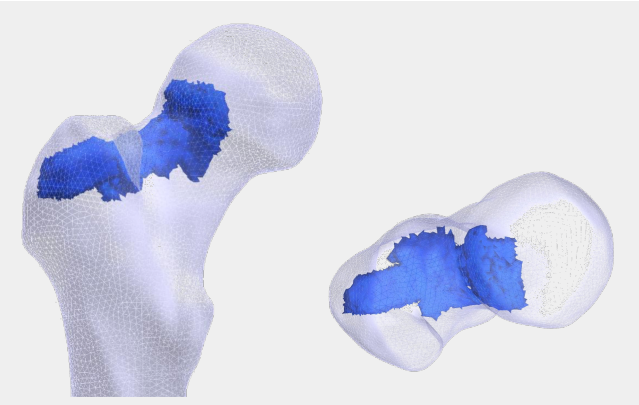

Figure 6.10: Patient-specific bone cement distribution for femur with T-Score -2.5.

6.4 Discussion

Mesh sensitivity is a common challenge when using FE methods to simulate damage and softening behaviour. When using local damage models, crack path and damage patterns are highly influenced by mesh orientation and size. In this case, as the mesh is refined, the failed region and energy dissipation shrink to unrealistic values. To avoid this issue, some proposed models include mesh regularization, consisting of adjusting the failure strain of each element based on its size (Hambli and Allaoui, 2013) or gradient-based nonlocal methods (Haider et al., 2018). In the present study, a nonlocal damage model was presented, where damage evolution was driven by an averaging of strains near a point. A similar technique, using weighted spatial averaging has been successfully applied in failure simulations of vertebral bone (Charlebois et al., 2010) and acrylic bone cement (Stolk et al., 2003). The method proposed in this chapter was implemented in a commercial FE package and tested through a mesh dependency analysis. Results showed

that the load-displacement curve and fracture pattern were not heavily influenced by mesh size, suggesting this technique can overcome mesh sensitivity issues.

In order to simulate bone fracture, a criterion based on the maximum principal strains in both tension and compression was incorporated in the damage model. Given the evidence suggesting that yield and fracture strain of bone tissue do not depend on bone density (Bayraktar et al., 2004; Morgan et al., 2004), fracture strain values were defined as constants (Reilly et al., 1974). However, some fracture models in the literature incorporate relationships between bone density and strain limit (Hambli and Allaoui, 2013; Dragomir-Daescu et al., 2011).

The predicted non-augmented femur fracture load ranged from 1864N to 4330N for a sideways fall configuration in femora with T-Score ranging from -1.0 to -3.5. On average, the femur fracture load for each T-Score was found to be 6% higher than the yield load calculated in Chapter 3. Failure loads for osteopenic and osteoporotic femora reported in this chapter were similar to the ones obtained in previous experimental studies that applied comparable loading conditions. For osteopenic femora, de Bakker et al. (2009) found an average fracture load of 3600N (average T-Score -1.74), similar to the fracture load of 3752N found in this chapter for the femur with T-Score -1.5. For osteoporotic femora, Schileo et al. (2014) found an average fracture load of 2516N (mean T-Score -2.97) and Pottecher et al. (2016) reported an average ultimate load of 2480N (mean T-Score -2.59). These are similar to the fracture loads of the femora with T-Score -2.5 and -3.0 presented in this chapter (2778N and 2283N respectively). Higher fracture loads have been found by Dragomir-Daescu et al. (2011) (average load of 4116N and 2362N for femora with average T-Score -1.78 and -3.47 respectively). Differences may be due to the femur lengths, differences in geometry and type of osteoporosis and/or load displacement rate (100mm/s for Dragomir-Daescu et al. (2011) and de Bakker et al. (2009); 17.5 to 32.5mm/s for Schileo et al. (2014)).

The fracture prediction study was also performed with augmented femora in order to identify the changes in fracture load and crack propagation. On average, augmenting

the femur with 7ml of bone cement in one cylinder (V1) increased the fracture load by 60% and the energy to fracture by 105%. These results can be compared to the experimental results of Beckmann et al. (2011); Springorum et al. (2014), who also injected bone cement in a single channel. Beckmann et al. (2011) performed a single centrodorsal augmentation using 12ml of bone cement and obtained a 35% and 164% increase in fracture load and energy to fracture respectively. Springorum et al. (2014) found similar results (33% increase in fracture load and 117% increase in energy until fracture), injecting less than 15ml of bone cement in a dorsocaudal drilling. In a computational study, Varga et al. (2017) also placed bone cement in cylindrical distributions and reported a 59% increase in fracture load with 12ml of bone cement. However, in their study bone cement extended through the femoral head, which may contribute to the difference in bone cement between this and the present study.

Results of this study also show that distributing 7ml of bone cement in two cylinders (V2), resulted in an average increase of 64% in fracture load and of 102% in energy to fracture. Femoral augmentation with two channels of bone cement (V-Shaped augmentation) has been experimentally performed in the literature by Fliri et al. (2013); Raas et al. (2016), resulting in increased energy to fracture but no changes in fracture load. However, in a V-Shaped augmentation the bone cement channel diverges from below the greater trochanter to the superior and inferior part of the femoral neck, while the two-channel distribution of this study consisted of one channel from the greater trochanter to the femoral neck and a small, second channel reinforcing the greater trochanter region. The superior performance of the augmentation strategies presented in this study, both in terms of bone cement volume and increase of strength, highlights the importance of bone cement placement in femoral augmentation. Furthermore, in agreement with previous computational and experimental studies (Springorum et al., 2014; Basafa et al., 2015; Varga et al., 2017), results presented in this chapter suggest that the effect of reinforcement is also related to original bone material properties (Figure 6.11). Therefore, using the same bone cement volume, weaker femora experienced a larger relative increase of biomechanical properties than stronger femora.

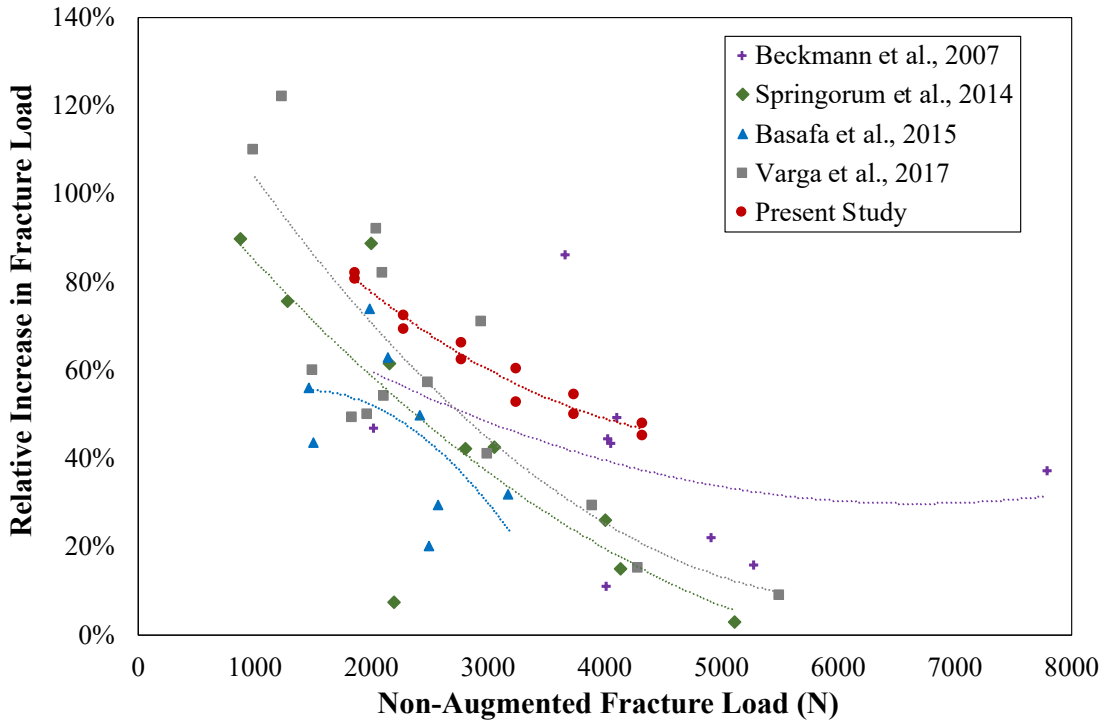

Figure 6.11: Relative increase in fracture load in previous femoral augmentation studies and present study.

Crack propagation leading to fracture in augmented and non-augmented femora was also studied in this chapter. According to (Cauley et al., 2009), fractures of the femoral neck and the intertrochanteric region account for over 90% of hip fractures and occur in nearly equal proportions. The type of fracture generally depends on multiple factors such as Bone Mineral Density (BMD), fall characteristics, sex, age and functional difficulties (Fox et al., 2000). In this study, femoral neck fractures were predicted for the six non-augmented femora. In all cases, fractures started with damage accumulation at the superior aspect of the femoral neck, and this damage increased and propagated through the neck. This is in agreement with the findings of de Bakker et al. (2009), who used loading conditions similar to the ones of this chapter and reported that femoral neck fractures initiate in the superior cortex of the neck due to high compressive strains and are followed by failure in the inferior aspect of the neck. Moreover, as can be seen in Figure 6.12 the fracture patterns obtained in this study are similar to fractures seen in experiments that apply lateral fall loading conditions (de Bakker et al., 2009; Dragomir-Daescu et al., 2011; Schileo

et al., 2014). Fracture paths of male, osteoporotic femora are shown, since the femur model of the present study is only valid for femora with senile osteoporosis (common in men).

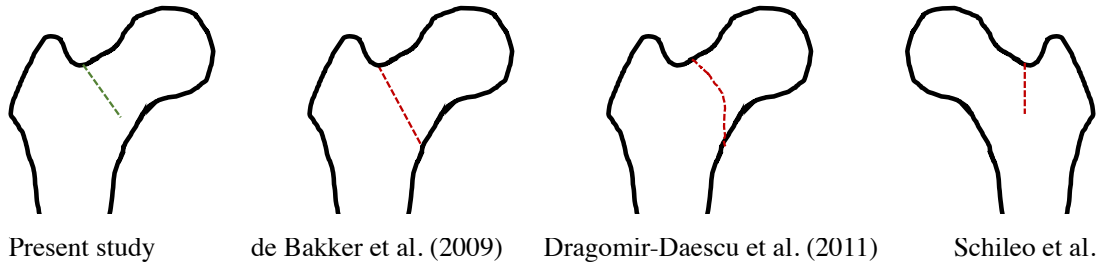

Figure 6.12: Fracture patterns obtained in previous experimental studies and in the present chapter.

Augmentation with approximately 7ml of bone cement increased fracture load but did not lead to significant changes in the main fracture path. This is consistent with previous experiments in the literature using less than 18ml of bone cement (Beckmann et al., 2011; Springorum et al., 2014) that reported no significant changes in fracture pattern or location after augmentation. Other experiments suggest that when using larger amounts of bone cement, fracture location changes significantly (Heini et al., 2004). Despite the main fracture location remaining unaltered, the present study shows that after augmentation, some smaller cracks were generated in different locations along the femoral neck. This suggests that fracture of an augmented femur could lead to a comminuted fracture and present complications in the fixation procedure. This phenomenon was also observed in the experiments performed by Beckmann et al. (2011), who reported an increase of multifragmentary fractures in the cemented femora. Additionally, as osteoporosis increased the changes between augmented and non-augmented fracture pattern also increased.

After studying the load-displacement curve and fracture pattern of bones augmented using two generalised strategies (V1, V2), a patient-specific distribution was found using an ESO algorithm. This distribution could be achieved in practice with two channels of bone cement diverging from the greater trochanter to the posterior and anterior region of the femoral head. Since osteoporosis was virtually introduced in the FE models (as

explained in Section 3.2.1), patient-specific bone cement distributions were similar for all T-Scores and patient-specific results are only applicable to the studied femur. Such configurations suggested that more reinforcement was needed in the superior aspect of the femoral neck, given it is the main region where fractures started. This bone cement distribution led to a higher increase of biomechanical properties than the two original distributions (average 85% increase in fracture load and 178% in energy to fracture). However, it also required a larger amount of bone cement (12ml) and was patient specific. The required increase in fracture load and energy to fracture in order to prevent an osteoporotic hip fracture in the event of a fall remains unclear (Fliri et al., 2013). Hence, it is difficult to decide whether the more complex injection pattern and increased bone cement volume in the patient-specific augmentation is justifiable.

Chapter 7

2D Modelling of Bone Cement Injection and Curing in Osteoporotic Femur

7.1 Introduction

Results obtained in previous chapters show that a predefined PMMA bone cement volume placed in a specific location can significantly improve the mechanical strength of osteoporotic femora. However, injecting bone cement into an osteoporotic bone presents certain risks that need to be investigated. Some potential complications of femoral augmentation are linked to bone cement leakage and increase of intraosseous pressure during the injection process (Xie et al., 2016). A further risk is thermal necrosis of tissues near the bone cement associated with the PMMA exothermic polymerisation process (Zeiser et al., 2008; Pearce et al., 2005). Additionally, shrinkage of bone cement during its solidification can lead to debonding or regions of high stress (Kwong and Power, 2006). Computational models could be able to predict some of the risks and

provide alternatives to minimise them. As an additional benefit, they could be used as a tool to support clinicians plan patient-specific interventions. Therefore, a first step is to study the flow behaviour of bone cement when injected into the trabecular bone. This will provide information about the bone cement distribution during injection and the possibility of developing non-filled cavities in the bone depending on factors like bone cement viscosity or bone cement porosity. Then, simulating the bone cement solidification process is necessary to evaluate the risk of thermal necrosis and regions of stress concentration.

Previous numerical work studying flow behaviour of bone cement in the femur focused on microscale models of trabecular bone specimens. In this field, Basafa et al. (2013) applied Smoothed Particle Hydrodynamics and created an experimentally validated model to study bone cement injection in small cubes of surrogate porous bone models. Similarly, Nawathe et al. (2014) investigated the flow of PMMA bone cement with different viscosities in small cubes with trabecular morphology using a Discrete Particle Model. Despite the limited extent of literature regarding the injection process in femoral augmentation, this matter has been examined using diverse computational approaches for vertebral augmentation. Meng (2008) employed Computational Fluid Dynamics (CFD) analysis to simulate PMMA flow into a macroscopic model of a vertebral body while applying Darcy's law. Given that this model omitted the trabecular microstructure of the bone, permeability values were extracted based on the Hounsfield Unit (HU) of the vertebral CT scan. Using the Theory of Porous Media (TPM), Bleiler et al. (2015) modelled simultaneously PMMA fluid flow and mechanical loading of the bone structure. Less common approaches such as lattice Boltzmann simulations (Zeiser et al., 2008) or time-lapse CT (Stadelmann et al., 2016) have also been used to investigate bone cement injection in vertebral bodies. However, one important difference between vertebral and femoral augmentation is the injection procedure. While in vertebral augmentation the cannula used to inject the bone cement does not move, in femoral augmentation the cannula is initially inside the bone and is retracted while injecting. Given this is an issue related to femoral augmentation that should be studied

with a macroscopic model, none of the aforementioned studies have adequately investigated bone cement flow under femoral augmentation conditions.

Developing a model of bone cement flow in femoral augmentation is a first step that should be followed by the simulation of the PMMA polymerisation process inside the bone. Generally, this process involves an exothermic reaction from the curing process and both chemical and thermal deformation in the bone cement. Some authors have focused on the temperature distribution in the bone cement during the curing process. For instance, Hansen (2003), who developed a heat transfer model based on the principles of polymerisation kinetics and Farvardin et al. (2018), who studied temperatures developed in a 3D model of augmented femur using data from experimental measurements. Stanczyk and Rietbergen (2004) also studied the temperature distribution at the bone-PMMA interface using a microstructural model of bovine trabecular bone. Other authors have proposed methods to simulate both heat transfer and PMMA deformation related to the polymerisation process. In this field, Pérez et al. (2009) evaluated temperature distribution and residual stresses after polymerisation for an idealised femoral stem, using a coefficient of thermal expansion dependant on the PMMA elastic modulus to model deformation. A similar approach was presented by Briscoe and New (2010), but shrinkage was modelled proportional to the degree of polymerisation. However, in both studies only a thin layer of bone cement was analysed in the context of prosthesis fixation, which differs from bone cement distributions required in femoroplasty. Using a trabecular microstructural model, Landgraf et al. (2015) simulated bone cement injection and solidification. Both chemical and thermal shrinkage were modelled, although the methodology was not applied to a full-scale model of the bone. None of the aforementioned macroscopic studies analyse the debonding that might occur between the bone and the PMMA. In this field, Hung and Chang (2010) modelled the debonding behaviour at the interface of these two materials measuring tensile and shear strength and validated their results experimentally. Similarly, Pérez and Palacios (2010) developed a more complex FE model to simulate the debonding process considering damage accumulation due to

normal and shear stresses.

The first objective in this chapter is to develop a 2D CFD model that can simulate bone cement injection in the framework of femoral augmentation and be applied to a macroscale femur model. Different injection velocities were studied and PMMA distribution and intraosseous pressure were monitored. After studying bone cement flow, the second objective was to simulate bone cement polymerisation inside the femur considering heat transfer as well as chemical and thermal expansion/shrinkage. Shear stresses at the PMMA-bone interface were examined and used to evaluate potential debonding regions.

7.2 Methods

7.2.1 Simulation of Bone Cement Injection

The simulation of bone cement injection was performed in a 2D femur model created using the CT scan and methodology described in Chapter 3. In order to replicate the femoral augmentation procedure, a cannula was included in the model as depicted in Figure 7.1. The diameter and length of the path drilled in the femur were 7mm and 67mm respectively. A triangular, unstructured mesh of the 2D femur and cannula was created, including boundary layers in the cannula walls.

Trabecular bone in the proximal femur is formed of bone tissue and bone marrow. However, given the complex structure of the trabecular bone tissue, simulating the flow of cement in a femur using micro-scale detailed geometry would result in a complex and computationally intensive model. For this reason, bone tissue was represented as a porous continuum medium filled with bone marrow. Bone marrow in the trabecular tissue was defined as a Newtonian fluid with constant viscosity (material properties according to Landgraf et al. (2015)). The fluid flow through a porous media is described

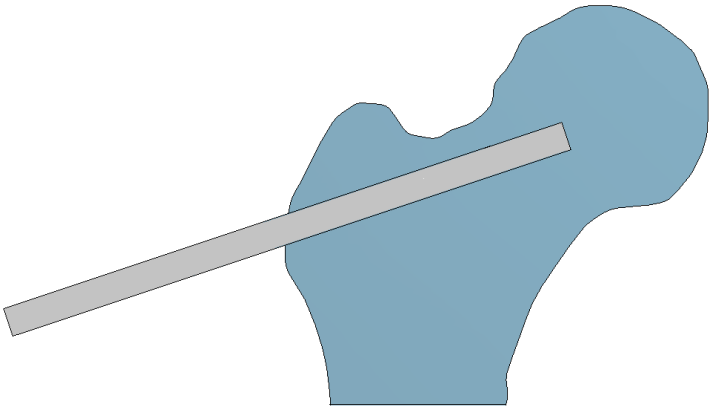

Figure 7.1: 2D femur and cannula model.

by the Darcy equation (Equation 7.1):

$$q = -\frac{kA}{\eta}\frac{dp}{dL} \tag{7.1}$$

where k is the permeability, representing the ability of the medium to transmit fluids; q is the volumetric flow; dp/dL is the pressure drop per unit length; η is the kinematic viscosity of the fluid; and A is the cross-sectional area.

The permeability of bone tissue depends on the morphological properties of the trabecular tissue and is independent of the nature of the fluid (Daish et al., 2017). In this study, the permeability of each bone tissue element was characterized as isotropic and as a function of bone porosity according to Equation 7.2 (Baroud et al., 2004):

$$k = B\frac{\psi}{1-\psi} \tag{7.2}$$

Where ψ is the bone porosity and B is a phenomenological parameter ($0.394 \cdot 10^{-8} m^2$) according to Baroud et al. (2004)). Bone porosity in an element is defined as the proportion of space not occupied by bone tissue and therefore, was calculated for each mesh element according to Equation 7.3:

$$\psi = 1 - BVF \tag{7.3}$$

Where BVF is the Bone Volume Fraction of each element, previously calculated in Chapter 4.

PMMA bone cement was modelled as a non-Newtonian fluid with shear thinning behaviour, which implied viscosity decreased as shear rate increased. To replicate this behaviour, PMMA viscosity was modelled in ANSYS Fluent with a User Defined Function (UDF) relating viscosity of PMMA (η), shear rate (γ) and time elapsed after mixing (t) as shown in Equation 7.4. This power law has been previously used in the literature to describe pseudoplastic and rheopectic behaviour of bone cements (Baroud and Yahia, 2004).

$$\eta = \left(a\frac{t}{t_s} + b\right)\left(\frac{\gamma}{\gamma_s}\right)^{c\left(\frac{t}{t_s}\right)+d} \tag{7.4}$$

Where a, b, c and d are constants that depend on the material. For this work, parameters of SimplexP bone cement were used ($a = 590$; $b = -1048.8$; $c = -0.026$; $d = 0.29$) (Baroud and Yahia, 2004). Characteristic time (t_s) was set to 1min and shear strain rate (γ_s) to $1s^{-1}$. Also, for the simulation it was considered that the cement injection started two minutes after mixing the PMMA. Material properties for both fluid phases are summarised in Table 7.1.

Table 7.1: Material properties for CFD simulation

Properties	**Bone marrow**	**PMMA**
Density, kg/m^3	1060	1480
Specific Heat, J/(kgK)	2670	1200
Thermal Conductivity, W/(mK)	0.28	0.25
Viscosity, kg/(ms)	0.0375	Eq. 7.4
Reference Temperature, K	310.15	293.15

The injection of bone cement into the bone was simulated using the CFD software ANSYS Fluent. An unsteady laminar flow in the porous medium was modelled to analyse flow characteristics and distribution of PMMA inside the femur. The simulation was conducted

using the Volume of Fluid (VOF) method for two immiscible fluids: bone marrow and PMMA bone cement. The VOF model is a surface-tracking technique designed for two or more immiscible fluids where the position of the interface between the fluids is of interest (Hirt and Nichols, 1981). Hence, at each time-step, the volume fraction (φ_{bc}) of each cell was computed according to:

$$\varphi_{bc} = 1 \quad \text{Bone Cement Cells} \tag{7.5}$$

$$0 < \varphi_{bc} < 1 \quad \text{Interfacial Cells} \tag{7.6}$$

$$\varphi_{bc} = 0 \quad \text{Bone Marrow Cells} \tag{7.7}$$

The variable φ_{bc} defines the volume fraction of the bone cement phase within a finite volume cell. Thus, $\varphi_{bc} = 1$ describes a finite volume cell containing only bone cement and a value of $\varphi_{bc} = 0$ denotes a cell containing only bone marrow. According to its volume fraction, the variables and properties in any given cell are either purely representative of one of the phases, or representative of a mixture of the phases.

The computational domain used for this study included the proximal femur and a retractable cannula. An inlet boundary condition, where PMMA entered the computational domain was defined at the right end of the cannula. Three different PMMA injection velocities were studied: 3.75mm/s, 7.5mm/s and 11.25mm/s. At the other side of the cannula, both phases could exit the domain through the outlet, which was set to atmospheric pressure. A dynamic mesh condition was created to simulate retraction of the cannula (at a velocity of 7.5mm/s) as the bone cement entered the domain. The rest of boundaries were defined as non-slip adiabatic walls. The temperature of bone marrow was set to 37°C to replicate the human body temperature and the PMMA temperature was set to ambient temperature (20°C). An initial pressure of 2.3kPa was also assigned to the bone tissue in order to simulate the average intraosseous pressure in the femur (Wingstrand et al., 1985). Furthermore, it was assumed that the computational domain did not contain any bone cement in the initial state.

7.2.2 Thermal-Structural Analysis of Bone Cement Polymerisation

After the injection simulation, the polymerisation of PMMA inside the bone was studied using FEA. The numerical model that defined the PMMA curing process was an adaptation of the one presented by Baliga et al. (1992); Lennon and Prendergast (2002); Pérez et al. (2009). In this model, the polymerisation fraction (p) of cement was defined as the ratio of the heat generated (S) at a time (t) divided by the total amount of heat liberated per unit volume during the complete polymerisation process ($Q_{tot} = 0.121 J/mm^3$ according to Maffezzoli et al. (1997)):

$$p = \frac{\int_0^t S dt}{Q_{tot}} \simeq \frac{\sum_{i=1}^{n} S_i \Delta t_i}{Q_{tot}} \tag{7.8}$$

The heat generation rate (S) was assumed to be a function of temperature and polymerisation fraction (p):

$$S = R(T) p^m (1-p)^n \tag{7.9}$$

Where R is an empirically obtained temperature-dependent function taken from the literature (Baliga et al., 1992) and m and n are equal to 1. Therefore, the following kinetic equation governed the bone cement polymerisation:

$$\dot{p} = \frac{1}{Q_{tot}} R(T)(p - p^2) \tag{7.10}$$

The modulus of elasticity of PMMA at every instant depended on the modulus of elasticity of the solidified PMMA ($E_{solidif} = 2300 MPa$) and the degree of polymerisation (p). This approach to simulate solidification, shown in Equation 7.11 was also adopted by Pérez and Palacios (2010).

$$E = E_{solidif} \cdot p \tag{7.11}$$

Material properties of bone tissue were derived from the CT scan following the methodology presented in Section 3.2.1.

A new assumption in the proposed computational model was the consideration of both thermal expansion ($\varepsilon_{thermal}$) and chemical shrinkage ($\varepsilon_{chemical}$) independently. Thermal expansion was modelled using a constant coefficient ($\phi = 72.2 \cdot 10^{-6} K^{-1}$) and chemical shrinkage was linearly related to the degree of polymerisation, with a maximum value of 2.56% (Gilbert, 2006).

$$\varepsilon_{total} = \varepsilon_{thermal} + \varepsilon_{chemical} \tag{7.12}$$

$$\varepsilon_{total} = \phi(T - T_{ref}) + (-2.56) \cdot p \tag{7.13}$$

This numerical model was applied to the 2D femur model and implemented in Matlab R2019. ANSYS Mechanical APDL was used in batch mode to solve the transient thermal-structural analysis at each time step. Results from the CFD simulation of Section 7.2.1 ($V_{injection}$=7.5mm/s) were exported as two files: one that contained the distribution of PMMA in the bone and other that contained the mesh of the model and the temperature field. These two files were combined and converted to Ansys Parametric Design Language (APDL) using a custom Matlab script.

A very small initial polymerisation fraction ($p=10^{-6}$) was defined for the first time step and after this, analyses were performed using a time increment of 1s for a total time of 1000s. Thermal boundary conditions were defined at the external femur walls: heat convection with ambient temperature of 20°C and a film coefficient of 1000W/(m^2K). Also, displacement of all external nodes of the bone (cortical tissue) were fixed. The complete iterative procedure is depicted in Figure 7.2.

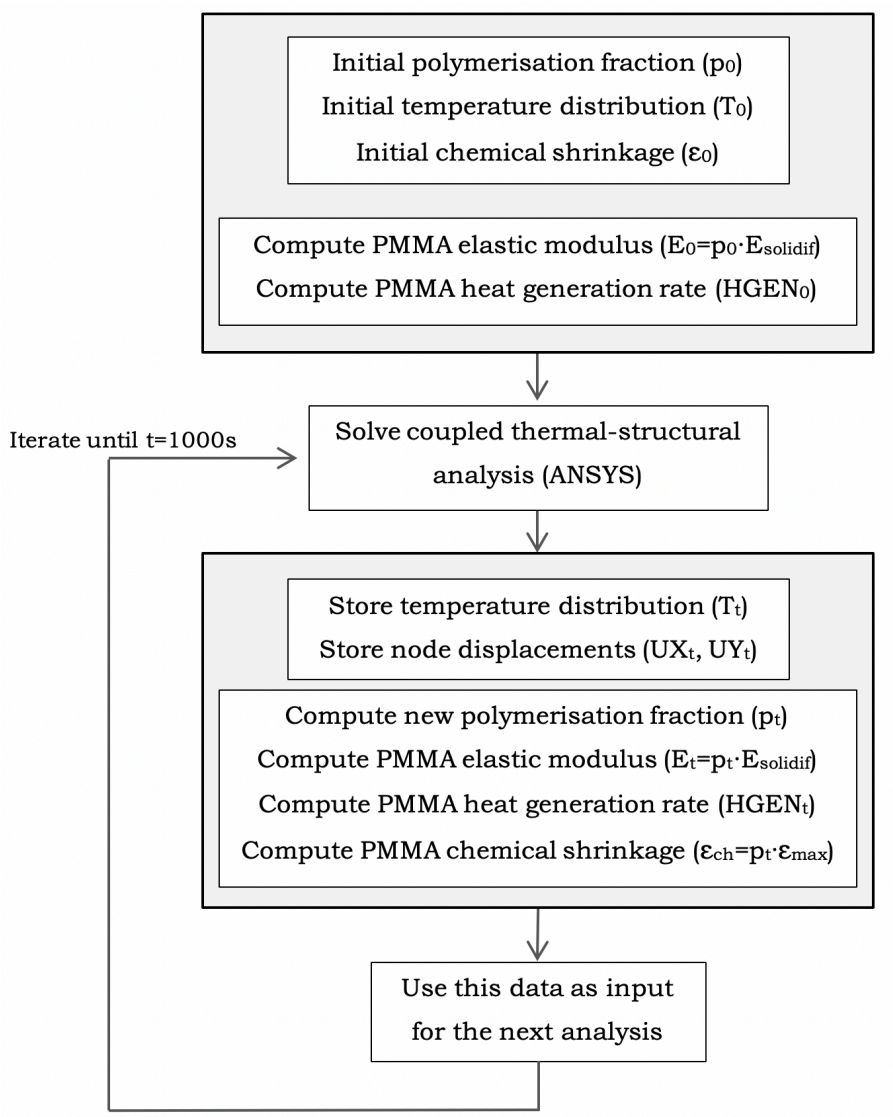

Figure 7.2: Algorithm for the simulation of bone cement polymerisation.

7.3 Results

The bone cement distribution at different stages of the injection process ($V_{injection}$=7.5mm/s) and cannula retraction are shown in Figure 7.4. In the figure, a PMMA volume fraction of 1 represents a cell containing only bone cement and a PMMA volume fraction of 0 represents a cell containing only bone tissue. The injection was

completed after approximately 8.5 seconds and due to the cannula retraction, the bone cement was able to fill the drilled cavity homogeneously.

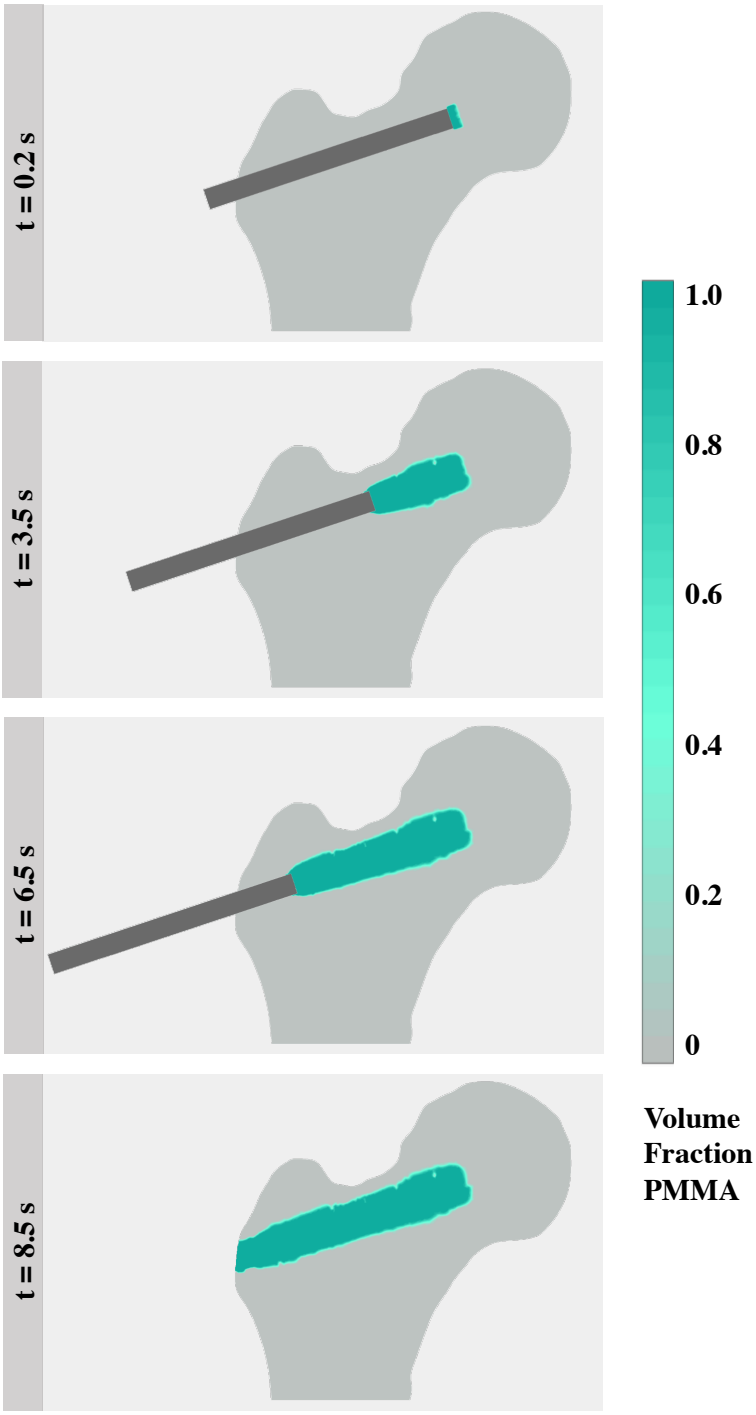

Figure 7.3: PMMA distribution at different time steps of the injection process.

Three different PMMA injection velocities (3.75mm/s, 7.5mm/s and 11.25mm/s) were studied, resulting in changes to the amount of injected bone cement. The final PMMA distribution for each aforementioned configuration is shown in Figure 7.4, covering an area of 6.3cm^2, 8.3cm^2 and 10.7cm^2 respectively. Assuming that bone cement spreads similarly in the third dimension, this would be equivalent to injecting 4.1ml, 7.3ml and 12.2ml of PMMA.

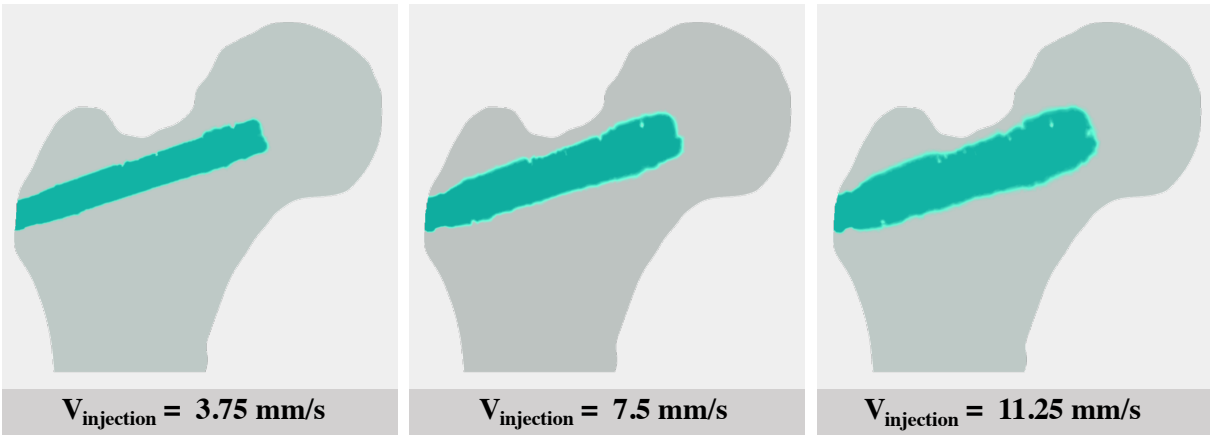

Figure 7.4: Final PMMA distribution for different injection velocities.

The average intraosseous pressure was also monitored during PMMA injection and is depicted in Figure 7.5. In all models, an initial intraosseous pressure of 2.3kPa was defined, which can be observed at t=0s. After this, pressure increased at different rates depending on the bone cement injection velocity. Higher velocities resulted in larger amounts of PMMA being injected and subsequently higher pressure. Maximum pressure increase recorded for each injection velocity was 6.45kPa (at 3.75mm/s), 10.52kPa (at 7.5mm/s), and 18.65kPa (at 11.25mm/s).

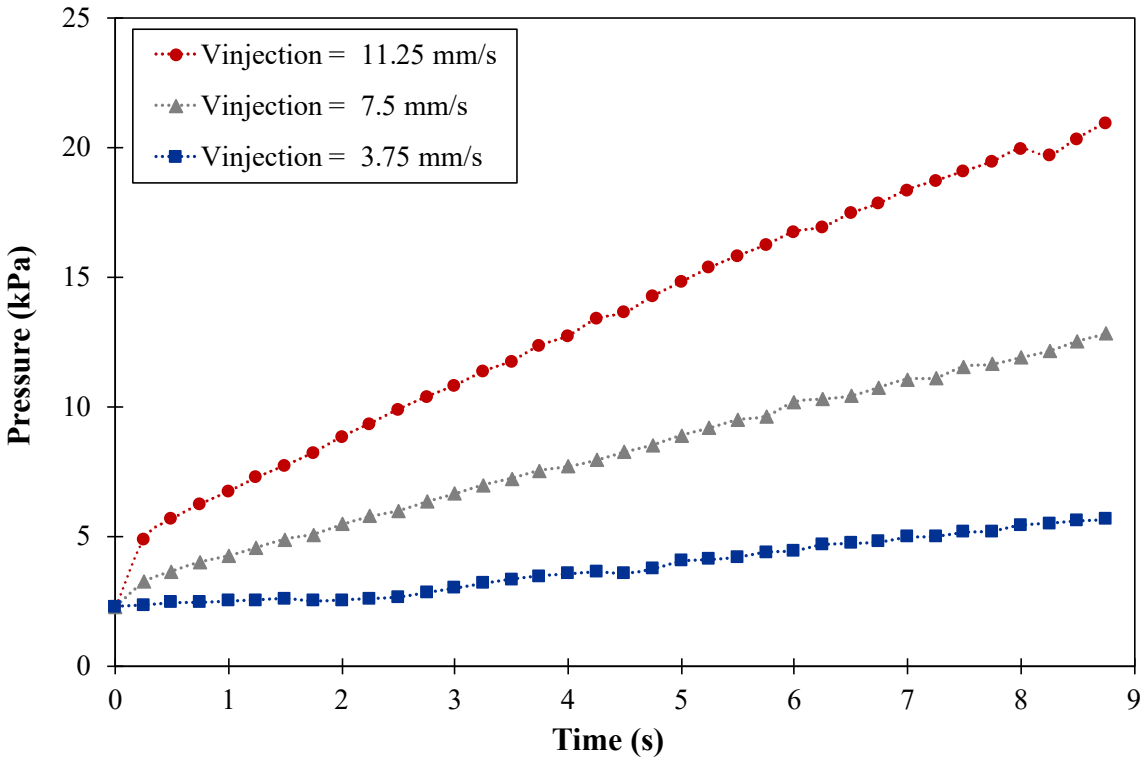

Figure 7.5: Pressure vs Time for all studied cases.

After the CFD analysis, a transient thermal-structural FE simulation was conducted to replicate the bone cement curing process. Figure 7.6 shows the evolution of the polymerisation fraction (p) over 1000s of the simulation in all the PMMA domain (shown in grey). The average degree of cure was also plotted (shown in red), which reaches a value of 1 approximately 400s after the simulation starts. It can be seen that the chemical process of polymerisation was different for each element yet completed within the specified time in all cases.

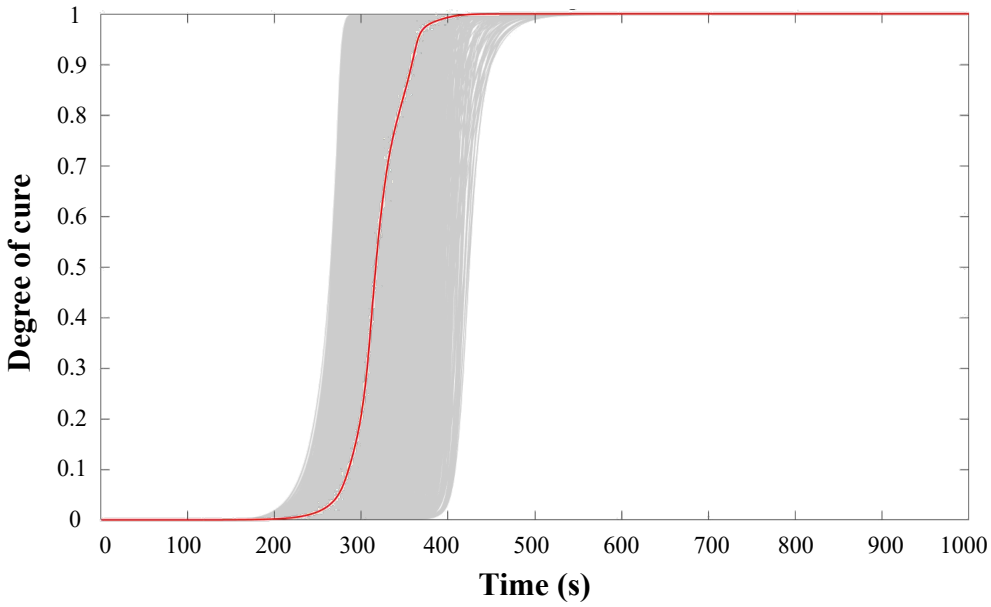

Figure 7.6: Evolution of the degree of cure with time.

The initial temperature distribution in the curing process was taken from the CFD simulation results (Figure 7.7). Hence, as PMMA was injected at ambient temperature (20°C), its initial temperature was lower than the femur temperature (37°C). After approximately 300 seconds, convection allows PMMA temperature to reach body temperature. Subsequently, the exothermic reaction associated with bone cement curing generates an increase in the PMMA temperature.

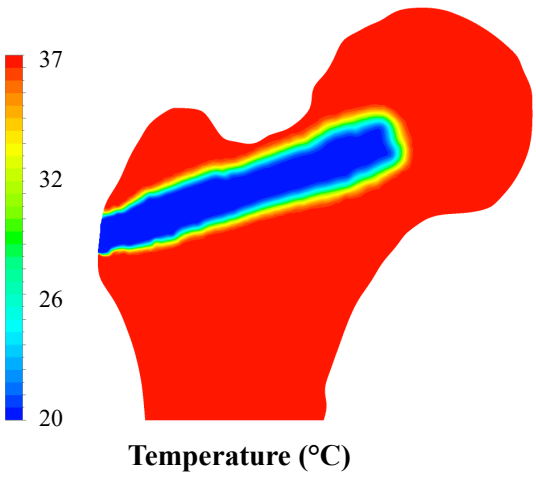

Figure 7.7: Initial temperature distribution from CFD calculations.

In Figure 7.8 it can be observed that peak temperatures reached at the PMMA-bone interface (locations A, B) were lower than the ones generated inside the PMMA (location D). Similarly, bone tissue sufficiently distant from the bone cement (location C) was not affected by the exothermic reaction of the curing process. The peak temperature reached in the bone cement mantle was 96°C, while maximum temperature recorded at the interface was 89°C.

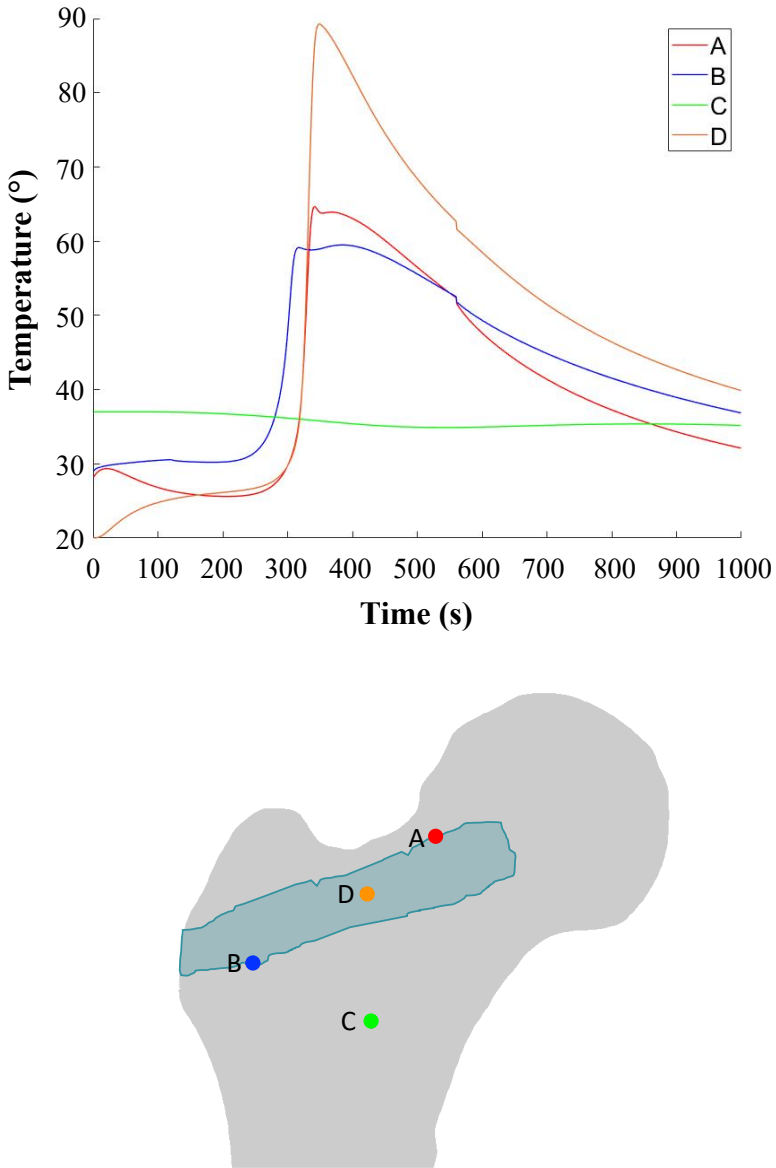

Figure 7.8: Evolution of the temperature during the bone cement curing process at different locations.

In order to evaluate the possibility of thermal necrosis, the proportion of bone tissue exposed to temperatures exceeding 40°C 50°C and 60°C was plotted against time (Figure 7.9). Over 20% of the bone was exposed to a temperature higher than 40°C during a large part of the study (after t=360s). Temperatures above 60°C occurred in a smaller fraction of the bone tissue (2%) and in smaller periods of time (from t=360s to t=520s).

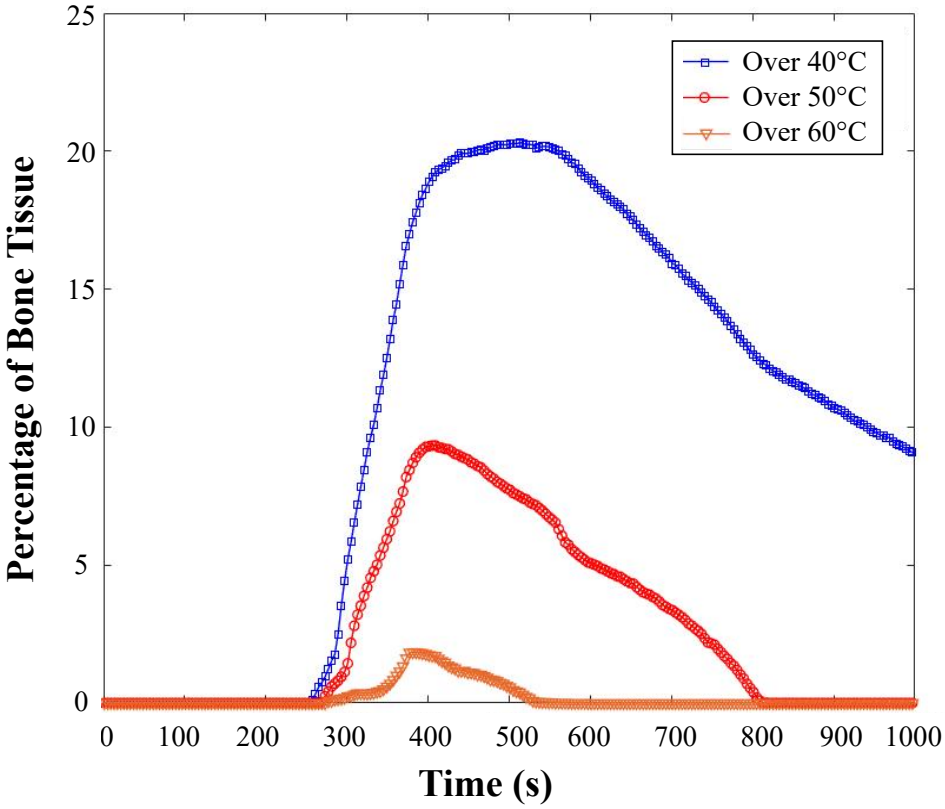

Figure 7.9: Percentage of tissue exposed to a temperature exceeding specific levels.

Besides the changes in temperature, the PMMA polymerisation process also has an effect on bone and PMMA mechanics. Stresses can arise in the bone tissue due to the thermal expansion and chemical shrinkage of bone cement. In the FE analysis all the femur external nodes were fixed and therefore, the total area of the domain was forced to remain constant. Several investigations have reported that shear stress can be studied to evaluate debonding between PMMA and bone tissue (Hung and Chang, 2010). In this study, the maximum developed shear stresses were within the range of 0.5 to 1.3MPa and found near the greater trochanter and the superior part of the PMMA distribution (Figure 7.10).

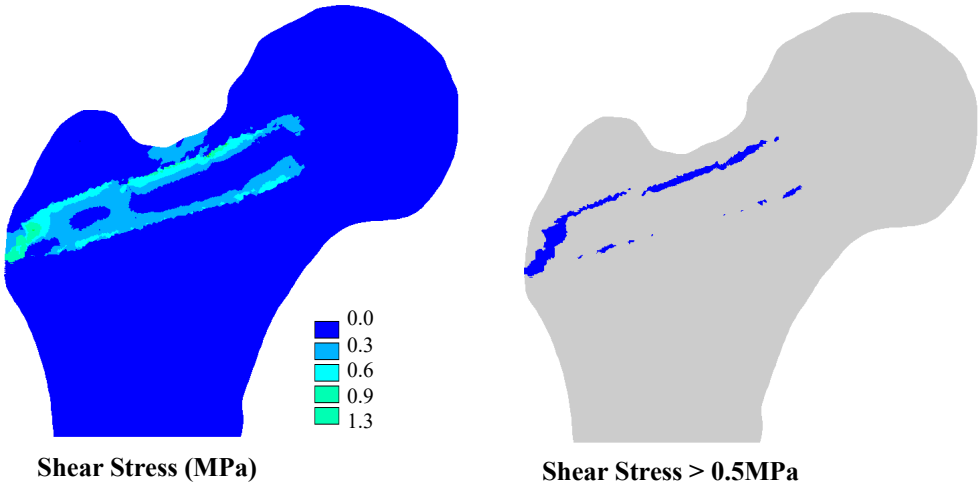

Figure 7.10: Shear stresses generated due to the PMMA curing process.

The Von Mises stress distribution generated due to the curing process is shown in Figure 7.11, reaching a maximum value of 3.6MPa near the cortical region and in the superior region of the PMMA distribution.

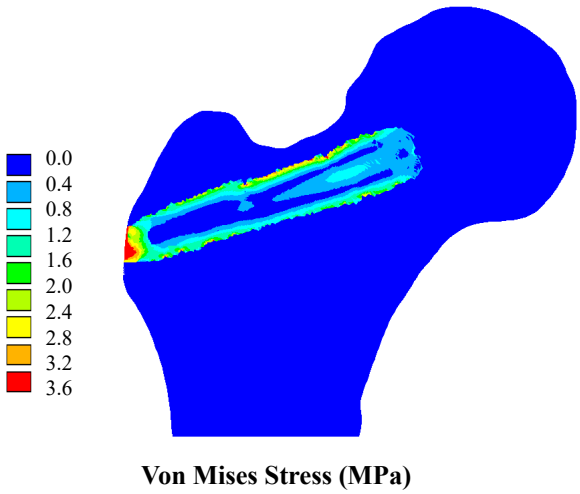

Figure 7.11: Von Mises stresses generated due to the PMMA curing process.

7.4 Discussion

A computational framework for modelling bone cement injection and polymerisation in the femoral augmentation procedure was presented in this chapter and applied to a 2D femur model. In the study, a CFD analysis was performed to investigate heat transfer and fluid flow characteristics during the PMMA injection process. Detailed material properties were applied to PMMA bone cement in order to replicate its rheological behaviour and bone tissue was modelled as a porous medium. After this, thermal-structural FE simulations were conducted to simulate bone cement curing. The model used to represent polymerisation included curing kinetics, heat generation, evolving mechanical properties, chemical shrinkage and thermal expansion.

Femoral augmentation was performed on a single specimen using three different PMMA injection velocities and hence, three related PMMA bone cement volumes. The generated femur was a two-dimensional macroscale FE model, assuming trabecular bone as a continuum solid. Although micro-FE models may have provided more accurate flow and bone cement distribution results, they also require very high computational resources. For this reason, most micro-FE models studied in the literature (Zeiser et al., 2008; Landgraf et al., 2015; Ramos-Infante et al., 2018) focus on an osteoporotic trabecular structure and do not consider the whole bone. Hence, such models do not allow for the visualization of the PMMA distribution after augmentation.

A power law was implemented based on the work of Baroud and Yahia (2004) capable of modelling both pseudoplastic (shear-rate dependent viscosity) and rheopectic (time dependent viscosity) behaviour of PMMA bone cement. CT scan data was used to create a femur geometry and derive the bone permeability of each mesh element. Permeability was the main factor affecting distribution of PMMA in the bone tissue and was modelled as an isotropic parameter, dependant on the bone volume fraction of each element. This assumption is acceptable for the 2D representation of vertebral bodies but

given the complex trabecular structure of the proximal femur (Syahrom et al., 2015) the validity of this simplification remains unclear. Homogeneous distributions of bone cement filling the pre-drilled channel were achieved at the end of the injection process. This was achieved by the inclusion of cannula retraction during the injection. Since the majority of investigations regarding bone cement injection in macroscale bone models are related to vertebroplasty, which does not involve cannula retraction, no other frameworks have considered cannula displacement. However, experimental studies of femoral augmentation using a pre-drilled channel (Beckmann et al., 2011; Steenhoven et al., 2011; Springorum et al., 2014) have found bone cement distributions similar to the ones of this chapter.

PMMA injection rate is an important parameter in any bone augmentation surgery, since it influences volume of injected PMMA, injection pressure and possibility of leakage. In this study, increasing PMMA injection velocity also increased the amount of bone cement injected in the cavity. Assuming bone cement spreads in a similar manner in the third dimension, volumes ranging from 4.1 to 12.2ml were introduced in the femur. Furthermore, depending on the PMMA injection velocity the peak pressure recorded in the simulation ranged from 6.45 to 18.65kPa. Higher pressures were found by Wang et al. (2013) who injected 2-6ml of PMMA in a vertebroplasty and reported an intraosseous peak pressure of 22.5±6.2kPa. However, Reidy et al. (2003) and Baroud et al. (2005) reported peak intravertebral pressures during vertebroplasty of 6.83±10.4kPa and 3.54±2.91kPa respectively. Peak intraosseous pressure during augmentation depends on a variety of factors such as rheology of the injected bone cement, velocity and type of injection, and material properties of the bone. This can explain variation in results obtained for in vitro vertebral augmentation cases and shows the importance of computational models. In the present study no gap was modelled between the cannula and the bone and therefore, leakage could not be studied.

One of the resultant CFD models, representing a PMMA injected volume of 7.3ml was converted into a FE model to investigate the bone cement curing process. 508 seconds

after injection the bone cement was fully cured, although the polymerisation rate of each element depended on its initial temperature. In the present study, high initial temperatures increased the rate of curing and heat evolution, as reported by Landgraf et al. (2015). Existing models considering PMMA polymerisation as a temperature-independent process (Jefferiss et al., 1975; Swenson et al., 1981) cannot account for this effect. On the other hand, more complex models also account for the leftover monomer concentration during solidification (Mazzullot et al., 1991; Stanczyk and Rietbergen, 2004) or three different phases of the polymerisation process (Hansen, 2003). These models may further enhance the findings presented this chapter, although the model used in this study was sufficient to predict the curing behaviour of the bone cement and results are in agreement with previous numerical and experimental studies (Landgraf et al., 2015; Arens et al., 2011).

The exothermic reaction generated during the PMMA polymerisation process can cause thermal necrosis in any bone augmentation procedure. Therefore, in order to evaluate risk of thermal necrosis in the femoral augmentation proposed in this chapter, results of the thermal-structural analysis were analysed. Thermal necrosis has been reported in bone tissue exposed to temperatures higher than 56°C for more than 10 seconds (Pearce et al., 2005). According to the present results, bone tissue regions adjacent to the injected PMMA are subject to temperatures of up to 89°C for over 50 seconds. It seems likely that those regions of the bone will suffer from thermal necrosis and not survive. However, since bone located at the interface is embedded within PMMA, it cannot remodel, and it is likely to remain intact and capable of transmitting loads (Stanczyk and Rietbergen, 2004). When checking temperatures in regions further away from the interface (5mm from the interface) figures are much lower, reaching a maximum of 55°C for 30 seconds. Hence, it is unlikely that thermal necrosis would propagate further away from the interface and affect bone tissue not embedded in bone cement.

Similar peak temperatures at the bone-cement interface were found by Stanczyk and Rietbergen (2004), who simulated the curing process in a 3D model of a bone trabecular

structure and reported a peak temperature of approximately 70°C, 19°C lower than the one found in this chapter. However, theirs is a microscale model and the bone cement volume studied is significantly smaller than the one of the present study. A computational study at macroscale level replicating a total hip arthroplasty was performed by Pérez et al. (2009), who reported peak temperatures between 46.3 and 54.9°C in the femoral stem. These lower temperatures are expected since the bone cement was spread in a 5mm layer around a steel cylinder and the temperature was measured in the steel stem. In addition to numerical simulations, experiments have also been performed in the past with the objective of measuring the bone cement temperature during the curing process (Arens et al., 2011; Jiang et al., 2015; Tai et al., 2016). In those experiments, bone cement was shaped into cylindrical samples similar to the bone cement distribution obtained in this chapter due to the cannula retraction. Therefore, temperature measurements from those experimental studies were compared against the temperature evolution at the bone-cement interface obtained in the present study (Figure 7.12). Results in terms of peak temperature and settling time are varied and depend on the size and geometry of the mold where bone cement was injected (Vallo, 2002), temperature measurement location, bone cement brand and ambient temperature. However, despite the differences all graphs show the same trend and the temperatures reached in the present study are within a reasonable range. Without any further experiments that replicate the same conditions applied in this chapter, it is not possible to fully validate our model, but results show the same trends found in experimental studies of cylindrical PMMA samples.

Apart from high temperatures generated in the curing process, changes in the bone cement volume can occur due to thermal expansion, chemical shrinkage and the applied boundary conditions. Bone cement is known to shrink up to 2.56% during polymerisation (Gilbert, 2006), and due to the high temperatures in the curing process, thermal expansion is also likely to occur. Stresses generated during the curing process by these effects may cause debonding and affect augmentation performance. Wide variability has been reported in previous studies evaluating the debonding of bone and PMMA. Hung and Chang (2010) found that shear stresses higher than 4.72-7.98MPa can lead to the separation of the

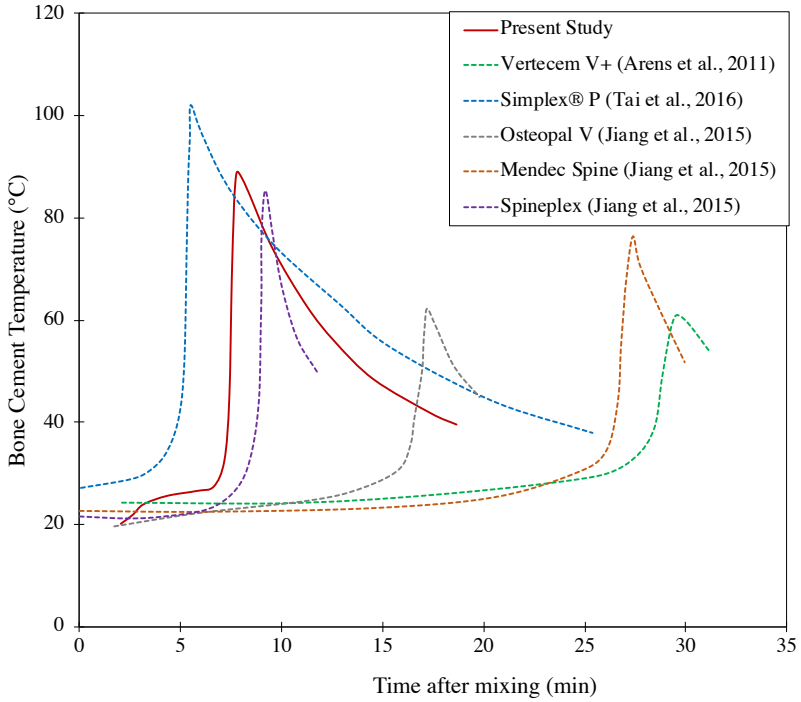

Figure 7.12: Temperatures developed in the PMMA curing process obtained in previous experimental studies and in the present chapter.

two materials. Similar values were presented by Dohmae et al. (1988), while Bean et al. (1987) reported stresses in the range of 6-15MPa. The highest shear stress found at the bone-cement interface in this study was 1.3MPa. However, obtained results can only be used as an indication of the locations that are likely to suffer debonding. More detailed modelling of the interface could help obtain more accurate results in this aspect.

Chapter 8

Conclusion and Future Work

8.1 Summary

The present study numerically investigated femoral augmentation in six femur models with different levels of osteoporosis and osteopenia. Osteoporosis was virtually introduced as a uniform reduction of the elastic modulus, which is a valid assumption for senile osteoporosis (Type 2), common in male population. The osteoporotic and osteopenic models were not validated experimentally, but a good agreement was found when comparing the yield load of the created models with the yield or fracture load found in previous experimental and computational studies (Sutter et al., 2010a,b; Falcinelli et al., 2014).

After developing the models, Chapter 3 focused on identifying the ideal bone cement volume and distribution needed to restore the load capacity of the examined femora. To do so, an Evolutionary Structural Optimisation (ESO) algorithm was applied to the FE models while replicating a lateral fall on the greater trochanter. The algorithm found the ideal locations where bone cement should be injected to increase the femur yield load by at least 100%. This ideal bone cement distribution comprised reinforcing the

greater trochanter, superior aspect of the femoral neck and, in some cases, a ring around the femoral neck. However, since the ESO was not constrained to create shapes that are injectable in practice, these distributions were formed of clusters of bone cement, not necessarily connected to each other. For this reason, in all femora the required volume of bone cement to at least duplicate the original femur yield load was small compared to previously published data from experiments or simulations. Additionally, a linear correlation between the femur T-Score and optimum volume of bone cement was demonstrated and as expected, larger volumes of bone cement were required to obtain a predefined level of augmentation in weaker femora (2.98ml in femur with T-Score -1.0 vs 18ml in femur with T-Score -3.5).

Some of the limitations of Chapter 3 were addressed in Chapter 4, such as the fact that in practice, bone cement is embedded in trabecular tissue and hence, the material properties of augmented tissue should also depend on the original properties of the bone. Besides, bone cement porosity, developed due to shrinkage and during the PMMA mixing phase, may also have an effect on the augmentation performance. Therefore, five different approaches were employed and compared to calculate the elastic modulus of the augmented tissue: pure PMMA, pure PMMA with porosity, bone-PMMA composite; bone-PMMA composite with porosity and bone-PMMA composite neglecting bone tissue. From these approaches, the first two are widely used in the literature and were proven to be significantly different to each other in the context of femoroplasty ($p=0.048$). The fourth scheme, which combined Voigt-Reuss-Hill average and bone cement porosity was considered to be the most physiologically realistic in femoral augmentation and provided results that were not statistically different to the rest of approaches. Hence, for the rest of the thesis this was the method used to simulate augmented tissue. Moreover, results from the sensitivity analysis conducted in Chapter 4 suggest that the two variables that have the highest influence in the augmentation requirements are the femoral rotation in the frontal plane (internal rotation) and the level of bone cement porosity. Increasing the femur internal rotation during a fall or using bone cement with high porosity has a negative effect in the augmentation result.

The ideal bone cement pattern found in Chapter 4 was used as a reference to propose several feasible, generalised augmentation strategies in Chapter 5. These augmentation strategies were chosen because they are achievable in practice and in most cases, there is experimental evidence that it is possible to create such distributions inside the femur. They comprised the injection of up to three spheres of bone cement or the injection of bone cement in up to two pre-drilled channels. For all proposed augmentation strategies, a Taguchi analysis was conducted and it was found that bone cement location was more important in the augmentation result than bone cement volume. Therefore, based on these results the location of bone cement in the proposed generalised augmentation approaches was optimised using a *patternsearch* algorithm. Once optimised, all augmentation strategies performed similarly (average increase of 71% with spheres of bone cement and average increase of 79% with pre-drilled paths), although injection of three spheres of bone cement required larger amounts of bone cement (8.6ml vs 7.3ml). Given the similarity of results, the choice between approaches should depend on replicability and potential clinical risks. Despite injecting three spheres of bone cement may reduce the risk of thermal necrosis (they can be injected separately, waiting until polymerisation of each sphere is completed), it is harder to control how the bone cement would spread, it may damage the cortical bone excessively if it needs to be drilled more than once and it may require detailed pre-operative planning. Augmentation in cylindrical pre-drilled channels may be easier to replicate in practice, although the risk of thermal necrosis may be higher and would need to be evaluated before the procedure.

Since most experimental work in femoral augmentation involves injecting bone cement in one or two pre-drilled channels, the fracture analysis of augmented femora (in Chapter 6) was conducted using the optimised results of the aforementioned approaches. A nonlocal damage model was applied to investigate bone fracture patterns, fracture load and energy to fracture in the augmented and non-augmented femur models with different degrees of osteoporosis and osteopenia. A significant increase in yield load, fracture load and energy to fracture was found after augmentation with approximately 7ml of bone cement: 74% increase of femur yield load, 62% increase of fracture load and

117% increase of energy to fracture in a femur with T-Score -2.5. Through comparison with existing literature it was found that the optimised augmentation strategies proposed in this study performed better than non-optimised existing approaches tested both numerically and experimentally. It was also shown that when using a predefined volume of bone cement, weaker bones obtained greater benefits from augmentation (relative fracture load increase of 81% in femur with T-Score -3.5 vs 45% in femur with T-Score -1.0). In the fracture analyses, the fracture paths generated in augmented and non-augmented femora were also studied and compared. Although fracture patterns did not change significantly after augmentation, small cracks were generated closer to the femoral head in augmented models, suggesting augmented femora may be at higher risk of comminuted fractures. However, despite results are in agreement with trends found in previous experiments, the findings of this study are only valid for a single femur and a larger sample size would be required to draw general conclusions.

Finally, Chapter 7 was dedicated to evaluate some of the risks involved in femoral augmentation such as thermal necrosis, excessive intraosseous pressure, and bone and cement debonding. Therefore, a methodology was proposed to simulate the bone cement injection and curing process and was applied to a 2D femoral augmentation procedure. Results showed that after injecting approximately 7ml of bone cement, the risk of thermal necrosis was limited to the regions in the bone-PMMA interface and debonding was not likely to happen. It was also shown that the regions more likely to suffer from debonding or stress concentration were near the superior aspect of the femoral neck. This might be a reason for concern since this is the initial region of failure in the event of a lateral fall onto the greater trochanter. Additionally, after comparison with existing literature it was found that results in terms of peak temperature and possibility of debonding depend on a variety of factors such as the brand and type of bone cement and its distribution inside the bone. Therefore, experiments that replicate the femoral augmentation procedure as depicted in Chapter 7 would be necessary to validate the model.

Despite the limitations of the present study and lack of direct experimental validation, the methodology developed in this thesis can be applied to plan and optimise a femoral augmentation intervention in any femur. After applying them to a single femur with different degrees of osteoporosis, we conclude that femoral augmentation with a limited volume of bone cement can result in significantly increased yield and fracture load without significant risks. So far, the requirements and risks of the procedure are subject-specific, although applying this study to a larger sample size could help in the development of augmentation strategies that are beneficial to a large part of the population at risk of osteoporotic fractures.

8.2 Limitations and Future Work

In the present study there are certain simplifications and limitations that could be addressed in future work. One of them concerns the fact that osteoporosis was virtually introduced in the developed models in a way that would only represent senile osteoporosis (in senile osteoporosis there is a uniform reduction of material properties in the cortical and trabecular tissue). However, hip fractures are also likely to occur in people with postmenopausal osteoporosis. In this case, the degradation of material properties is not homogeneous in the cortical and trabecular tissue and therefore, the requirements and outcome of femoral augmentation might be different. Hence, despite the yield and fracture loads of the developed models were compared and showed good agreement with experimental data from previous studies, only one femur geometry was studied with senile osteoporosis. A larger sample size, including male and female osteoporotic models, with different geometry and type of osteoporosis (I and II) could help derive more meaningful results.

In addition to a larger sample size, suitable experiments fracturing augmented and non-augmented femora could be performed in order to validate the results obtained in this

numerical study. Cadaveric or synthetic femora could be augmented by injecting cement in pre-drilled channels or in spheres and test conditions that replicate a lateral fall could be applied. With this, it would be possible to find the augmented yield and fracture load and potential changes in fracture patterns due to augmentation. Other test conditions that have not been investigated in this research could also be applied. Although most osteoporotic hip fractures occur due to a fall, patients with severe osteoporosis might develop a fracture when walking or climbing stairs. As expected, the sensitivity analysis conducted in Section 4.2.2 found that fall direction affects augmentation requirements. However, a more detailed study of different boundary conditions, from standing to fall in different directions could improve the efficacy of the augmentation strategies. Similarly, combining results from these simulations with epidemiological data of the most common types of fall could enhance the augmentation requirements.

All the simulations performed in this thesis were static due to the complexity and computational costs of dynamic simulations. However, they do not accurately represent a dynamic event like a fall on the side. Hence, changing the existing simulations to a dynamic impact analysis, accounting for the person's height and weight and the damping effects of soft tissue would increase the accuracy in representing a fall.

The present study also included the development of a framework to simulate bone cement injection and solidification, but it was only applied to a 2D femur model. This could be enhanced by small modifications that allow application to a 3D model, considering anisotropic permeability of trabecular tissue. Additionally, in order to validate the model, bone cement could be injected into cadaveric or synthetic femora while monitoring the temperature with thermocouples in different locations. The final bone cement distribution in simulations and experiments could also be compared after performing X-ray in the augmented bone. Given the different available commercial bone cements and the sensitivity of the curing process to the type of bone cement, this methodology could be used to study the effect of the fluid rheology in the risks involved in femoral augmentation. Besides, cooling the femur prior to augmentation may be

studied as an alternative to minimise the risk of thermal necrosis and changes in the bone cement injection and solidification process could be monitored.

Finally, all the methodologies developed in this study could be combined to build a tool that could help surgeons plan the augmentation procedure. This tool should use the femur CT scan as input and provide realistic and easy to implement augmentation strategies for the specific femur (such as filling with bone cement one or two pre-drilled cavities). Variables like the type of bone cement and ambient temperature in the operation room could be changed. The risks and benefits involved with each bone cement and augmentation strategy would be provided and may help the surgeon in the decision-making process. In order to replicate in practice the simulated augmentation, parameters such as the inclination of the drill, diameter of the drill bits and injection velocity would be provided.

Appendix A

Publications

1.Santana Artiles, María E. & Venetsanos, Demetrios T. (2017) A new evolutionary optimization method for osteoporotic bone augmentation, *Computer Methods in Biomechanics and Biomedical Engineering*. 20&1) pp. 691-700 .
Available at https://doi.org/10.1080/10255842.2017.1291805

2. Santana Artiles, María E. & Venetsanos, Demetrios T. (2018) Numerical investigation of the effect of bone cement porosity on osteoporotic femoral augmentation. *International Journal for Numerical Methods in Biomedical Engineering*, 34(8) pp. e2989.
Available at https://doi.org/10.1002/cnm.2989

References

Abrahamsen, B. (2017). The calcium and vitamin D controversy. *Therapeutic Advances in Musculoskeletal Disease*, 9(5):107–114.

Albrektsson, T. and Linder, L. (1984). Bone injury caused by curing bone cement. A vital microscopic study in the rabbit tibia. *Clinical orthopaedics and related research*, 183:280–287.

Ali, A. A., Cristofolini, L., Schileo, E., Hu, H., Taddei, F., Kim, R. H., Rullkoetter, P. J., and Laz, P. J. (2014). Specimen-specific modeling of hip fracture pattern and repair. *Journal of Biomechanics*, 47(2):536–543.

Alonso, J., Volgas, D., Giordano, V., and Stannard, J. (2000). A review of the treatment of hip dislocations associated with acetabular fractures. *Clinical orthopaedics and related research*, 377:32–43.

Altai, Z., Qasim, M., Li, X., and Viceconti, M. (2019). The effect of boundary and loading conditions on patient classification using finite element predicted risk of fracture. *Clinical Biomechanics*, 68:137–143.

Arens, D., Rothstock, S., Windolf, M., and Boger, A. (2011). Bone marrow modified acrylic bone cement for augmentation of osteoporotic cancellous bone. *Journal of the Mechanical Behavior of Biomedical Materials*, 4(8):2081–2089.

Badilatti, S. D., Christen, P., Ferguson, S. J., and Müller, R. (2017). Computational modeling of long-term effects of prophylactic vertebroplasty on bone adaptation.

Proceedings of the Institution of Mechanical Engineers, Part H: Journal of Engineering in Medicine, 231(5):423–431.

Baliga, B. R., Rose, P. L., and Ahmed, A. M. (1992). Thermal modeling of polymerizing polymethylmethacrylate, considering temperature-dependent heat generation. *Journal of Biomechanical Engineering*, 114(2):251–259.

Baroud, G., Falk, R., Crookshank, M., Sponagel, S., and Steffen, T. (2004). Experimental and theoretical investigation of directional permeability of human vertebral cancellous bone for cement infiltration. *Journal of Biomechanics*, 37(2):189–196.

Baroud, G., Vant, C., Giannitsios, D., Bohner, M., and Steffen, T. (2005). Effect of vertebral shell on injection pressure and intravertebral pressure in vertebroplasty. *Spine*, 30(1):68–74.

Baroud, G. and Yahia, F. B. (2004). A finite element rheological model for polymethylmethacrylate flow: Analysis of the cement delivery in vertebroplasty. *Proceedings of the Institution of Mechanical Engineers, Part H: Journal of Engineering in Medicine*, 218(5):331–338.

Basafa, E. and Armand, M. (2013). Cement placement optimization in femoral augmentation using an evolutionary algorithm. In *Proceedings of the ASME Design Engineering Technical Conference*, volume 4.

Basafa, E. and Armand, M. (2014). Subject-specific planning of femoroplasty: A combined evolutionary optimization and particle diffusion model approach. *Journal of Biomechanics*, 47(10):2237–2243.

Basafa, E., Murphy, R. J., Kutzer, M. D., Otake, Y., and Armand, M. (2013). A particle model for prediction of cement infiltration of cancellous bone in osteoporotic bone augmentation. *PLoS ONE*, 8(6).

Basafa, E., Murphy, R. J., Otake, Y., Kutzer, M. D., Belkoff, S. M., Mears, S. C., and Armand, M. (2015). Subject-specific planning of femoroplasty: An experimental verification study. *Journal of Biomechanics*, 48(1):59–64.

Bayraktar, H. H., Morgan, E. F., Niebur, G. L., Morris, G. E., Wong, E. K., and Keaveny, T. M. (2004). Comparison of the elastic and yield properties of human femoral trabecular and cortical bone tissue. *Journal of Biomechanics*, 37(1):27–35.

Bean, D. J., Convery, F. R., Woo, S. L. Y., and Lieber, R. L. (1987). Regional variation in shear strength of the bone-polymethylmethacrylate interface. *Journal of Arthroplasty*, 2(4):293–298.

Beckmann, J., Ferguson, S. J., Gebauer, M., Luering, C., Gasser, B., and Heini, P. (2007). Femoroplasty - augmentation of the proximal femur with a composite bone cement - feasibility, biomechanical properties and osteosynthesis potential. *Medical Engineering and Physics*, 29(7):755–764.

Beckmann, J., Springorum, R., Vettorazzi, E., Bachmeier, S., Lüring, C., Tingart, M., Püschel, K., Stark, O., Grifka, J., Gehrke, T., Amling, M., and Gebauer, M. (2011). Fracture prevention by femoroplasty-cement augmentation of the proximal femur. *Journal of Orthopaedic Research*, 29(11):1753–1758.

Belkoff, S. M., Mathis, J. M., Jasper, L. E., and Deramond, H. (2001). The biomechanics of vertebroplasty: The effect of cement volume on mechanical behavior. *Spine*, 26(14):1537–1541.

Benca, E., Synek, A., Amini, M., Kainberger, F., Hirtler, L., Windhager, R., Mayr, W., and Pahr, D. H. (2019). QCT-based finite element prediction of pathologic fractures in proximal femora with metastatic lesions. *Scientific Reports*, 9(1):10305.

Bergeles, C., Gosline, A. H., Vasilyev, N. V., Codd, P. J., Nido, P. J. D., and Dupont, P. E. (2015). Concentric tube robot design and optimization based on task and anatomical constraints. *IEEE Transactions on Robotics*, 31(1):67–84.

Bessho, M., Ohnishi, I., Matsumoto, T., Ohashi, S., Matsuyama, J., Tobita, K., Kaneko, M., and Nakamura, K. (2009). Prediction of proximal femur strength using a CT-based nonlinear finite element method: Differences in predicted fracture load and site with changing load and boundary conditions. *Bone*, 45(2):226–231.

Bessho, M., Ohnishi, I., Matsuyama, J., Matsumoto, T., Imai, K., and Nakamura, K. (2007). Prediction of strength and strain of the proximal femur by a CT-based finite element method. *Journal of Biomechanics*, 40(8):1745–1753.

Bischoff-Ferrari, H. A., Bhasin, S., and Manson, J. E. (2018). Preventing fractures and falls: A limited role for calcium and vitamin D supplements? *JAMA - Journal of the American Medical Association*, 319(15):1552–1553.

Bischoff-Ferrari, H. A., Willett, W. C., Wong, J. B., Stuck, A. E., Staehelin, H. B., Orav, E. J., Thoma, A., Kiel, D. P., and Henschkowski, J. (2009). Prevention of nonvertebral fractures with oral vitamin D and dose dependency: A meta-analysis of randomized controlled trials. *Archives of Internal Medicine*, 169(6):551–561.

Black, D. M., Thompson, D. E., Bauer, D. C., Ensrud, K., Musliner, T., Hochberg, M. C., Nevitt, M. C., Suryawanshi, S., and Cummings, S. R. (2000). Fracture risk reduction with alendronate in women with osteoporosis: The fracture intervention trial. *Journal of Clinical Endocrinology and Metabolism*, 85(11):4118–4124.

Blake, A. J., Morgan, K., Bendall, M. J., Dallosso, H., Ebrahim, S. B. J., Arie, T. H. D., Fentem, P. H., and Bassey, E. J. (1988). Falls by elderly people at home: Prevalence and associated factors. *Age and Ageing*, 17(6):365–372.

Bleiler, C., Wagner, A., Stadelmann, V. A., Windolf, M., Köstler, H., Boger, A., Gueorguiev-Rüegg, B., Ehlers, W., and Röhrle, O. (2015). Multiphasic modelling of bone-cement injection into vertebral cancellous bone. *International Journal for Numerical Methods in Biomedical Engineering*, 31(1):37–57.

Bohner, M. (2007). Reactivity of calcium phosphate cements. *Journal of Materials Chemistry*, 17(38):3980–3986.

Bohner, M., Doebelin, N., and Baroud, G. (2006). Theoretical and experimental approach to test the cohesion of calcium phosphate pastes. *European Cells and Materials*, 12:26–35.

Bolland, M. J., Grey, A., and Reid, I. R. (2015). Should we prescribe calcium or vitamin D supplements to treat or prevent osteoporosis? *Climacteric*, 18:22–31.

Boyd, D., Clarkin, O. M., Wren, A. W., and Towler, M. R. (2008a). Zinc-based glass polyalkenoate cements with improved setting times and mechanical properties. *Acta Biomaterialia*, 4(2):425–431.

Boyd, D., Li, H., Tanner, D. A., Towler, M. R., and Wall, J. G. (2006). The antibacterial effects of zinc ion migration from zinc-based glass polyalkenoate cements. *Journal of Materials Science: Materials in Medicine*, 17(6):489–494.

Boyd, D., Towler, M. R., Wren, A., and Clarkin, O. M. (2008b). Comparison of an experimental bone cement with surgical Simplex® P, Spineplex® and Cortoss®. *Journal of Materials Science: Materials in Medicine*, 19(4):1745–1752.

Brand, R. A. (2011). The Classic: The architecture of the trabecular bone (tenth contribution on the mechanics of the human skeletal framework). *Clinical orthopaedics and related research*, 469(11):3079–3084.

Briscoe, A. and New, A. (2010). Polymerisation stress modelling in acrylic bone cement. *Journal of Biomechanics*, 43(5):978–983.

Cameron, I. D., Murray, G. R., Gillespie, L. D., Robertson, M. C., Hill, K. D., Cumming, R. G., and Kerse, N. (2010). Interventions for preventing falls in older people in nursing care facilities and hospitals. *Cochrane database of systematic reviews*, (1).

Cameron, I. D., Venman, J., Kurrle, S. E., Lockwood, K., Birks, C., Cumming, R. G., Quine, S., and Bashford, G. (2001). Hip protectors in aged-care facilities: A randomized trial of use by individual higher-risk residents. *Age and Ageing*, 30(6):477–481.

Campbell, A. J., Reinken, J., Allan, B. C., and Martinez, G. S. (1981). Falls in old age: A study of frequency and related clinical factors. *Age and Ageing*, 10(4):264–270.

Carte, D. R. and Hayes, W. C. (1977). The compressive behavior of bone as a two-phase porous structure. *Journal of Bone and Joint Surgery - Series A*, 59(7):954–962.

Cauley, J. A., Lui, L.-Y., Genant, H. K., Salamone, L., Browner, W., Fink, H. A., Cohen, P., Hillier, T., Bauer, D. C., and Cummings, S. R. (2009). Risk factors for severity and type of the hip fracture. *Journal of Bone and Mineral Research*, 24(5):943–955.

Chan, D. K., Hillier, G., Coore, M., Cooke, R., Monk, R., Mills, J., and Hung, W. T. (2000). Effectiveness and acceptability of a newly designed hip protector: A pilot study. *Archives of Gerontology and Geriatrics*, 30(1):25–34.

Chang, J. T., Morton, S. C., Rubenstein, L. Z., Mojica, W. A., Maglione, M., Suttorp, M. J., Roth, E. A., and Shekelle, P. G. (2004). Interventions for the prevention of falls in older adults: Systematic review and meta-analysis of randomised clinical trials. *British medical journal*, 328(7441):680–683.

Chapuy, M. C., Arlot, M. E., Duboeuf, F., Brun, J., Crouzet, B., Arnaud, S., Delmas, P. D., and Meunier, P. J. (1992). Vitamin D3 and calcium to prevent hip fractures in elderly women. *New England Journal of Medicine*, 327(23):1637–1642.

Charlebois, M., Jirásek, M., and Zysset, P. K. (2010). A nonlocal constitutive model for trabecular bone softening in compression. *Biomechanics and Modeling in Mechanobiology*, 9(5):597–611.

Chen, G., Wu, F. Y., Liu, Z. C., Yang, K., and Cui, F. (2015). Comparisons of node-based and element-based approaches of assigning bone material properties onto subject-specific finite element models. *Medical Engineering and Physics*, 37(8):808–812.

Chevalier, Y., Pahr, D., Charlebois, M., Heini, P., Schneider, E., and Zysset, P. (2008). Cement distribution, volume, and compliance in vertebroplasty: Some answers from an anatomy-based nonlinear finite element study. *Spine*, 33(16):1722–1730.

Clarkin, O. M., Boyd, D., Madigan, S., and Towler, M. R. (2009). Comparison of an experimental bone cement with a commercial control, hydroset. *Journal of Materials Science: Materials in Medicine*, 20(7):1563–1570.

Cody, D. D., Gross, G. J., Hou, F. J., Spencer, H. J., Goldstein, S. A., and Fyhrie, D. P. (1999). Femoral strength is better predicted by finite element models than QCT and DXA. *Journal of Biomechanics*, 32(10):1013–1020.

Compston, J., Cooper, A., Cooper, C., Gittoes, N., Gregson, C., Harvey, N., Hope, S., Kanis, J. A., McCloskey, E. V., Poole, K. E. S., Reid, D. M., Selby, P., Thompson, F., Thurston, A., Vine, N., and Osteoporosis, G. G. T. N. (2017). UK clinical guideline for the prevention and treatment of osteoporosis. *Archives of Osteoporosis*, 12(1):43.

Cranney, A., Tugwell, P., Zytaruk, N., Robinson, V., Weaver, B., Adachi, J., Wells, G., Shea, B., and Guyatt, G. (2002). Meta-analysis of raloxifene for the prevention and treatment of postmenopausal osteoporosis. *Endocrine reviews*, 23(4):524–528.

Cummings, S. R. and Melton, L. J. (2002). Epidemiology and outcomes of osteoporotic fractures. *The Lancet*, 359(9319):1761–1767.

Cummings, S. R., Nevitt, M. C., Browner, W. S., Stone, K., Fox, K. M., Ensrud, K. E., Cauley, J., Black, D., and Vogt, T. M. (1995). Risk factors for hip fracture in white women. *New England Journal of Medicine*, 332(12):767–773.

Daish, C., Blanchard, R., Gulati, K., Losic, D., Findlay, D., Harvie, D. J. E., and Pivonka, P. (2017). Estimation of anisotropic permeability in trabecular bone based on microCT imaging and pore-scale fluid dynamics simulations. *Bone Reports*, 6:129–139.

Darling, M. and Hill, R. (1994). Novel polyalkenoate (glass-ionomer) dental cements based on zinc silicate glasses. *Biomaterials*, 15(4):299–306.

de Bakker, P. M., Manske, S. L., Ebacher, V., Oxland, T. R., Cripton, P. A., and Guy, P. (2009). During sideways falls proximal femur fractures initiate in the superolateral cortex: Evidence from high-speed video of simulated fractures. *Journal of Biomechanics*, 42(12):1917–1925.

Dell, R. M., Adams, A. L., Greene, D. F., Funahashi, T. T., Silverman, S. L., Eisemon, E. O., Zhou, H., Burchette, R. J., and Ott, S. M. (2012). Incidence of atypical

nontraumatic diaphyseal fractures of the femur. *Journal of Bone and Mineral Research*, 27(12):2544–2550.

Dohmae, Y., Bechtold, J. E., Sherman, R. E., Puno, R. M., and Gustilo, R. B. (1988). Reduction in cement-bone interface shear strength between primary and revision arthroplasty. *Clinical orthopaedics and related research*, (236):214–220.

Dragomir-Daescu, D., Buijs, J. O. D., McEligot, S., Dai, Y., Entwistle, R. C., Salas, C., Melton, L. J., Bennet, K. E., Khosla, S., and Amin, S. (2011). Robust QCT/FEA models of proximal femur stiffness and fracture load during a sideways fall on the hip. *Annals of Biomedical Engineering*, 39(2):742–755.

Drake, A. J., Armstrong, D. W., and Shakir, K. M. M. (2004). Bone mineral density and total body bone mineral content in 18- to 22-year-old women. *Bone*, 34(6):1037–1043.

Eggermont, F., Derikx, L. C., Verdonschot, N., van der Geest I.C.M., de Jong M.A.A., Snyers, A., van der Linden Y.M., and Tanck, E. (2018). Can patient-specific finite element models better predict fractures in metastatic bone disease than experienced clinicians?: Towards computational modelling in daily clinical practice. *Bone & joint research*, 7(6):430–439.

Engelke, K., Lang, T., Khosla, S., Qin, L., Zysset, P., Leslie, W. D., Shepherd, J. A., and Schousboe, J. T. (2015). Clinical use of quantitative computed tomography (qct) of the hip in the management of osteoporosis in adults: the 2015 ISCD official positions-part I. *Journal of Clinical Densitometry*, 18(3):338–358.

Erbe, E. M., Clineff, T. D., and Gualtieri, G. (2001). Comparison of a new bisphenol-a-glycidyl dimethacrylate-based cortical bone void filler with polymethyl methacrylate. *European Spine Journal*, 10:S147–S152.

Falcinelli, C., Schileo, E., Balistreri, L., Baruffaldi, F., Bordini, B., Viceconti, M., Albisinni, U., Ceccarelli, F., Milandri, L., Toni, A., and Taddei, F. (2014). Multiple loading conditions analysis can improve the association between finite element bone

strength estimates and proximal femur fractures: A preliminary study in elderly women. *Bone*, 67:71–80.

Farvardin, A., Basafa, E., Bakhtiarinejad, M., and Armand, M. (2019). Significance of preoperative planning for prophylactic augmentation of osteoporotic hip: A computational modeling study. *Journal of Biomechanics*, 94:75–81.

Farvardin, A., Nejad, M. B., Pozin, M., and Armand, M. (2018). A biomechanical and thermal analysis for bone augmentation of the proximal femur. In *ASME International Mechanical Engineering Congress and Exposition, Proceedings (IMECE)*, volume 3.

Feith, R. (1975). Side effects of acrylic cement implanted into bone. A histological (micro)angiographic, fluorescence microscopic and autoradiographic study in the rabbit femur. *Acta Orthopaedica Scandinavica*, 46(sup 161).

Feng, X. and McDonald, J. M. (2011). Disorders of bone remodeling. *Annual Review of Pathology: Mechanisms of Disease*, 6(1):121–145.

Ferizi, U., Besser, H., Hysi, P., Jacobs, J., Rajapakse, C. S., Chen, C., Saha, P. K., Honig, S., and Chang, G. (2019). Artificial intelligence applied to osteoporosis: A performance comparison of machine learning algorithms in predicting fragility fractures from mri data. *Journal of Magnetic Resonance Imaging*, 49(4):1029–1038.

Fisher, A., Srikusalanukul, W., Davis, M., and Smith, P. (2010). Hip fracture type: Important role of parathyroid hormone (PTH) response to hypovitaminosis D. *Bone*, 47(2):400–407.

Fleps, I., Vuille, M., Melnyk, A., Ferguson, S. J., Guy, P., Helgason, B., and Cripton, P. A. (2018). A novel sideways fall simulator to study hip fractures ex vivo. *PLOS ONE*, 13(7):e0201096.

Fliri, L., Sermon, A., Wähnert, D., Schmoelz, W., Blauth, M., and Windolf, M. (2013). Limited V-shaped cement augmentation of the proximal femur to prevent secondary hip fractures. *Journal of Biomaterials Applications*, 28(1):136–143.

Floerkemeier, T., Lutz, A., Nackenhorst, U., Thorey, F., Waizy, H., Windhagen, H., and von Lewinski, G. (2011). Core decompression and osteonecrosis intervention rod in osteonecrosis of the femoral head: clinical outcome and finite element analysis. *International orthopaedics*, 35(10):1461–1466.

Ford, T. M., Keaveny, T. M., and Hayes, W. C. (1996). The effect of impact direction on the structural capacity of the proximal femur during falls. *Journal of Bone and Mineral Research*, 11(3):377–383.

Fox, K. M., Cummings, S. R., Williams, E., and Stone, K. (2000). Femoral neck and intertrochanteric fractures have different risk factors: A prospective study. *Osteoporosis International*, 11(12):1018–1023.

Fox, K. M., Magaziner, J., Hebel, J. R., Kenzora, J. E., and Kashnei, T. M. (1999). Intertrochanteric versus femoral neck hip fractures: Differential characteristics, treatment, and sequelae. *The Journals of Gerontology: Series A*, 54(12):M635–M640.

Frankenburg, E. P., Goldstein, S. A., Bauer, T. W., Harris, S. A., and Poser, R. D. (1998). Biomechanical and histological evaluation of a calcium phosphate cement. *Journal of Bone and Joint Surgery - Series A*, 80(8):1112–1124.

Geraci, G., Iacono, G. L., Nigro, C. L., Cannizzaro, F., Cajozzo, M., and Modica, G. (2013). Asymptomatic bone cement pulmonary embolism after vertebroplasty: case report and literature review. *Case reports in surgery*, 2013:591432.

Geusens, P., van Geel, T., and den Bergh van (2010). Can hip fracture prediction in women be estimated beyond bone mineral density measurement alone? *Therapeutic advances in musculoskeletal disease*, 2(2):63–77.

Gilbert, J. L. (2006). Complexity in modeling of residual stresses and strains during polymerization of bone cement: Effects of conversion, constraint, heat transfer, and viscoelastic property changes. *Journal of Biomedical Materials Research - Part A*, 79(4):999–1014.

Gilchrist, S., Nishiyama, K. K., de Bakker, P., Guy, P., Boyd, S. K., Oxland, T., and Cripton, P. A. (2014). Proximal femur elastic behaviour is the same in impact and constant displacement rate fall simulation. *Journal of Biomechanics*, 47(15):3744–3749.

Gillespie, L. D., Robertson, M. C., Gillespie, W. J., Sherrington, C., Gates, S., Clemson, L. M., and Lamb, S. E. (2012). Interventions for preventing falls in older people living in the community. *Cochrane Database of Systematic Reviews*, 2012(9).

Ginebra, M. P., Canal, C., Espanol, M., Pastorino, D., and Montufar, E. B. (2012). Calcium phosphate cements as drug delivery materials. *Advanced Drug Delivery Reviews*, 64(12):1090–1110.

Ginebra, M. P., Traykova, T., and Planell, J. A. (2006). Calcium phosphate cements as bone drug delivery systems: A review. *Journal of Controlled Release*, 113(2):102–110.

Gomez-Alonso, C., Curiel, M., Carranza, F., Cano, R., and Pérez, A. (2000). Femoral bone mineral density, neck-shaft angle and mean femoral neck width as predictors of hip fracture in men and women. *Osteoporosis International*, 11:714–720.

Grassi, L., Schileo, E., Taddei, F., Zani, L., Juszczyk, M., Cristofolini, L., and Viceconti, M. (2012). Accuracy of finite element predictions in sideways load configurations for the proximal human femur. *Journal of Biomechanics*, 45(2):394–399.

Grassi, L., Väänänen, S. P., Ristinmaa, M., Jurvelin, J. S., and Isaksson, H. (2017). Prediction of femoral strength using 3D finite element models reconstructed from DXA images: validation against experiments. *Biomechanics and Modeling in Mechanobiology*, 16(3):989–1000.

Gullberg, B., Johnell, O., and Kanis, J. (1997). World-wide projections for hip fracture. *Osteoporosis International*, 7:407–413.

Gultepe, E., Jin, Q., Choi, A., Abramson, A., and Gracias, D. H. (2015). *Miniaturized Untethered Tools for Surgery*, pages 201–234. Micro- and Nanomanipulation Tools.

Gunantara, N. (2018). A review of multi-objective optimization: Methods and its applications. *Cogent Engineering*, 5(1):1–16.

Haider, I. T., Goldak, J., and Frei, H. (2018). Femoral fracture load and fracture pattern is accurately predicted using a gradient-enhanced quasi-brittle finite element model. *Medical Engineering and Physics*, 55:1–8.

Hambli, R. and Allaoui, S. (2013). A robust 3D finite element simulation of human proximal femur progressive fracture under stance load with experimental validation. *Annals of Biomedical Engineering*, 41(12):2515–2527.

Hambli, R., Bettamer, A., and Allaoui, S. (2012). Finite element prediction of proximal femur fracture pattern based on orthotropic behaviour law coupled to quasi-brittle damage. *Medical Engineering and Physics*, 34(2):202–210.

Hansen, E. (2003). Modelling heat transfer in a bone-cement-prosthesis system. *Journal of Biomechanics*, 36(6):787–795.

Harmata, A. J., Uppuganti, S., Granke, M., Guelcher, S. A., and Nyman, J. S. (2015). Compressive fatigue and fracture toughness behavior of injectable, settable bone cements. *Journal of the Mechanical Behavior of Biomedical Materials*, 51:345–355.

Harvey, N. C., Biver, E., Kaufman, J. M., Bauer, J., Branco, J., Brandi, M. L., Bruyère, O., Coxam, V., Cruz-Jentoft, A., Czerwinski, E., Dimai, H., Fardellone, P., Landi, F., Reginster, J. Y., Dawson-Hughes, B., Kanis, J. A., Rizzoli, R., and Cooper, C. (2017). The role of calcium supplementation in healthy musculoskeletal ageing. *Osteoporosis International*, 28(2):447–462.

He, Z., Zhai, Q., Hu, M., Cao, C., Wang, J., Yang, H., and Li, B. (2015). Bone cements for percutaneous vertebroplasty and balloon kyphoplasty: Current status and future developments. *Journal of Orthopaedic Translation*, 3(1):1–11.

Heini, P. and Berlemann, U. (2001). Bone substitutes in vertebroplasty. *European Spine Journal*, 10(2):S205–S213.

Heini, P. F., Franz, T., Fankhauser, C., Gasser, B., and Ganz, R. (2004). Femoroplasty-augmentation of mechanical properties in the osteoporotic proximal femur: A biomechanical investigation of PMMA reinforcement in cadaver bones. *Clinical Biomechanics*, 19(5):506–512.

Higgs, W. A. J., Lucksanasombool, P., Higgs, R. J. E. D., and Swain, M. V. (2001). Comparison of the material properties of PMMA and glass-ionomer based cements for use in orthopaedic surgery. *Journal of Materials Science: Materials in Medicine*, 12(5):453–460.

Hirt, C. W. and Nichols, B. D. (1981). Volume of fluid (VOF) method for the dynamics of free boundaries. *Journal of Computational Physics*, 39(1):201–225.

Hung, J. P. and Chang, F. C. (2010). Computational modeling of debonding behavior at the bone/cement interface with experimental validation. *Materials Science and Engineering C*, 30(3):445–453.

Järvinen, T., Jokihaara, J., Guy, P., Alonso-Coello, P., Collins, G. S., Michaëlsson, K., and Sievänen, H. (2014). Conflicts at the heart of the FRAX™ tool. *CMAJ : Canadian Medical Association journal*, 186(3):165–167.

Jefferiss, C. D., Lee, A. J. C., and Ling, R. S. M. (1975). Thermal aspects of self curing polymethylmethacrylate. *Journal of Bone and Joint Surgery - Series B*, 57(4):511–518.

Jiang, H.-J., Xu, J., Qiu, Z.-Y., Ma, X.-L., Zhang, Z.-Q., Tan, X.-X., Cui, Y., and Cui, F.-Z. (2015). Mechanical properties and cytocompatibility improvement of vertebroplasty pmma bone cements by incorporating mineralized collagen. *Materials*, 8(5):2616–2634.

Kanis, J. A. (2002). Osteoporosis III: Diagnosis of osteoporosis and assessment of fracture risk. *Lancet*, 359(9321):1929–1936.

Kanis, J. A., Johnell, O., Oden, A., Johansson, H., and McCloskey, E. (2008). FRAX™ and the assessment of fracture probability in men and women from the UK. *Osteoporosis International*, 19(4):385–397.

Kanis, J. A., McCloskey, E. V., Johansson, H., Cooper, C., Rizzoli, R., and Reginster, J. Y. (2013). European guidance for the diagnosis and management of osteoporosis in postmenopausal women. *Osteoporosis International*, 24(1):23–57.

Kannus, P., Parkkari, J., Niemi, S., Pasanen, M., Palvanen, M., Järvinen, M., and Vuori, I. (2000). Prevention of hip fracture in elderly people with use of a hip protector. *New England Journal of Medicine*, 343(21):1506–1513.

Kaptoge, S., Beck, T. J., Reeve, J., Stone, K. L., Hillier, T. A., Cauley, J. A., and Cummings, S. R. (2008). Prediction of incident hip fracture risk by femur geometry variables measured by hip structural analysis in the study of osteoporotic fractures. *Journal of bone and mineral research : the official journal of the American Society for Bone and Mineral Research*, 23(12):1892–1904.

Kaufman, J. M., Palacios, S., Silverman, S., Sutradhar, S., and Chines, A. (2013). An evaluation of the fracture risk assessment tool (FRAX™) as an indicator of treatment efficacy: The effects of bazedoxifene and raloxifene on vertebral, nonvertebral, and all clinical fractures as a function of baseline fracture risk assessed by FRAX™. *Osteoporosis International*, 24(10):2561–2569.

Keller, T. S. (1994). Predicting the compressive mechanical behavior of bone. *Journal of Biomechanics*, 27(9):1159–1168.

Keyak, J. H. (2001). Improved prediction of proximal femoral fracture load using nonlinear finite element models. *Medical Engineering & Physics*, 23(3):165–173.

Keyak, J. H. and Falkinstein, Y. (2003). Comparison of in situ and in vitro CT scan-based finite element model predictions of proximal femoral fracture load. *Medical Engineering and Physics*, 25(9):781–787.

Keyak, J. H., Skinner, H. B., and Fleming, J. A. (2001). Effect of force direction on femoral fracture load for two types of loading conditions. *Journal of Orthopaedic Research*, 19(4):539–544.

Khader, B. A., Rodriguez, O., and Towler, M. R. (2018). The effect of Mg2+ incorporation into the glass phase of zinc-based glass polyalkenoate cements. *Journal of Non-Crystalline Solids*, 483:106–117.

Khosla, S. and Riggs, B. L. (2005). Pathophysiology of age-related bone loss and osteoporosis.

Kiel, D. P., Magaziner, J., Zimmerman, S., Ball, L., Barton, B. A., Brown, K. M., Stone, J. P., Dewkett, D., and Birge, S. J. (2007). Efficacy of a hip protector to prevent hip fracture in nursing home residents: The HIP PRO randomized controlled trial. *Journal of the American Medical Association*, 298(4):413–422.

Kinzl, M., Boger, A., Zysset, P. K., and Pahr, D. H. (2011). The effects of bone and pore volume fraction on the mechanical properties of PMMA/bone biopsies extracted from augmented vertebrae. *Journal of Biomechanics*, 44(15):2732–2736.

Kinzl, M., Boger, A., Zysset, P. K., and Pahr, D. H. (2012). The mechanical behavior of PMMA/bone specimens extracted from augmented vertebrae: A numerical study of interface properties, PMMA shrinkage and trabecular bone damage. *Journal of Biomechanics*, 45(8):1478–1484.

Kinzl, M., Schwiedrzik, J., Zysset, P. K., and Pahr, D. H. (2013). An experimentally validated finite element method for augmented vertebral bodies. *Clinical Biomechanics*, 28(1):15–22.

Klotzbuecher, C. M., Ross, P. D., Landsman, P. B., Abbott, T. A., and Berger, M. (2000). Patients with prior fractures have an increased risk of future fractures: A summary of the literature and statistical synthesis. *Journal of Bone and Mineral Research*, 15(4):721–739.

Kothawala, P., Badamgarav, E., Ryu, S., Miller, R. M., and Halbert, R. J. (2007). Systematic review and meta-analysis of real-world adherence to drug therapy for osteoporosis. *Mayo Clinic Proceedings*, 82(12):1493–1501.

Kruse, C., Eiken, P., and Vestergaard, P. (2017). Machine learning principles can improve hip fracture prediction. *Calcified tissue international*, 100(4):348–360.

Kwong, F. N. K. and Power, R. A. (2006). A comparison of the shrinkage of commercial bone cements when mixed under vacuum. *Journal of Bone and Joint Surgery - Series B*, 88(1):120–122.

LaFleur, J., McAdam-Marx, C., Kirkness, C., and Brixner, D. I. (2008). Clinical risk factors for fracture in postmenopausal osteoporotic women: A review of the recent literature. *Annals of Pharmacotherapy*, 42(3):375–386.

Laing, A. C. and Robinovitch, S. N. (2010). Characterizing the effective stiffness of the pelvis during sideways falls on the hip. *Journal of Biomechanics*, 43(10):1898–1904.

Landgraf, R., Ihlemann, J., Kolmeder, S., Lion, A., Lebsack, H., and Kober, C. (2015). Modelling and simulation of acrylic bone cement injection and curing within the framework of vertebroplasty. *ZAMM Zeitschrift fur Angewandte Mathematik und Mechanik*, 95(12):1530–1547.

Langton, C. M., Pisharody, S., and Keyak, J. H. (2009). Generation of a 3D proximal femur shape from a single projection 2D radiographic image. *Osteoporosis International*, 20(3):455–461.

Larsson, S. and Bauer, T. W. (2002). Use of injectable calcium phosphate cement for fracture fixation: A review. *Clinical orthopaedics and related research*, (395):23–32.

Lauritzen, J. B., Petersen, M. M., and Lund, B. (1993). Effect of external hip protectors on hip fractures. *The Lancet*, 341(8836):11–13.

Leibson, C. L., Tosteson, A. N. A., Gabriel, S. E., Ransom, J. E., and Melton, L. J. (2002). Mortality, disability, and nursing home use for persons with and without hip fracture: A population-based study. *Journal of the American Geriatrics Society*, 50(10):1644–1650.

Lennon, A. B. and Prendergast, P. J. (2002). Residual stress due to curing can initiate

damage in porous bone cement: experimental and theoretical evidence. *Journal of Biomechanics*, 35(3):311–321.

Lieberman, I. H., Togawa, D., and Kayanja, M. M. (2005). Vertebroplasty and kyphoplasty: Filler materials. *Spine Journal*, 5(6):305S–361S.

Looker, A. C., Borrud, L. G., Hughes, J. P., Fan, B., Shepherd, J. A., and 3rd., L. J. M. (2012). Lumbar spine and proximal femur bone mineral density, bone mineral content, and bone area: United states, 2005-2008. *Vital and health statistics.Series 11, Data from the national health survey*, (251):1–132.

Lu, J. X., Huang, Z. W., Tropiano, P., d'Orval, B. C., Remusat, M., Dejou, J., Proust, J. P., and Poitout, D. (2002). Human biological reactions at the interface between bone tissue and polymethylmethacrylate cement. *Journal of Materials Science: Materials in Medicine*, 13(8):803–809.

Lu, Y., Maquer, G., Museyko, O., Püschel, K., Engelke, K., Zysset, P., Morlock, M., and Huber, G. (2014). Finite element analyses of human vertebral bodies embedded in polymethylmethalcrylate or loaded via the hyperelastic intervertebral disc models provide equivalent predictions of experimental strength. *Journal of Biomechanics*, 47(10):2512–2516.

Maffezzoli, A., Ronca, D., Guida, G., Pochini, I., and Nicolais, L. (1997). In-situ polymerization behaviour of bone cements. *Journal of Materials Science: Materials in Medicine*, 8(2):75–83.

Majumder, S., Roychowdhury, A., and Pal, S. (2007). Simulation of hip fracture in sideways fall using a 3D finite element model of pelvis–femur–soft tissue complex with simplified representation of whole body. *Medical Engineering & Physics*, 29(10):1167–1178.

Makras, P., Delaroudis, S., and Anastasilakis, A. D. (2015). Novel therapies for osteoporosis. *Metabolism: Clinical and Experimental*, 64(10):1199–1214.

Marco, M., Giner, E., Larraínzar, R., Caeiro, J. R., and Miguélez, M. H. (2017). Numerical modelling of femur fracture and experimental validation using bone simulant. *Annals of Biomedical Engineering*, 45(10):1–14.

Marco, M., Giner, E., Larraínzar-Garijo, R., Caeiro, J. R., and Miguélez, M. H. (2018). Modelling of femur fracture using finite element procedures. *Engineering Fracture Mechanics*, 196:157–167.

Marks, R. (2010). Hip fracture epidemiological trends, outcomes, and risk factors, 1970-2009. *International journal of general medicine*, 3:1–17.

Masud, T. and Morris, R. O. (2001). Epidemiology of falls. *Age and Ageing*, 30(4):3–7.

Mazzullot, S., Paolini, M., and Verdi, C. (1991). Numerical simulation of thermal bone necrosis during cementation of femoral prostheses. *Journal of mathematical biology*, 29(5):475–494.

McClung, M. R., Geusens, P., Miller, P. D., Zippel, H., Bensen, W. G., Roux, C., Adami, S., Fogelman, I., Diamond, T., Eastell, R., Meunier, P. J., Reginster, J. Y., Wasnich, R. D., Greenwald, M., Kaufman, J. M., and III, C. H. C. (2001). Effect of risedronate on the risk of hip fracture in elderly women. *New England Journal of Medicine*, 344(5):333–340.

Meng, J. T. C. (2008). Patient specific finite volume modeling for intraosseous pmma cement flow simulation in vertebral cancellous bone.

Morgan, E. F., Bayraktar, H. H., and Keaveny, T. M. (2003). Trabecular bone modulus-density relationships depend on anatomic site. *Journal of Biomechanics*, 36(7):897–904.

Morgan, E. F., Bayraktar, H. H., Yeh, O. C., Majumdar, S., Burghardt, A., and Keaveny, T. M. (2004). Contribution of inter-site variations in architecture to trabecular bone apparent yield strains. *Journal of Biomechanics*, 37(9):1413–1420.

Morgan, E. F., Yetkinler, D. N., Constantz, B. R., and Dauskardt, R. H. (1997). Mechanical properties of carbonated apatite bone mineral substitute: Strength, fracture

and fatigue behaviour. *Journal of Materials Science: Materials in Medicine*, 8(9):559–570.

Mullender, M. G. and Huiskes, R. (1995). Proposal for the regulatory mechanism of Wolff's law. *Journal of Orthopaedic Research*, 13(4):503–512.

Muller, S. D., Green, S. M., and McCaskie, A. W. (2002). The dynamic volume changes of polymerising polymethyl methacrylate bone cement. *Acta Orthopaedica Scandinavica*, 73(6):684–687.

Nachreiner, N. M., Findorff, M. J., Wyman, J. F., and McCarthy, T. C. (2007). Circumstances and consequences of falls in community-dwelling older women. *Journal of Women's Health*, 16.

Nalla, R. K., Stölken, J. S., Kinney, J. H., and Ritchie, R. O. (2005). Fracture in human cortical bone: Local fracture criteria and toughening mechanisms. *Journal of Biomechanics*, 38(7):1517–1525.

Nawathe, S., Akhlaghpour, H., Bouxsein, M. L., and Keaveny, T. M. (2014). Microstructural failure mechanisms in the human proximal femur for sideways fall loading. *Journal of Bone and Mineral Research*, 29(2):507–515.

Nazarian, A., Stechow, D. V., Zurakowski, D., Müller, R., and Snyder, B. D. (2008). Bone volume fraction explains the variation in strength and stiffness of cancellous bone affected by metastatic cancer and osteoporosis. *Calcified tissue international*, 83(6):368–379.

Neuburger, J., Currie, C., Wakeman, R., Tsang, C., Plant, F., Stavola, B. D., Cromwell, D. A., and der Meulen van (2015). The impact of a national clinician-led audit initiative on care and mortality after hip fracture in england: an external evaluation using time trends in non-audit data. *Medical care*, 53(8):686–691.

Nguyen, N. D., Eisman, J. A., Center, J. R., and Nguyen, T. V. (2007a). Risk factors for fracture in nonosteoporotic men and women. *The Journal of Clinical Endocrinology & Metabolism*, 92(3):955–962.

Nguyen, N. D., Frost, S. A., Center, J. R., Eisman, J. A., and Nguyen, T. V. (2007b). Development of a nomogram for individualizing hip fracture risk in men and women. *Osteoporosis International*, 18(8):1109–1117.

NIH Consensus Development Panel on Osteoporosis Prevention, Diagnosis, a. T. (2001). Osteoporosis prevention, diagnosis, and therapy. *JAMA - Journal of the American Medical Association*, 285(6):785–795.

Nobile, S. and Nobile, L. (2019). Assessment of fracture toughness in bone tissue engineering. *Polymer Engineering & Science*, 59(12):2402–2405.

O'Flaherty, E. J. (2000). Modeling normal aging bone loss, with consideration of bone loss in osteoporosis. *Toxicological Sciences*, 55(1):171–188.

Ovesen, J., Møller-Madsen, B., Thomsen, J. S., Danscher, G., and Mosekilde, L. (2001). The positive effects of zinc on skeletal strength in growing rats. *Bone*, 29(6):565–570.

Parkkari, J., Kannus, P., Palvanen, M., Natri, A., Vainio, J., Aho, H., Vuori, I., and Järvinen, M. (1999). Majority of hip fractures occur as a result of a fall and impact on the greater trochanter of the femur: A prospective controlled hip fracture study with 206 consecutive patients. *Calcified tissue international*, 65(3):183–187.

Pearce, G., Bainbridge, C., Patrick, J., Kibble, K., Lenz, M., and Jones, G. (2005). *An investigation into thermal necrosis of bone associated with surgical procedures*, volume 6. WitPress.

Pérez, M. A., no, N. N., Madrala, A., García-Aznar, J. M., and Doblaré, M. (2009). Computational modelling of bone cement polymerization: Temperature and residual stresses. *Computers in biology and medicine*, 39(9):751–759.

Pérez, M. A. and Palacios, J. (2010). Comparative finite element analysis of the debonding process in different concepts of cemented hip implants. *Annals of Biomedical Engineering*, 38(6):2093–2106.

Pinilla, T. P., Boardman, K. C., Bouxsein, M. L., Myers, E. R., and Hayes, W. C. (1996). Impact direction from a fall influences the failure load of the proximal femur as much as age-related bone loss. *Calcified tissue international*, 58(4):231–235.

Pistoia, W., Rietbergen, B. V., Lochmüller, E. M., Lill, C. A., Eckstein, F., and Rüegsegger, P. (2002). Estimation of distal radius failure load with micro-finite element analysis models based on three-dimensional peripheral quantitative computed tomography images. *Bone*, 30(6):842–848.

Polizzi, S., Pira, E., Ferrara, M., Bugiani, M., Papaleo, A., Albera, R., and Palmi, S. (2002). Neurotoxic effects of aluminium among foundry workers and alzheimer's disease. *Neurotoxicology*, 23(6):761–774.

Pomrink, G. J., DiCicco, M. P., Clineff, T. D., and Erbe, E. M. (2003). Evaluation of the reaction kinetics of CORTOSS®, a thermoset cortical bone void filler. *Biomaterials*, 24(6):1023–1031.

Pottecher, P., Engelke, K., Duchemin, L., Museyko, O., Moser, T., Mitton, D., Vicaut, E., Adams, J., Skalli, W., Laredo, J. D., and Bousson, V. (2016). Prediction of hip failure load: In vitro study of 80 femurs using three imaging methods and finite element models - the european fracture study (effect). *Radiology*, 280(3):837–847.

Pulkkinen, P., Glüer, C. C., and Jämsä, T. (2011). Investigation of differences between hip fracture types: A worthy strategy for improved risk assessment and fracture prevention. *Bone*, 49(4):600–604.

Raas, C., Hofmann-Fliri, L., Hörmann, R., and Schmoelz, W. (2016). Prophylactic augmentation of the proximal femur: an investigation of two techniques. *Archives of orthopaedic and trauma surgery*, 136(3):345–351.

Ramos-Infante, S. J. and Pérez, M. A. (2019). High- and low-viscosity cement for osteoporotic femoral augmentation: A computational subject-specific approach. *Engineering Fracture Mechanics*, 219.

Ramos-Infante, S. J., Ten-Esteve, A., Alberich-Bayarri, A., and Pérez, M. A. (2018). Discrete particle model for cement infiltration within open-cell structures: Prevention of osteoporotic fracture. *PLoS ONE*, 13(6).

Reidy, D., Ahn, H., Mousavi, P., Finkelstein, J., and Whyne, C. M. (2003). A biomechanical analysis of intravertebral pressures during vertebroplasty of cadaveric spines with and without simulated metastases. *Spine*, 28(14):1534–1539.

Reilly, D. T., Burstein, A. H., and Frankel, V. H. (1974). The elastic modulus for bone. *Journal of Biomechanics*, 7(3):271–272,IN9–IN12,273–275.

Riggs, B. L., Khosla, S., and Melton, L. J. (2001). *Chapter 38 - The Type I/Type II Model for Involutional Osteoporosis: Update and Modification Based on New Observations*. ELSEVIER.

Riggs, B. L., Wahner, H. W., Seeman, E., Offord, K. P., Dunn, W. L., Mazess, R. B., Johnson, K. A., and Melton, L. J. (1982). Changes in bone mineral density of the proximal femur and spine with aging: Differences between the postmenopausal and senile osteoporosis syndromes. *The Journal of clinical investigation*, 70(4):716–723.

Robertson, M. C., Campbell, A. J., Gardner, M. M., and Devlin, N. (2002). Preventing injuries in older people by preventing falls: A meta-analysis of individual-level data. *Journal of the American Geriatrics Society*, 50(5):905–911.

Rohlmann, A., Boustani, H. N., Bergmann, G., and Zander, T. (2010). A probabilistic finite element analysis of the stresses in the augmented vertebral body after vertebroplasty. *European Spine Journal*, 19(9):1585–1595.

Rossouw, J. E., Anderson, G. L., Prentice, R. L., LaCroix, A. Z., Kooperberg, C., Stefanick, M. L., Jackson, R. D., Beresford, S. A. A., Howard, B. V., Johnson, K. C., Kotchen, J. M., and Ockene, J. (2002). Risks and benefits of estrogen plus progestin in healthy postmenopausal women: Principal results from the women's health initiative randomized controlled trial. *Journal of the American Medical Association*, 288(3):321–333.

Rubin, L. A., Hawker, G. A., Peltekova, V. D., Fielding, L. J., Ridout, R., and Cole, D. E. C. (1999). Determinants of peak bone mass: Clinical and genetic analyses in a young female Canadian cohort. *Journal of Bone and Mineral Research*, 14(4):633–643.

Sanders, K. M., Lim, K., Stuart, A. L., Macleod, A., Scott, D., Nicholson, G. C., and Busija, L. (2017). Diversity in fall characteristics hampers effective prevention: the precipitants, the environment, the fall and the injury. *Osteoporosis International*, 28(10):3005–3015.

Schileo, E., Balistreri, L., Grassi, L., Cristofolini, L., and Taddei, F. (2014). To what extent can linear finite element models of human femora predict failure under stance and fall loading configurations? *Journal of Biomechanics*, 47(14):3531–3538.

Schileo, E., Dall'Ara, E., Taddei, F., Malandrino, A., Schotkamp, T., Baleani, M., and Viceconti, M. (2008a). An accurate estimation of bone density improves the accuracy of subject-specific finite element models. *Journal of Biomechanics*, 41(11):2483–2491.

Schileo, E., Taddei, F., Cristofolini, L., and Viceconti, M. (2008b). Subject-specific finite element models implementing a maximum principal strain criterion are able to estimate failure risk and fracture location on human femurs tested in vitro. *Journal of Biomechanics*, 41(2):356–367.

Schoor, N. M. V., Smit, J. H., Twisk, J. W. R., Bouter, L. M., and Lips, P. (2003). Prevention of hip fractures by external hip protectors: A randomized controlled trial. *Journal of the American Medical Association*, 289(15):1957–1962.

Soyka, R. P. W., Helgason, B., Marangalou, J. H., Bergh, J. P. V. D., Rietbergen, B. V., and Ferguson, S. J. (2016). The effectiveness of percutaneous vertebroplasty is determined by the patient-specific bone condition and the treatment strategy. *PLoS ONE*, 11(4).

Spierings, P. T. J. (2005). *Testing and Performance of Bone Cements*, pages 67–78. The Well-Cemented Total Hip Arthroplasty: Theory and Practice. Springer Berlin Heidelberg, Berlin, Heidelberg.

Springorum, H. R., Gebauer, M., Mehrl, A., Stark, O., Craiovan, B., Püschel, K., Amling, M., Grifka, J., and Beckmann, J. (2014). Fracture prevention by prophylactic femoroplasty of the proximal femur-metallic compared with cemented augmentation. *Journal of orthopaedic trauma*, 28(7):403–409.

Stadelmann, V. A., Zderic, I., Baur, A., Unholz, C., Eberli, U., and Gueorguiev, B. (2016). Composite time-lapse computed tomography and micro finite element simulations: A new imaging approach for characterizing cement flows and mechanical benefits of vertebroplasty. *Medical Engineering and Physics*, 38(2):97–107.

Stanczyk, M. and Rietbergen, B. V. (2004). Thermal analysis of bone cement polymerisation at the cement-bone interface. *Journal of Biomechanics*, 37(12):1803–1810.

Steenhoven, T. J. V. D., Schaasberg, W., Vries, A. C. D., Valstar, E. R., and Nelissen, R. G. H. H. (2011). Elastomer femoroplasty prevents hip fracture displacement: In vitro biomechanical study comparing two minimal invasive femoroplasty techniques. *Clinical Biomechanics*, 26(5):464–469.

Steenhoven, T. J. V. D., Schaasberg, W., Vries, A. C. D., Valstar, E. R., and Nelissen, R. G. H. H. (2012). Cyclic loading of fractured cadaveric femurs after elastomer femoroplasty: An in vitro biomechanical study. *Clinical Biomechanics*, 27(8):819–823.

Stolk, J., Verdonschot, N., Mann, K. A., and Huiskes, R. (2003). Prevention of mesh-dependent damage growth in finite element simulations of crack formation in acrylic bone cement. *Journal of Biomechanics*, 36(6):861–871.

Stroncek, J. D., Shaul, J. L., Favell, D., Hill, R. S., Huber, B. M., Howe, J. G., and Bouxsein, M. L. (2019). In vitro injection of osteoporotic cadaveric femurs with a triphasic calcium-based implant confers immediate biomechanical integrity. *Journal of Orthopaedic Research*, 37(4):908–915.

Sutter, E. G., Mears, S. C., and Belkoff, S. M. (2010a). A biomechanical evaluation of

femoroplasty under simulated fall conditions. *Journal of orthopaedic trauma*, 24(2):95–99.

Sutter, E. G., Wall, S. J., Mears, S. C., and Belkoff, S. M. (2010b). The effect of cement placement on augmentation of the osteoporotic proximal femur. *Geriatric orthopaedic surgery & rehabilitation*, 1(1):22–26.

Svedbom, A., Hernlund, E., Ivergård, M., Compston, J., Cooper, C., Stenmark, J., McCloskey, E. V., Jönsson, B., Kanis, J. A., and the EU review (2013). Osteoporosis in the european union: a compendium of country-specific reports. *Archives of Osteoporosis*, 8(1):137.

Swenson, L. W., Schurman, D. J., and Piziali, R. L. (1981). Finite element temperature analysis of a total hip replacement and measurement of pmma curing temperatures. *Journal of Biomedical Materials Research*, 15(1):83–96.

Syahrom, A., Kadir, M. R. A., Harun, M. N., and Öchsner, A. (2015). Permeability study of cancellous bone and its idealised structures. *Medical Engineering & Physics*, 37(1):77–86.

Tai, C.-L., Lai, P.-L., Lin, W.-D., Tsai, T.-T., Lee, Y.-C., Liu, M.-Y., and Chen, L.-H. (2016). Modification of mechanical properties, polymerization temperature, and handling time of polymethylmethacrylate cement for enhancing applicability in vertebroplasty. *BioMed Research International*, 2016:7901562.

Trivedi, D. P., Doll, R., and Khaw, K. T. (2003). Effect of four monthly oral vitamin d3 (cholecalciferol) supplementation on fractures and mortality in men and women living in the community: Randomised double blind controlled trial. *British medical journal*, 326(7387):469–472.

Turner, C. H. (2002). Biomechanics of bone: Determinants of skeletal fragility and bone quality. *Osteoporosis International*, 13(2):97–104.

Turner, C. H. (2006). Bone strength: Current concepts. *Annals of the New York Academy of Sciences*, 1068(1):429–446.

Ueyama, Y., Ishikawa, K., Mano, T., Koyama, T., Nagatsuka, H., Matsumura, T., and Suzuki, K. (2001). Initial tissue response to anti-washout apatite cement in the rat palatal region: Comparison with conventional apatite cement. *Journal of Biomedical Materials Research*, 55(4):652–660.

Väänänen, S. P., Yavari, S. A., Weinans, H., Zadpoor, A. A., Jurvelin, J. S., and Isaksson, H. (2013). Repeatability of digital image correlation for measurement of surface strains in composite long bones. *Journal of Biomechanics*, 46(11):1928–1932.

Vallo, C. I. (2002). Theoretical prediction and experimental determination of the effect of mold characteristics on temperature and monomer conversion fraction profiles during polymerization of a pmma-based bone cement. *Journal of Biomedical Materials Research*, 63(5):627–642.

van den Munckhof, S. and Zadpoor, A. A. (2014). How accurately can we predict the fracture load of the proximal femur using finite element models? *Clinical Biomechanics*, 29(4):373–380.

van der Steenhoven, T. J., Schaasberg, W., de Vries, A. C., Valstar, E. R., and Nelissen, R. G. H. H. (2009). Augmentation with silicone stabilizes proximal femur fractures: An in vitro biomechanical study. *Clinical Biomechanics*, 24(3):286–290.

van der Velde, R. Y., Brouwers, J. R. B. J., Geusens, P. P., Lems, W. F., and den Bergh van (2014). Calcium and vitamin D supplementation: state of the art for daily practice. *Food & Nutrition Research*, 58(1):21796.

Varga, P., Inzana, J. A., Schwiedrzik, J., Zysset, P. K., Gueorguiev, B., Blauth, M., and Windolf, M. (2017). New approaches for cement-based prophylactic augmentation of the osteoporotic proximal femur provide enhanced reinforcement as predicted by non-linear finite element simulations. *Clinical Biomechanics*, 44:7–13.

Varga, P., Schwiedrzik, J., Zysset, P. K., Fliri-Hofmann, L., Widmer, D., Gueorguiev, B., Blauth, M., and Windolf, M. (2016). Nonlinear quasi-static finite element simulations

predict in vitro strength of human proximal femora assessed in a dynamic sideways fall setup. *Journal of the Mechanical Behavior of Biomedical Materials*, 57:116–127.

Vazquez, B., Levenfeld, B., and Roman, J. S. (1998). Role of amine activators on the curing parameters, properties and toxicity of acrylic bone cements. *Polymer International*, 46(3):241–250.

Verhulp, E., van Rietbergen, B., and Huiskes, R. (2008). Load distribution in the healthy and osteoporotic human proximal femur during a fall to the side. *Bone*, 42(1):30–35.

Verron, E., Bouler, J. M., and Guicheux, J. (2012). Controlling the biological function of calcium phosphate bone substitutes with drugs. *Acta Biomaterialia*, 8(10):3541–3551.

Wang, Y., Huang, F., Chen, L., Ke, Z. Y., and Deng, Z. L. (2013). Clinical measurement of intravertebral pressure during vertebroplasty and kyphoplasty. *Pain Physician*, 16(4):E411–E418.

Watts, N. B., Ettinger, B., and LeBoff, M. S. (2009). FRAX™ facts. *Journal of Bone and Mineral Research*, 24(6):975–979.

Weber, N. K., Fidler, J. L., Keaveny, T. M., Clarke, B. L., Khosla, S., Fletcher, J. G., Lee, D. C., Pardi, D. S., Loftus, E. V., Kane, S. V., Barlow, J. M., Murthy, N. S., Becker, B. D., and Bruining, D. H. (2014). Validation of a CT-derived method for osteoporosis screening in IBD patients undergoing contrast-enhanced CT enterography. *American Journal of Gastroenterology*, 109(3):401–408.

Wijayathunga, V. N., Oakland, R. J., Jones, A. C., Hall, R. M., and Wilcox, R. K. (2013). Vertebroplasty: Patient and treatment variations studied through parametric computational models. *Clinical Biomechanics*, 28(8):860–865.

Wingstrand, H., Egund, N., Carlin, N. O., Forsberg, L., Gustafson, T., and Sundén, G. (1985). Intracapsular pressure in transient synovitis of the hip. *Acta Orthopaedica*, 56(3):204–210.

Winter, A., Bradman, H., Fraser, C., and Holt, G. (2016). The management of intracapsular hip fractures. *Orthopaedics and Trauma*, 30(2):93–102.

Wolfram, U., Wilke, H.-J., and Zysset, P. K. (2011). Damage accumulation in vertebral trabecular bone depends on loading mode and direction. *Journal of Biomechanics*, 44(6):1164–1169.

Wren, A., Boyd, D., and Towler, M. R. (2008). The processing, mechanical properties and bioactivity of strontium based glass polyalkenoate cements. *Journal of Materials Science: Materials in Medicine*, 19(4):1737–1743.

Xie, W., Jin, D., Ma, H., Ding, J., Xu, J., Zhang, S., and Liang, D. (2016). Cement leakage in percutaneous vertebral augmentation for osteoporotic vertebral compression fractures analysis of risk factors. *Clinical Spine Surgery*, 29(4):E171–E176.

Xie, Y. M. and Steven, G. P. (1996). Evolutionary structural optimization for dynamic problems. *Computers & Structures*, 58(6):1067–1073.

Yosibash, Z., Tal, D., and Trabelsi, N. (2010). Predicting the yield of the proximal femur using high-order finite-element analysis with inhomogeneous orthotropic material properties. *Philosophical Transactions of the Royal Society A: Mathematical, Physical and Engineering Sciences*, 368(1920):2707–2723.

Zani, L., Erani, P., Grassi, L., Taddei, F., and Cristofolini, L. (2015). Strain distribution in the proximal human femur during in vitro simulated sideways fall. *Journal of Biomechanics*, 48(10):2130–2143.

Zeiser, T., Bashoor-Zadeh, M., Darabi, A., and Baroud, G. (2008). Pore-scale analysis of newtonian flow in the explicit geometry of vertebral trabecular bones using lattice Boltzmann simulation. *Proceedings of the Institution of Mechanical Engineers, Part H: Journal of Engineering in Medicine*, 222(2):185–194.

Zhang, J., Liu, W., Schnitzler, V., Tancret, F., and Bouler, J. M. (2014). Calcium phosphate cements for bone substitution: Chemistry, handling and mechanical properties. *Acta Biomaterialia*, 10(3):1035–1049.

Zhang, Y., Zhong, W., Zhu, H., Chen, Y., Xu, L., and Zhu, J. (2013). Establishing the 3d finite element solid model of femurs in partial by volume rendering.

Zijlstra, G. A. R., Haastregt, J. C. M. V., Rossum, E. V., Eijk, J. T. M. V., Yardley, L., and Kempen, G. I. J. M. (2007). Interventions to reduce fear of falling in community-living older people: A systematic review. *Journal of the American Geriatrics Society*, 55(4):603–615.

Zimmerman, S., Magaziner, J., Birge, S. J., Barton, B. A., Kronsberg, S. S., and Kiel, D. P. (2010). Adherence to hip protectors and implications for U.S. long-term care settings. *Journal of the American Medical Directors Association*, 11(2):106–115.